UTS UNIVERSITY OF TECHNOLOGY SYDNEY

Probabilistic Safe Fault-Tolerant Control: A Gaussian Process-Based Approach

by Linhao Zhao

Thesis submitted in fulfilment of the requirements for the degree of

Doctor of Philosophy

under the supervision of Prof. Shiping Wen

University of Technology Sydney
Faculty of Engineering and Information Technology

June 2025

CERTIFICATE OF ORIGINAL AUTHORSHIP

I, *Linhao Zhao* declare that this thesis, is submitted in fulfilment of the requirements for the award of Doctor of Philosophy, in the Australian Artificial Intelligence Institute, Faculty of Engineering and Information Technology at the University of Technology Sydney.

This thesis is wholly my own work unless otherwise referenced or acknowledged. In addition, I certify that all information sources and literature used are indicated in the thesis.

This document has not been submitted for qualifications at any other academic institution.

This research is supported by the Australian Government Research Training Program.

Signature: Production Note:
Signature removed prior to publication.

Date: June 2025

Abstract

Fault-tolerant control (FTC) aims to preserve system functionality and ensure stability in the presence of unknown faults, such as actuator faults. However, existing FTC methods do not explicitly guarantee safety and may fail to mitigate potential risks to surrounding systems in practical environments. Accordingly, this research investigates the impact of unknown actuator gain and bias faults on system dynamics, which may result from partial degradation of physical components or long-term wear. In addition, model uncertainty is an inherent property of systems due to randomness and limited system knowledge, which degrades the performance of FTC methods. Two types of uncertainty are considered in this thesis: aleatoric uncertainty, arising from randomness, and epistemic uncertainty, resulting from incomplete system knowledge. To address these challenges, probabilistically safe FTC methods, which integrate GPs and control barrier functions (CBFs) into FTC frameworks, are proposed to ensure safe and reliable control of autonomous systems.

Firstly, this thesis proposes probabilistic adaptive FTC approaches to compensate for unknown actuator bias faults and to approximate unknown system dynamics through GP regression. Since GPs are sensitive to the quality and quantity of training data, two data collection strategies are investigated: offline data collection and online event-triggered learning. Sufficient conditions are derived to ensure the probabilistic stability of the closed-loop system. Secondly, to ensure both stability and safety of systems with high relative degrees, a learning-based safe FTC method is presented by integrating a

high-order CBF (HOCBF) method and GP regression into the FTC framework. Theoretical feasibility conditions are derived to ensure probabilistic constraint satisfaction. Thirdly, a novel GP-based safe control approach is proposed to handle challenges arising from actuator gain faults. The approach incorporates the CBF method and online fault parameter estimation and is further extended to the HOCBF framework. Several theoretical results are derived to ensure stability of the estimator and probabilistic safety of uncertain systems. Lastly, to overcome the conservative assumptions about the structure of model uncertainty, particularly those adopted in HOCBF methods, a novel unified GP modelling strategy with compound kernels is introduced and integrated with HOCBFs into the FTC framework. Theoretical conditions are established to guarantee its feasibility. Numerical examples demonstrate the effectiveness and competitiveness of proposed methods compared to existing methods.

Overall, this thesis proposes novel methodologies to address unknown actuator faults and model uncertainty, with a focus on enhancing the safety and stability of autonomous systems in practical environments.

Dedication

To girlfriend, family, friends, and myself.

Acknowledgments

My Ph.D. journey at the University of Technology Sydney (UTS) over the past four years has been both challenging and rewarding. This experience has not only shaped me as a researcher but also enriched my personal growth. I would like to extend my sincere appreciation to all those who have supported, inspired, and accompanied me throughout this memorable period.

First and foremost, I express my deepest gratitude to my principal supervisor, Professor Shiping Wen, for his unwavering support, expert guidance, and invaluable mentorship. Professor Wen's profound knowledge, academic insight, and dedication have been instrumental in shaping the direction of my research. His trust in my abilities and consistent encouragement have empowered me to pursue ambitious ideas, overcome challenges, and continuously improve. I am truly honored to have worked under the guidance of such a distinguished scholar and generous mentor.

I am also deeply thankful to my co-supervisors, Dr. Feng Liu, for his continuous support and insightful advice throughout my Ph.D. studies. His mentorship has played a pivotal role in my development as an independent researcher. His thoughtful feedback, rigorous academic perspective, and encouragement during difficult times have been invaluable in expanding my research capabilities and confidence.

I would like to express my heartfelt gratitude to the Australian Artificial Intelligence Institute and the Faculty of Engineering and Information Technology at UTS for providing an excellent research environment and generous support. Their resources, facilities, and academic community have greatly contributed to the successful completion

of my doctoral studies.

I am also grateful to the members of my research group. Dr. Zhencheng Fan, Dr. Ziyu Sheng, Dr. Boqian Li, and Dr. Guangyang Tian, for their collaboration, intellectual exchange, and constant encouragement. Their companionship has made my research journey more enjoyable and fulfilling.

Special thanks to Dr. Jiahao Xia and Dr. Shengbo Wang, whose support and guidance have been instrumental from my master's years through to my Ph.D. Their mentorship, encouragement, and unwavering belief in my abilities have served as a cornerstone of my academic and personal development. I am profoundly grateful for their significant and continued contributions to my journey.

I would like thank my parents for their unwavering support, unconditional love, belief in my abilities, and financial assistances. Their enduring belief in me has been the foundation upon which I have built this achievement. This journey would not have been possible without their sacrifices and unwavering encouragement.

Finally, and most importantly, I would like to express my deepest love and heartfelt appreciation to my girlfriend, Dr. Lu Wang, who brings warmth, meaning, and strength to my life. Her companionship has been a steady source of comfort and encouragement during difficult and uncertain times. To her, I wish to say: "I love three things in this world: the Sun, the Moon, and You. The Sun for the day, the Moon for the night, and You forever."

List of Publications

Related to the Thesis :

1. L. Zhao, G. Wen, Z. Guo, et al., “Probabilistic model-based fault-tolerant control for uncertain nonlinear systems," *IEEE Transactions on Cybernetics*, vol. 55, no. 4, pp. 1838-1847, April 2025.

2. L. Zhao, L. Wang, Y. Cao, et al., “Learning-based fault-tolerant control with high-order control barrier functions," *IEEE Transactions on Automation Science and Engineering*, vol. 22, pp. 14689-14698, 2025.

3. L. Zhao, C. Hu, S. Zhu, et al., “Safe learning for adaptive fault-tolerant control with probabilistic control barrier function," *IEEE Transactions on Automation Science and Engineering*, Under Review.

4. L. Zhao, T. Huang, and S. Wen, “Probabilistic safe control using learning-based high-order control barrier functions," *IEEE Transactions on Automatic Control*, Under Review.

Others :

5. L. Zhao and B. Li, “Adaptive fixed-time control for multiple switched coupled neural networks," *International Journal of Network Dynamics and Intelligence*, vol. 3, no. 3, pp. 100018. Sept. 2024.

6. L. Zhao, S. Wen, S. Zhu, et al., “Robust $\mathscr{H}_\infty$ pinning synchronization for multi-weighted coupled reaction-diffusion neural networks," *IEEE Transactions on Cybernetics*, vol. 53, no. 10, pp. 6549-6561, Oct. 2023.

7. L. Zhao, S. Wen, Z. Guo, et al.: Finite-time nonchattering synchronization of coupled neural networks with multi-weights, *IEEE Transactions on Network Science and Engineering*, vol. 10, no. 4, pp. 2212-2225, 1 July-Aug. 2023.

8. L. Zhao, S. Wen, C. Li, et al.: A recent survey on control for synchronization and passivity of complex networks, *IEEE Transactions on Network Science and Engineering*, vol. 9, no. 6, pp. 4235-4254, 1 Nov.-Dec. 2022.

9. L. Zhao, S. Wen, M. Xu, et al.: PID control for output synchronization of multiple output coupled complex networks, *IEEE Transactions on Network Science and Engineering*, vol. 9, no. 3, pp. 1553-1566, 1 May-June 2022.

List of Abbreviations

ACC	Adaptive Cruise Control
CBFs	Control Barrier Functions
CLFs	Control Lyapunov Functions
FTC	Fault-Tolerant Control
GPs	Gaussian Processes
HOCBFs	High-Order Control Barrier Functions
HJ	Hamilton-Jacobi
MASs	Multi-Agent Systems
MPC	Model Predictive Control
MRAC	Model Reference Adaptive Control
NNs	Neural Networks
PD	Proportional-Derivative
PID	Proportional-Integral-Derivative
QP	Quadratic Programming
RL	Reinforcement Learning
RBF	Radial Basis Function
RBFNNs	Radial Basis Function Neural Networks
UAVs	Unmanned Aerial Vehicles
UGVs	Unmanned Ground Vehicles
SOCP	Second Order Cone Programming

Table of Contents

LIST OF FIGURES

FIGURE **Page**

CHAPTER 1

INTRODUCTION

1.1 Background and Motivations

With the advancement of modern control systems, autonomous systems such as unmanned aerial vehicles (UAVs) and unmanned ground vehicles (UGVs) have been widely deployed in real-world scenarios, including exploration [1, 2] and delivery [3, 4]. These systems are expected to become a major trend in future development; however, these systems may experience unexpected faults (e.g. unknown actuator faults or failure) during real-time operation. For example, after long-term operation, both UAVs and UGVs are prone to faults: the actuating rotors of an UAV may fail due to motor degradation or propeller damage [5], while wear and tear of internal components in UGVs can lead to actuator faults [6], potentially resulting in emergency situations, such as operating with partial or degraded capabilities in unknown environments, which may ultimately lead to mission failure or environmental damage. Considering the importance of tasks such as transportation and soil data collection, it is essential to guarantee that they can safely reach a designated location (typically one

accessible to humans), even in the presence of actuator faults. In addition, model uncertainty, arising from a lack of true system knowledge, poses further risks to control performance and system safety [7]. This thesis aims to build probabilistically safe fault-tolerant control methods to guarantee both stability and safety for uncertain systems subject to unknown actuator faults in the practical environments. Figure 1.1 shows the illustration of our proposed methods in this thesis.

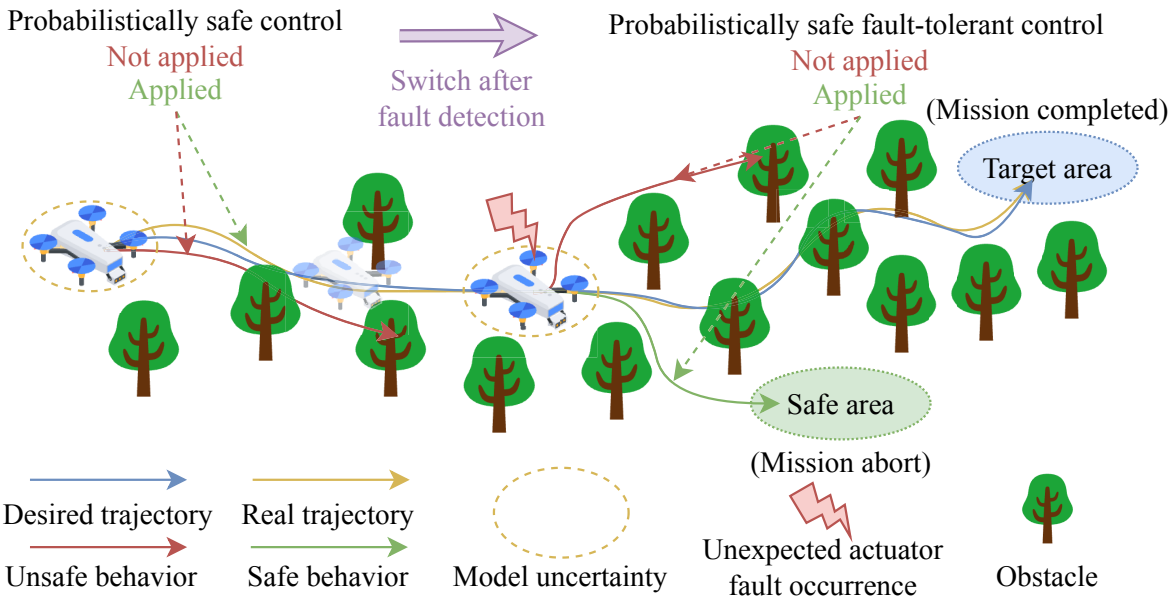

Figure 1.1: Intuitive illustration of the probabilistic safety problems through a UAV system. The blue trajectory presents a desired trajectory, while the yellow trajectory reflects the real trajectory under probabilistically safe control in the presence of model uncertainty. After the fault detection the quadrotor with model uncertainty will follow the green trajectory to reach safe area using the probabilistically safe fault-tolerant control method. Application of unsafe control input results in the red trajectory. The goal of this thesis is to present probabilistically safe fault-tolerant control method to ensure both stability and safety for uncertain systems with unexpected actuator faults.

In the context of machine learning [8], aleatoric uncertainty and epistemic uncertainty can be seen as two different sources of model uncertainty. Aleatoric uncertainty arises from inherent randomness or noise within the system, but epistemic uncertainty is caused by a lack of knowledge, such as insufficient or unrepresentative training data.

From the viewpoint of control theory, model uncertainty is modelled as additive model uncertainty and bias model uncertainty. To mitigate the influence of model uncertainty for control performance, prior studies have explored both robust control [9] and adaptive control [10]. In robust control, model uncertainty is typically assumed to satisfy a norm-bounded condition, and the controller is designed based on the upper bound, such as $\mathscr{H}_\infty$ control. In contrast, adaptive control methods aim to approximate or estimate model uncertainty using online adaptive laws or parameter estimation strategies. Their theoretical results are generally established through Lyapunov-based stability analysis. However, in above two methods, robust control considers the worst-case scenario for controller design, while adaptive control relies heavily on accurate output measurements and designed adaptation laws. In practical applications, robust control tends to be more conservative and may incur higher performance costs, particularly when uncertainty bounds are overestimated. Although adaptive control can estimate model uncertainty but its effectiveness is limited by sensor noise or measurement inaccuracies. To handle these issues, researchers have explored Gaussian Processes (GPs) to build probabilistic models for learning uncertain system dynamics [11]. Unlike robust and adaptive control methods, GP regression provides a distribution over possible functions to represent model uncertainty, which offers better robustness and performance against observation noise and imperfect measurements.

For handling actuator faults, researchers have explored the fault-tolerant control (FTC) methods aimed at maintaining system functionality [12, 13]. From the viewpoint of control theory, actuator faults are typically modelled as actuator gain faults and an actuator bias faults [14]. The former reduces the effectiveness of the control input, thereby degrading overall control performance, while the latter introduces a constant offset to the applied control signal. Since the performance of FTC depends on an accurate system model, robust FTC [15] and adaptive FTC [16] have been proposed to address uncertain

systems subject to unknown actuator faults. However, the above methods [15, 16] are still limited by sensor noise and measurement inaccuracies, which can degrade estimation and control performance. To address this, a few researchers have further explored GP-based FTC methods to handle both model uncertainty and unknown actuator faults [17], with the goal of designing controllers based on probabilistic system models. Although the above FTC methods are designed to actuator faults and model uncertainty, they do not provide formal safety guarantees for systems during real-time operation. Ensuring the safety of faulty systems is essential for mitigating potential risks to surrounding systems in practical deployment scenarios.

To guarantee system safety, researchers have developed various safety-critical control methods, including control barrier functions (CBFs) [18], Hamilton-Jacobi (HJ) reachability analysis [19], and safe reinforcement learning (RL) [20]. Unlike HJ reachability and safe RL, CBFs enforce forward invariance of safe sets, thereby providing rigorous safety guarantees for control systems. They have been widely applied in robotics, particularly in legged robots [21]. Researchers have further developed high-order CBFs (HOCBFs), which extend CBFs to systems with high relative degrees [22]. However, both CBFs and HOCBFs rely heavily on accurate system models, and their effectiveness can be influenced and even destroyed under model uncertainty. Although researchers have proposed robust adaptive CBFs, RL-based CBFs, and learning-based HOCBFs [23], these methods still struggle to address aleatoric and epistemic uncertainties effectively. Consequently, few studies have explored GP-based CBFs [24] and GP-based HOCBFs [25], which aim to enable probabilistic safety for uncertain systems. Since unknown actuator faults alter system dynamics, existing CBF and HOCBF methods cannot effectively handle such faults. Research on fault-tolerant CBFs and HOCBFs remains at an early stage and limited in scope. Although the mathematical formulations of model uncertainty and actuator faults share similarities, actuator faults are

random and unexpected, often lacking effective training data. Moreover, actuator gain faults and bias faults pose distinct challenges for the design of CBF- and HOCBF-based controllers. A few recent studies have proposed fault-tolerant CBFs [26] and HOCBFs [27] to ensure safety under unknown actuator bias faults, but these methods still face difficulties in addressing actuator gain faults as well as underlying model uncertainty.

Therefore, addressing model uncertainty is essential to ensuring the stability and safety of autonomous systems, particularly in the presence of unknown actuator faults. In practical applications, model-based control design often relies on nominal or imprecise models, which limits control performance. In contrast to worst-case analysis and deterministic estimation approaches, probabilistic system models provide a more effective way to handle model uncertainty. Moreover, developing FTC strategies is critical for autonomous systems to maintain system functionality under unknown actuator faults. In conclusion, this thesis aims to propose probabilistically safe FTC methods by integrating CBFs and GP regression into the FTC framework.

1.2 Research Questions and Objectives

1.2.1 Research Questions

The challenges of model uncertainty and unknown actuator faults remain largely open problems in the field. This thesis focuses on the following research questions:

RESEARCH QUESTION 1 (RQ1): *How to handle model uncertainty, compensate for unknown actuator bias faults, and ensure stability of systems?*

Model uncertainty is a fundamental challenge in control system design, typically categorized into aleatoric uncertainty, arising from inherent randomness, and epistemic uncertainty, caused by incomplete system knowledge. Robust control methods handle

these uncertainties using fixed upper bounds, but this often leads to overly conservative performance. While adaptive control can reduce conservatism through online estimation, it heavily depends on measurement accuracy and may converge to incorrect estimates under noisy observations. These limitations become more severe when unknown actuator bias faults occur. To handle bias faults, one can increase the fixed upper bound, but this leads to even more conservative results. Although adaptive fault estimators can mitigate bias faults, their design still relies on accurate system models. As a result, the combined effects of uncertainty and faults can not only hinder the performance of uncertainty-aware control methods but also influence system stability.

RESEARCH QUESTION 2 (RQ2): *How to guarantee the safety of uncertain systems with unknown actuator bias faults?*

Although existing FTC methods such as reconfigurable and adaptive FTC can mitigate the influence of unknown actuator bias faults, they mainly focus on maintaining system functionality after fault detection rather than ensuring safety. Consequently, traditional FTC frameworks often fail to guarantee safety and may expose the system to additional risks. The challenge becomes even greater in uncertain systems, where model mismatches interact with actuator bias faults and make safety constraints difficult to satisfy. These limitations raise the research question of how to design a fault-tolerant control framework with explicit safety guarantees that can handle unknown actuator bias faults under model uncertainty.

RESEARCH QUESTION 3 (RQ3): *How to address unknown actuator gain faults and guarantee the safety of uncertain systems?*

Compared with actuator bias faults, actuator gain faults present more severe challenges for safety-critical control design. A gain fault scales the control input by unknown and time-varying factors, which reduces control effectiveness and may render safety constraints infeasible. This problem becomes even harder when gain faults interact with

model uncertainty, as both effects distort the system dynamics and invalidate fixed robustness margins. These challenges raise the central research question: how to design a safe control framework that can compensate for unknown actuator gain faults and still guarantee provable safety in uncertain systems.

RESEARCH QUESTION 4 (RQ4): *How to model unknown drift and gain dynamics and ensure system safety under unknown actuator bias faults?*

In practical applications, autonomous systems are affected by both drift and gain uncertainties, which pose significant challenges for the design of model-based controllers. Existing approaches often attempt to estimate or approximate these unknown dynamics using estimation techniques or data-driven methods. However, such methods face difficulties when dealing with high-dimensional systems and often lack rigorous theoretical guarantees. When unknown actuator bias faults are also present, the performance of these uncertainty-aware learning approaches can be further degraded. These limitations raise the open question of how to effectively model unknown drift and gain dynamics in a way that enables reliable and safe fault-tolerant control.

1.2.2 Research Objectives

To answer these research questions, we provide the following Research Objectives (ROs):

RESEARCH OBJECTIVE 1 (RO1): *To develop learning-based adaptive FTC methods using GP regression.* (Aims to answer RQ1)

This thesis uses the GP regression to model the unknown system dynamics. Compared to adaptive estimation or robust control techniques, GP regression aims to build a probabilistic model and can effectively reduce the influences of aleatoric uncertainty and epistemic uncertainty. Considering that the quality and quantity of training data can impact the performance GP regression, this research respectively discusses two

cases of offline learning and event-triggered learning strategies for GPs and investigates the non-ignorable computational time. Furthermore, to compensate for unknown actuator bias faults, an adaptive FTC approach is presented. The proposed learning-based adaptive FTC methods can effectively address the unknown system dynamics and actuator bias faults and ensure the probabilistic stability of systems.

RESEARCH OBJECTIVE 2 (RO2): *To propose a GP-based safe FTC method by integrating HOCBFs into FTC frameworks.* (Aims to answer RQ2)

To ensure the safety of uncertain systems subject to unknown actuator bias faults, this thesis proposes a learning-based safe FTC method that integrates HOCBFs and GP regression into fault-tolerant control frameworks. Existing studies on fault-tolerant HOCBFs are limited, and these methods fail to remain effective under unknown actuator bias faults. To overcome this limitation, we design a novel fault-tolerant HOCBF formulation that achieves improved robustness against actuator unknown bias faults. Moreover, since HOCBF constraints typically involve uncertain system dynamics that are difficult to model explicitly, we directly use GP to fit uncertain terms with scalar dimension in the HOCBF constraint, thereby reducing the learning complexity while retaining safety guarantees. To ensure system stability, GP-based control Lyapunov functions (CLFs) are constructed to provide probabilistic stability guarantees for uncertain systems affected by unknown actuator bias faults.

RESEARCH OBJECTIVE 3 (RO3): *To build safe learning-based adaptive FTC methods based on GP regression and online estimation.* (Aims to answer RQ3)

In addition to considering actuator bias faults, this thesis further explores the influence of actuator gain faults on uncertain systems. To address these issues, an online estimator is designed to estimate gain fault parameters, and a probabilistic system model is provided using GP regression. Furthermore, this research integrates online estimation and GP regression into a CBF framework to guarantee system safety, extending the

approach to HOCBFs to handle systems with high relative degrees. In particular, the thesis investigates the effect of different initial estimation values on the performance of CBFs and HOCBFs. Unlike existing methods on robust safe HOCBFs, adaptive safety-critical control methods are proposed to deal with actuator gain faults.

RESEARCH OBJECTIVE 4 (RO4): *To propose a probabilistically safe FTC method using novel compound kernel methods and HOCBFs* (Aims to answer RQ4)

In practical applications, model uncertainty affects not only the drift dynamics but also the gain dynamics, posing additional challenges for system modelling and the design of HOCBFs. Although a few researchers have proposed GP-based HOCBF methods using affine dot product kernels, such approaches often lack feasibility and encounter difficulties in practical applications, such as mobile robotic systems. Considering these limitations, this thesis proposes a novel compound kernel method for GP regression to jointly address drift and gain uncertainties. Furthermore, a probabilistically safe FTC method is developed to deal with actuator bias faults by integrating the proposed GP regression approach into the HOCBF framework.

1.3 Research Contributions

This thesis aims to propose novel probabilistically safe FTC approaches to address model uncertainty and unknown actuator faults, developing reliable and adaptive control frameworks to overcome these challenges. The key contributions of this thesis are summarized as follows:

1) A novel online learning-based FTC method to handle faults and uncertainty

- This thesis proposes two probabilistic model-based adaptive FTC methods by integrating the GP regression technique into the adaptive FTC method. Compared with existing results on GP-based control [28–36], our approaches explicitly con-

sider non-ignored computational delays during real-time predictions. To explore GP-based control performance, two types of sampling methods are studies: offline training data collection and event-triggered online strategies.

- Four theoretical criteria are established to guarantee probabilistic stability for closed-loop systems. Additionally, this research derives probabilistic tracking error bounds with upper computational delay bounds and the event-triggered condition to ensure the convergence of tracking errors. Unlike the existing works on event-triggered sampling strategies for GP regression [28, 29, 36], a less conservative event-triggered condition is developed.

- Three numerical examples are conducted to show the effectiveness and competitiveness of our control methods. Comparison results demonstrate the importance of data efficiency and exhibit the competitive performance of proposed control methods compared to the neural network-based finite-time adaptive FTC method and the event-triggered GP-based online learning strategy.

2) A novel safe FTC method to guarantee both stability and safety of uncertain systems with actuator bias faults

- This thesis proposes a novel probabilistically fault-tolerant CLF-HOCBF method that integrates GP regression and HOCBFs into FTC methods. Compared to existing works on GP-based CBFs [34, 37] and HOCBFs [25, 38], our approach extends their applicability to cases involving unknown actuation bias faults.

- To address model uncertainty, GP regression is employed to construct GP-based CLF and HOCBF constraints. Based on these formulations, two design criteria are developed to support the controller design.

- Building on these criteria, two theoretical conditions are further derived to formally guarantee the effectiveness of the fault-tolerant GP-CLF-HOCBF method, ensuring stability and safety with high probability during control operation.

3) A novel adaptive safe control method to handle actuator gain faults

- This thesis proposes probabilistically and adaptively safe control frameworks that integrate GP regression and adaptive fault estimation into CBF and HOCBF constraints. Compared to [25–27, 34], our methods effectively address cases involving both model uncertainty and unknown actuator gain faults.

- A theoretical condition is derived to guarantee unknown actuator gain faults estimation, and four probabilistic conditions are established to guarantee the safety of uncertain faulty systems with high probability.

- Two simulation case studies validate the effectiveness and competitiveness of the proposed methods against existing approaches.

4) A novel probabilistically safe control method to address drift and gain uncertainties

- Compared to existing works on GP-based CBFs [34, 39] and HOCBFs [25, 38], this thesis proposes a novel compound kernel to model uncertain terms arising from model uncertainty in the HOCBF constraint, enabling a more flexible and general GP-based modelling strategy.

- Leveraging this strategy, an EGPBarrier method is developed to guarantee probabilistic safety guarantees for systems with model uncertainty. Moreover, three theoretical conditions are derived to ensure the feasibility of the proposed con-

trol formulation. To address the actuator bias faults, this research integrates the EGPBarrier method into the FTC framework.

1.4 Research Significance

The theoretical and practical significance of this thesis is organized as follows:

Theoretical significane: This research investigates the theoretical challenges posed by model uncertainty and unknown actuator faults in autonomous systems. These challenges, particularly those arising from drift and gain uncertainties, significantly hinder the effectiveness and reliability of existing robust and adaptive FTC methods.

To tackle the above challenges, this research builds upon a class of learning-based safe FTC control approaches that incorporate GP regression for modelling uncertain system dynamics. By constructing a probabilistic system model, the proposed method improves robustness against observation noise and imperfect measurements, thereby enabling more reliable FTC design. In particular, a novel compound kernel is introduced to jointly capture both drift and gain uncertainties, extending the current works on GP-based CBFs and HOCBFs. Furthermore, this thesis explores the integration of CBF-based safety constraints into FTC frameworks, formulating a unified strategy that ensures system stability and safety in the presence of unknown actuator faults. Both actuator gain and bias faults are considered and analyzed their challenges on the feasibility and design of CBFs and HOCBFs. Overall, this research establishes a solid foundation for safe and adaptive FTC methods and offers research directions for dealing with the issues of model uncertainty and unknown actuator faults.

Practical significane:

The contributions of this thesis hold significant practical value for real-world autonomous systems. By integrating GP regression and CBFs into FTC frameworks, this

research develops effective learning-based control strategies that enhance the stability and safety of uncertain systems. The proposed methods are validated through two representative applications: an adaptive cruise control (ACC) system and a mobile robotic system, demonstrating competitiveness compared with existing approaches. Furthermore, to assess real-time implementability and practicality, a virtual vehicular platform is constructed using the CARLA simulator. Extensive simulations under various conditions, including model uncertainty and actuator faults, verify the robustness, feasibility, and reliability of the proposed approaches. Overall, this research provides practical and generalizable learning-based FTC strategies with probabilistic safety guarantees for autonomous systems subject to actuator faults operating in uncertain environments.

1.5 Thesis Structure

Building on the above discussion, we organize the following chapters, and the structure of this thesis is outlined through the following chapters, as illustrated in Figure 1.2.

- **CHAPTER 2**: This chapter provides a comprehensive literature review that forms the foundation for the subsequent research in this thesis. It begins with an introduction to GP regression, including its basic definition and existing studies on GP-based control methods. Then, it discusses the formulation of two types of actuator faults, namely gain and bias faults, and outlines the concepts of passive FTC and active FTC. Within this context, existing work on adaptive FTC methods is analyzed. Finally, it reviews the definitions of CBFs and HOCBFs and introduces more existing work on uncertainty-aware CBFs and HOCBFs.

- **CHAPTER 3**: This chapter proposes two types of learning-based adaptive FTC methods using GP regression, with the goal of ensuring the stability of uncertain systems under actuator bias faults. GP regression is used to model the unknown

system dynamics and provide predictions, which are integrated into an adaptive FTC framework to handle both model uncertainty and actuator bias faults. Considering the computational complexity of GP regression, this chapter also examines the case where the computational cost during operation is non-ignorable. In addition, an event-triggered online learning strategy is introduced to study the effect of data efficiency on GP regression. Based on these results, two theoretical conditions are derived to ensure the closed-loop stability of uncertain systems. Experimental results on a pendulum system show the effectiveness and competitiveness of the proposed methods in comparison with existing approaches. This chapter addresses RQ1 and meets RO1.

- **CHAPTER 4**: This chapter proposes a GP-based safe FTC method that incorporates GP regression and HOCBFs into the FTC framework. The goal is to ensure both stability and safety of uncertain systems subject to actuator bias faults. GP regression is used to model an uncertain term in HOCBF constraint and to formulate a probabilistic HOCBF approach. In addition, a GP-based CLF approach is developed to ensure the stability of uncertain systems. To handle actuator bias faults, the FTC strategy is embedded within the GP-CLF and GP-HOCBF constraints. Two theoretical conditions are derived to ensure probabilistic stability and safety of uncertain systems under actuator bias faults. Numerical examples are conducted on an ACC system using the CARLA simulator to validate the effectiveness of the proposed methods. This chapter addresses RQ2 and meets RO2.

- **CHAPTER 5**: This chapter proposes learning-based safe FTC methods. The goal is to ensure probabilistic safety of uncertain systems subject to actuator gain faults. Unlike actuator bias faults, actuator gain faults directly affect the control input and can significantly degrade system performance. To address this challenge, an online estimator is developed to estimate faulty parameters, and a suf-

ficient condition is derived to ensure its stability. In addition, a probabilistic CBF constraint is formulated, and this approach is further extended to the HOCBF framework. Two theoretical conditions are established to ensure the feasibility of the proposed methods. Experimental results on an ACC system and a mobile robotic system demonstrate the effectiveness of the proposed methods in comparison with existing approaches. This chapter addresses RQ3 and meets RO3.

- **CHAPTER 6**: This chapter proposes probabilistically safe FTC methods, aiming to ensure the safety of faulty systems under drift and gain uncertainties. Existing GP-based HOCBF methods often face feasibility issues and encounter difficulties when applied to robotic systems with high relative degrees. To address these issues, a novel compound kernel is designed to jointly model the unknown drift and gain dynamics. Based on this kernel, a probabilistic HOCBF approach is formulated, and three theoretical conditions are derived to ensure its feasibility. The method is then extended to accommodate actuator bias faults. Numerical examples on an ACC system and a mobile robotic system demonstrate the effectiveness and competitiveness of the proposed methods in comparison with existing approaches. This chapter addresses RQ4 and meets RO4.

- **CHAPTER 7**: In the chapter, we conclude this thesis and discuss the potential directions for future research.

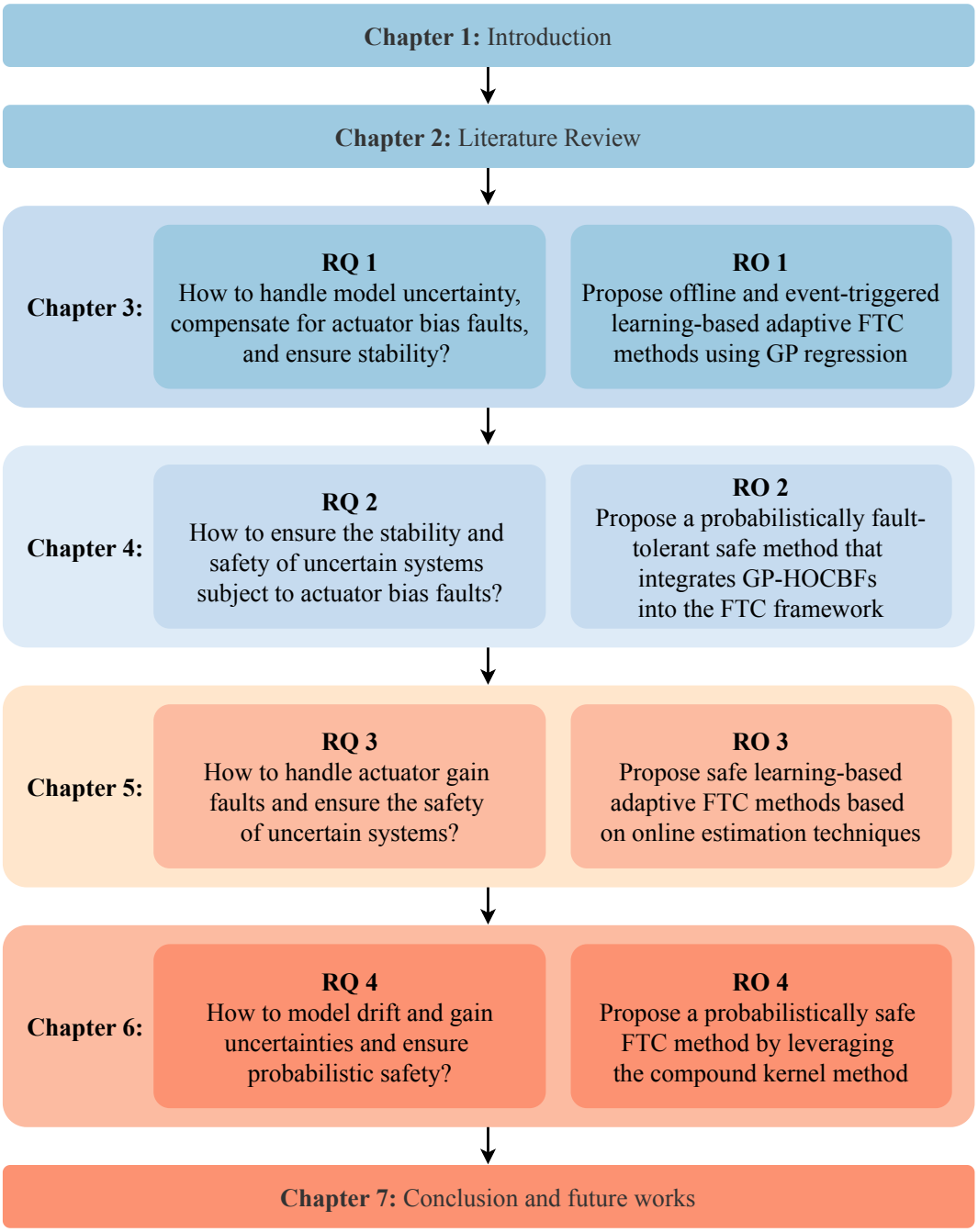

Figure 1.2: The structure of this thesis.

CHAPTER 2

LITERATURE REVIEW

This chapter provides a comprehensive survey of the literature related to this research and necessary fundamental concepts, and its structure is illustrated in Figure 2.1. Section 2.1 introduces the definition of GPs, particularly for use in regression, and further discusses the different structures of kernels. Then, Section 2.2 considers the problems of unknown actuator faults and the fundamental concepts of FTC, along with a review of recent developments in adaptive FTC methods. Finally, Sections 2.3 and 2.4 provide the definitions of CBFs and HOCBFs, discussing review recent literature on uncertainty-aware CBFs and HOCBFs.

2.1 Gaussian Processes

For learning unknown functions, there exist many ways, such as online estimation [40] and neural networks (NNs) [41], but one particularly elegant way is by probabilistic inference [42]. As a kernel method, GPs can capture many types of statistical structures, such as symmetries, periodicity, and additivity, which can be encoded through kernels selected by experts. In this section, we focus on fundamental concepts of GPs and the

structure of kernels, along with recent literature on GP-based control methods for ensuring stability.

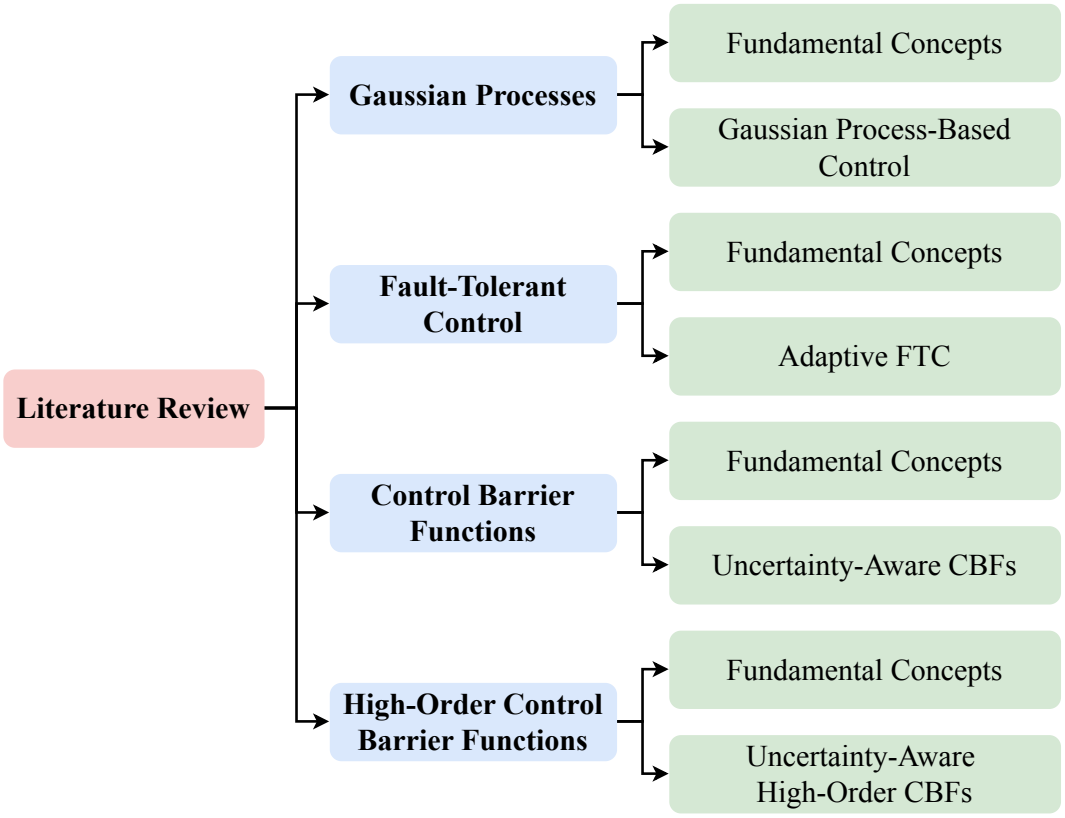

Figure 2.1: Structure of literature review.

2.1.1 Fundamental Concepts

Gaussian process (GP) regression serves as an effective machine learning technique for prediction tasks, especially in scenarios involving uncertainty. From a conceptual standpoint, a GP characterizes a probability distribution over functions, enabling inference to be conducted directly within the function space. This leads naturally to the formal definition presented below:

Definition 2.1.1 (Gaussian process [11])**.** *A GP is a collection of random variables, any finite number of which have a joint Gaussian distribution.*

For a GP model $f(\boldsymbol{x}) : \mathbb{R}^n \to \mathbb{R}$, the function is characterized by a mean function $m(\boldsymbol{x}) = \mathbb{E}[f(\boldsymbol{x})]$ and a covariance function $k(\boldsymbol{x}, \boldsymbol{x}') = \mathbb{E}[(f(\boldsymbol{x}) - m(\boldsymbol{x}))(f(\boldsymbol{x}') - m(\boldsymbol{x}'))]$. The process is thus expressed as $f(\boldsymbol{x}) \sim \mathcal{GP}(m(\boldsymbol{x}), k(\boldsymbol{x}, \boldsymbol{x}'))$. In practical scenarios, the function values are not directly observable; instead, one obtains noisy measurements $y_i = s(\boldsymbol{x}_i) + \varepsilon$, where the noise $\varepsilon \sim (0, \sigma_n^2)$. Given the training data $\boldsymbol{x}_i \in \mathbb{R}^n$ and corresponding output $y_i \in \mathbb{R}$, a training dataset is formed as $\mathcal{D}_{\text{train}} = \{\boldsymbol{x}_i, y_i\}_{i=1}^N$, with $X = \{\boldsymbol{x}_1, \cdots, \boldsymbol{x}_N\} \in \mathbb{R}^{n \times N}$ and $\boldsymbol{y} = \{y_1, \cdots, y_N\} \in \mathbb{R}^N$.

The joint Gaussian distribution over the training outputs $\boldsymbol{y}$ and test output $f^\star$ can be written as follows:

$$\begin{bmatrix} \boldsymbol{y} \\ f^\star \end{bmatrix} \sim \mathcal{N}\left(\begin{bmatrix} \boldsymbol{m} \\ f^\star \end{bmatrix}, \begin{bmatrix} K(X,X) + \sigma_n^2 I & K(X, \boldsymbol{x}^\star) \\ K(\boldsymbol{x}^\star, X) & k^\star \end{bmatrix} \right), \tag{2.1}$$

where $\boldsymbol{m} = [m(z_1), \cdots, m(z_N)]^\top \in \mathbb{R}^N$. $K(\boldsymbol{x}^\star, X) = [k(\boldsymbol{x}^\star, \boldsymbol{x}_1), \cdots, k(\boldsymbol{x}^\star, \boldsymbol{x}_N)] \in \mathbb{R}^{1 \times N}$ stands for covariance matrix between $\boldsymbol{x}^\star$ and X with $K(X, \boldsymbol{x}^\star) = K(\boldsymbol{x}^\star, X)^\top \in \mathbb{R}^N$. Function $k^\star = k(\boldsymbol{x}^\star, \boldsymbol{x}^\star) \in \mathbb{R}$. Matrix $K(X,X) \in \mathbb{R}^{N \times N}$ has entries defined by $[K(X,X)]_{ij} = k(\boldsymbol{x}_i, \boldsymbol{x}_j)$.

Based on the properties of multivariate Gaussian distributions, the conditional distribution of the test output given the training data and the test input is also Gaussian:

$$f^\star | X, \boldsymbol{y}, x^\star \sim \mathcal{N}\left(m(\boldsymbol{x}^\star), \mathrm{Cov}(x^\star)\right), \tag{2.2}$$

where the predictive mean and variance are given by

$$\begin{aligned} \bar{f}_\star &= \mathbb{E}[f^\star | X, \boldsymbol{y}, x^\star] = K(\boldsymbol{x}^\star, X)\left[K(X,X) + \sigma_n^2 I\right]^{-1} \boldsymbol{y}, \\ \mathbb{V}[x^\star] &= K(\boldsymbol{x}^\star, \boldsymbol{x}^\star) - K(\boldsymbol{x}^\star, X)\left[K(X,X) + \sigma_n^2 I\right]^{-1} K(X, \boldsymbol{x}^\star). \end{aligned} \tag{2.3}$$

Then, one has the following assumption and lemma:

Assumption 2.1.1 (Kernel Capacity [29, 43])**.** *The function $f(\cdot)$ has a bounded reproducing kernel Hilbert space norm with respect to a covariance function kernel $k(\cdot,\cdot)$, and a known upper bound $0 < B_f \in \mathbb{R}$ satisfies $\|f(\cdot)\|_k^2 \leqslant B_f$.*

Lemma 2.1.1 (Probabilistic Bound [43, 44])**.** *Suppose that Assumption 2.1.1 holds and there exists a compact set* $\mathbb{X} \subset \mathbb{R}^n$*, then*

$$\Pr\left\{|m(\boldsymbol{x}) - f(\boldsymbol{x})| \leqslant \psi \mathrm{Cov}(\boldsymbol{x}), \forall \boldsymbol{x} \in \mathbb{X}\right\} \geqslant 1 - \varrho \tag{2.4}$$

for any probability $\varrho \in (0,1)$*, parameters* $\psi = \sqrt{2B_f + 300\gamma \ln^3\left(\frac{N+1}{\varrho}\right)}$ *and the maximum information gain* $\gamma = \max_{\boldsymbol{x} \in \mathbb{X}} \frac{1}{2}\log\left(\det\left(I + \sigma_n^{-2}K(\boldsymbol{x},\boldsymbol{x}')\right)\right)$ *with* $\boldsymbol{x},\boldsymbol{x}' \in \{\boldsymbol{x}^{[1]}, \cdots, \boldsymbol{x}^{N+1}\}$.

Since the GPs belong to a kernel method, one introduces a commonly used kernels: the squared-exponential (SE) kernel with noisy observations

$$k(x,x') = \sigma_f^2 \exp\left(-\frac{(x-x')^2}{2l^2}\right) + \sigma_n^2 \delta_{ij}, \tag{2.5}$$

where l stands for length-scale, σ_f^2 represents the signal variance, and δ_{ij} refers to a Kronecker delta which is one if $i = j$ and zero otherwise. These quantities are collectively referred to as hyperparameters. The predictive capability of GP is closely influenced by these hyperparameters. The SE kernel, also commonly known as the radial basis function (RBF) kernel, is frequently used in practice.

As a simple illustrative case, consider the one-dimensional function $f(x) = x\sin(x)$ with noisy measurements given by $y_i = f(x_i) + \varepsilon$ with $\varepsilon \sim \mathcal{N}(0, 0.25)$.

The corresponding simulation outcomes are depicted in Figure 2.2. Based on the same signal variance $\sigma_f^2 = 1$ in Figures 2.2(a) and 2.2(b), increasing the length-scale l leads to enhanced regression accuracy. Moreover, as depicted in Figures 2.2(b) and 2.2(c), a higher signal variance improves the predictive performance of the GP model. Notably, among all configurations, Figure 2.2(d) achieves the best regression performance, which can be attributed to the use of an optimally selected set of hyperparameters, outperforming the cases shown in Figures 2.2(a) and 2.2(c).

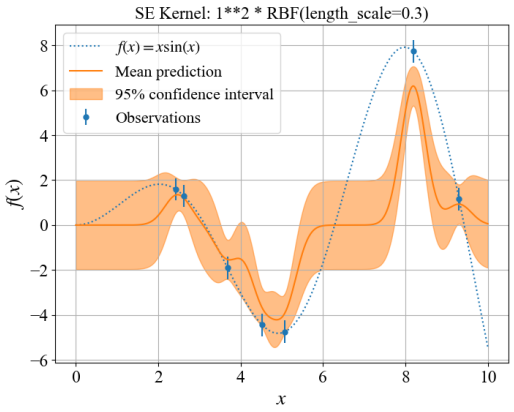

(a) $l = 0.3$ and $\sigma_f = 1$.

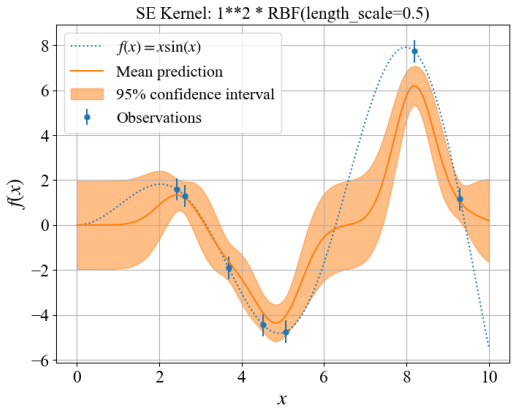

(b) $l = 0.5$ and $\sigma_f = 1$.

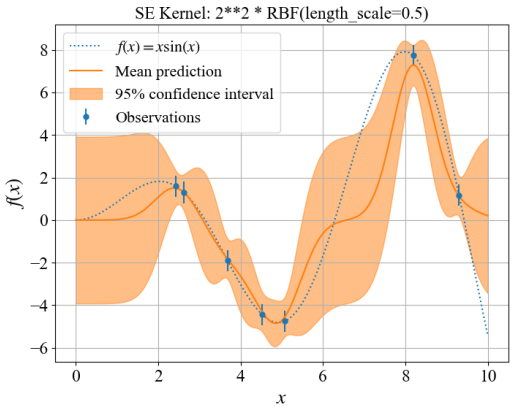

(c) $l = 0.5$ and $\sigma_f = 2$.

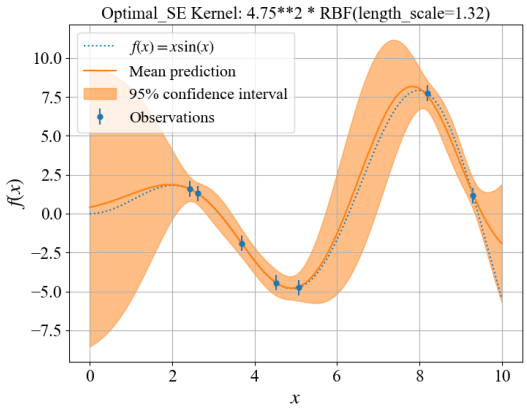

(d) $l = 1.32$ and $\sigma_f = 4.75$.

Figure 2.2: Profiles of SE kernel with different hyperparamters.

Therefore, one concludes that the optimizated hyperparameters can enhance the performance of GP regression. To optimize the hyperparameters, the log marginal likelihood conditioned on the parameters of the covariance function $\boldsymbol{\theta} = (l, \sigma_f, \sigma_n)$ can be computed as

$$\log p(\boldsymbol{y}|X,\boldsymbol{\theta}) = -\frac{1}{2}\boldsymbol{y}^\top \left(K + \sigma_n^2 I\right)^{-1} \boldsymbol{y} - \frac{1}{2}\log\left|K + \sigma_n^2 I\right| - \frac{1}{2}\log 2\pi. \tag{2.6}$$

Furthermore, the selection of the kernel function plays a crucial role in determining the effectiveness of GP regression when approximating an unknown target function.

To demonstrate this effect, two distinct kernels are employed: the SE kernel (2.5), and the periodic kernel given by $\sigma_f^2 \exp(-\frac{2}{l^2}\sin^2(\pi\frac{x-x'}{p}))$ also known as the Exp-Sine-Squared kernel. These kernels are used to fit the one-dimensional function $f(x) = \sin^2(x) - \cos^2(x)$ and its observations $y_i = f(x_i) + \varepsilon$ with $\varepsilon \sim \mathcal{N}(0, 0.01)$. As illustrated in Figure 2.3(a), even though the hyperparameters are optimized using the marginal likelihood method (2.6), the GP model using the periodic kernel yields more accurate predictions than the SE kernel case shown in Figure 2.3(b).

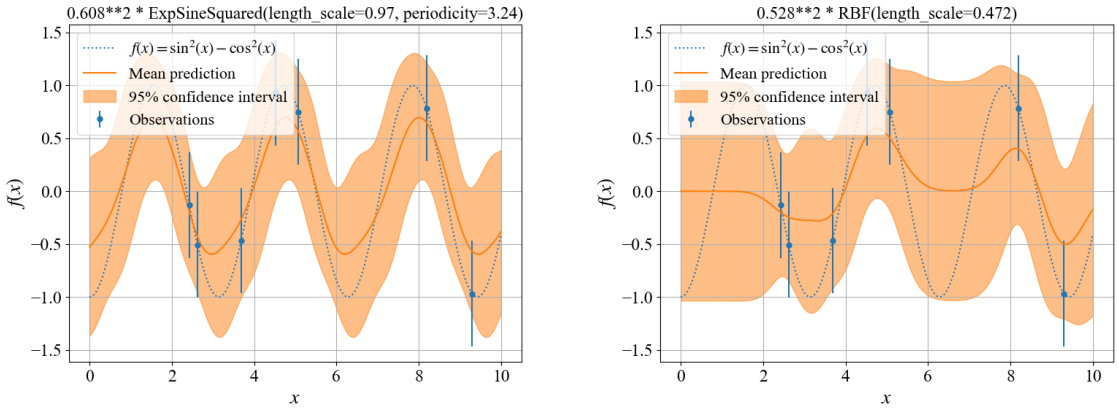

(a) Periodic kernel. (b) SE kernel.

Figure 2.3: Profiles of two different kernels.

To fit different structures of unknown functions, it is possible to build a “made to order" kernel with the desired properties. Given this, this subsection further discusses two combining kernel: addition and multiplication by a known function. To begin with, the additive formulation can be written as $f(\boldsymbol{x}) = f_\beta(\boldsymbol{x}) + f_\gamma(\boldsymbol{x})$. Assume functions f_β and f_γ are independently and satisfy $f_\beta \sim \mathcal{GP}(m_\beta, k_\beta)$ and $f_\gamma \sim \mathcal{GP}(m_\gamma, k_\gamma)$. In this case, their sum also yields a GP, and the resulting distribution is given by:

$$f_\beta + f_\gamma \sim \mathcal{GP}(m_\beta + m_\gamma, k_\beta + k_\gamma),$$

where kernels f_β and f_γ can be chosen different types.

The noisy observations $y_i = f_\beta(\boldsymbol{x}_i) + f_\gamma(\boldsymbol{x}_i) + \varepsilon$, where $\varepsilon \sim (0, \sigma_n^2)$. Denote $\mathscr{D} = \{\boldsymbol{x}_i, y_i\}_{i=1}^N$ and assume the functions f_β and f_γ are a prior independent, then the joint distribution can be written as follows:

$$\begin{bmatrix} \boldsymbol{y} \\ f_\beta^\star + f_\gamma^\star \\ f_\beta^\star \\ f_\gamma^\star \end{bmatrix} \sim \mathcal{N} \begin{bmatrix} K_\beta + K_\gamma + \sigma_n^2 I & K_\beta^\star + K_\gamma^\star & K_\beta^\star & K_\gamma^\star \\ (K_\beta^\star + K_\gamma^\star)^\top & k_\beta^{\star\star} + k_\gamma^{\star\star} & k_\beta^{\star\star} & 0 \\ (K_\beta^\star)^\top & k_\beta^{\star\star} & k_\beta^{\star\star} & k_\gamma^{\star\star} \\ (K_\gamma^\star)^\top & 0 & k_\gamma^{\star\star} & k_\gamma^{\star\star} \end{bmatrix}. \tag{2.7}$$

where $K_i = K_i(X, X) \in \mathbb{R}^{N\times N}$, $K_i^\star = K_i(X, \boldsymbol{x}^\star) \in \mathbb{R}^N$, and $k_i^{\star\star} = k_i(\boldsymbol{x}^\star, \boldsymbol{x}^\star) \in \mathbb{R}$.

As a result, the essential predictive formulations for GP regression are as follows:

$$\begin{aligned} f_\beta(\boldsymbol{x}^\star)|\boldsymbol{y} &\sim \mathcal{N}\left((K_\beta^\star)^\top K_{\text{sum}}^{-1}\boldsymbol{y},\ k_\beta^{\star\star} - (K_\beta^\star)^\top K_{\text{sum}}^{-1} K_\beta^\star\right), \\ f_\gamma(\boldsymbol{x}^\star)|\boldsymbol{y} &\sim \mathcal{N}\left((K_\gamma^\star)^\top K_{\text{sum}}^{-1}\boldsymbol{y},\ k_\gamma^{\star\star} - (K_\gamma^\star)^\top K_{\text{sum}}^{-1} K_\gamma^\star\right), \end{aligned} \tag{2.8}$$

where $K_{\text{sum}} = K_\beta + K_\gamma + \sigma_n^2 I$.

Furthermore, an unknown function $f(\boldsymbol{x})$ can also be modelled by any fixed known function $\xi(\boldsymbol{x})$ as well as an known function $q(\boldsymbol{x}) \sim \mathcal{GP}(0, k(\boldsymbol{x}, \boldsymbol{x}'))$, one has

$$f(\boldsymbol{x}) = \xi(\boldsymbol{x}) q(\boldsymbol{x}), \quad f(\boldsymbol{x}) \sim (0, \xi(\boldsymbol{x}) k(\boldsymbol{x}, \boldsymbol{x}') \xi(\boldsymbol{x}')), \tag{2.9}$$

then noisy observations $y_i = \xi(\boldsymbol{x}_i) q(\boldsymbol{x}_i) + \varepsilon$ and the joint distribution can be obtained as:

$$\begin{bmatrix} \boldsymbol{y} \\ f^\star \end{bmatrix} = \begin{bmatrix} \Xi(X) K(X, X) \Xi(X) + \sigma_n^2 I & \Xi(X) K(X, \boldsymbol{x}^\star) \\ K(\boldsymbol{x}^\star, X) \Xi(X) & k^\star \end{bmatrix}, \tag{2.10}$$

where $\Xi(X) = \text{diag}[\xi(\boldsymbol{x})_1, \xi(\boldsymbol{x})_2, \cdots, \xi(\boldsymbol{x})_N)] \in \mathbb{R}^{N\times N}$.

Consequently, the fundamental equations governing GP prediction are given below:

$$f(\boldsymbol{x}^\star)|\boldsymbol{y} \sim \mathcal{N}\left(K_\Xi K_{\text{multi}}^{-1}\boldsymbol{y},\ k(\boldsymbol{x}^\star, \boldsymbol{x}^\star) - K_\Xi K_{\text{multi}}^{-1} K_\Xi^\top\right). \tag{2.11}$$

where $K_\Xi = K(\boldsymbol{x}^\star, X)\Xi(X)$ and $K_{\text{multi}} = \Xi(X) K(X, X) \Xi(X) + \sigma_n^2 I$.

2.1.2 Gaussian Process-Based Stabilizing Controller

Owing to the strong modelling capabilities of GP regression, many researchers have investigated its integration with various control strategies, such as GP-based feedback control [45–48], GP-based adaptive control [49–51], and GP-based model predictive control (MPC) [52–54]. For instance, as discussed in [45], Lederer et al. established a uniform error bound under relaxed assumptions to improve the approximation performance of GP regression, and analyzed the stability of probabilistic models under a feedback control framework. In [47], Umlauft et al. proposed a control approach based on differential dynamic programming to solve optimal control problems in uncertain systems modelled via GP regression. Departing from the conventional construction of probabilistic system models, Castañeda et al. [48] developed a probabilistic constraint formulation for control Lyapunov functions by embedding an affine dot product kernel within the GP regression process. In the context of adaptive control, Chowdhary et al. [50] designed a model reference adaptive control (MRAC) framework that leverages GP regression to counteract model uncertainty, thereby enhancing control robustness. Building upon this work, Joshi et al. [51] incorporated generative networks to further improve the performance of the GP-MRAC scheme, especially in handling complex model variations. Regarding MPC-based methods, Hewing et al. [52] utilized GP regression to capture system dynamics and proposed a cautious MPC framework capable of accounting for prediction uncertainty. Similarly, Cao et al. [54] presented a hierarchical control structure that combines GP modelling with MPC techniques to address trajectory tracking tasks for unmanned quadrotors, demonstrating its effectiveness in high-dimensional nonlinear environments.

However, the aforementioned methods are mainly designed for guaranteeing the stability for uncertain systems and may lose effectiveness in the presence of unknown faults. Different from model uncertainty, faults are unexpected and can cause signifi-

cant damage to the controlled system. Given this, it is essential to ensure that uncertain systems with faults remain both stable and functional.

2.2 Fault-Tolerant Control

FTC aims to maintain the essential functionality of autonomous systems after completing fault detection. To enhance control performance under model uncertainty, adaptive FTC has been proposed and widely used to estimate unknown dynamics. This section introduces the fundamental concepts of actuator faults and FTC approaches, discussing the corresponding literature on adaptive FTC methods against both uncertainty and actuator faults that are closely related to the focus of this research.

2.2.1 Fundamental Concepts

Before introducing the definition of FTC method, this subsection begins with the common type of actuator faults in controlled systems. Actuator faults can be modelled as actuator bias faults [55] and gain faults [56], resulting in the following definition [14]:

$$\boldsymbol{u}_F = \Theta \boldsymbol{u} + \Delta \boldsymbol{u}_F, \quad t \geqslant t_F, \tag{2.12}$$

where $0 < t_F \in \mathbb{R}$ represents an unknown fault occurrence time. $\boldsymbol{u}_F \in \mathbb{R}^m$ is actuator output after $t \geqslant t_F$, and $\boldsymbol{u} \in \mathbb{R}^m$ refers to actuator input. $\Theta = \text{diag}[\theta_1, \theta_2, \cdots, \theta_m] \in \mathbb{R}^{m \times m}$ stands for the unknown parameterized matrix of actuation effectiveness with $\theta_i \in (0, 1]$, $i = 1, 2, \cdots, m$. $\Delta \boldsymbol{u}_F \in \mathbb{R}^m$ is unknown and time-varied actuator bias faults. Accordingly, the unknown actuator faults (2.12) can be divided into the following cases:

1) $\Theta = I_m$ and $\Delta \boldsymbol{u}_F = 0$ represent a fault-free case.

2) $0 < \theta_i < 1, i = 1, 2, \cdots, m$ and $\Delta \boldsymbol{u}_F = 0$ denote the partial loss of actuation effectiveness.

3) $\Theta = I_m$ and $\Delta \boldsymbol{u}_F \neq 0$ mean the actuator bias faults.

4) $0 < \theta_i < 1, i = 1, 2, \cdots, m$ and $\Delta \boldsymbol{u}_F \neq 0$ indicate both partial loss of actuation effectiveness and the actuator bias faults.

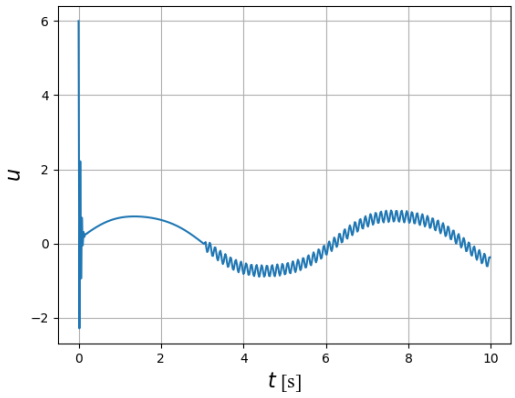

(a) Without actuator fault.

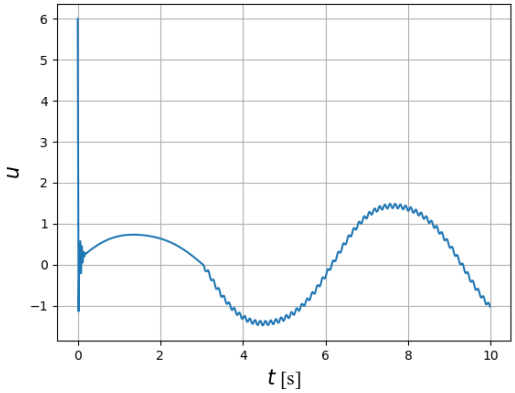

(b) Actuator gain fault.

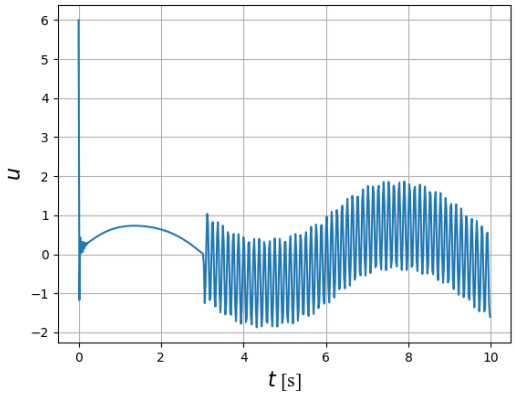

(c) Actuator bias fault.

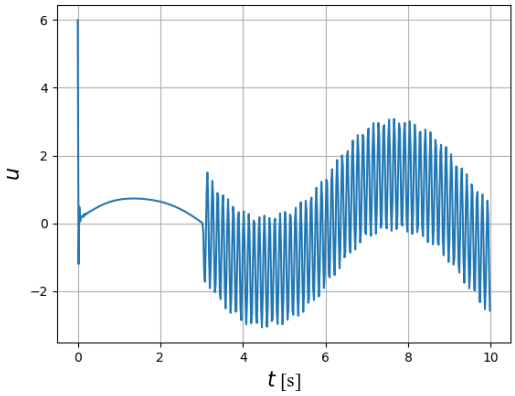

(d) With both actuator gain and bias faults.

Figure 2.4: Profiles of actuator outputs under different fault conditions.

To illustrate the impact of unknown faults on actuator output, results are presented in Figure 2.4. In this simulation, a pendulum system with $n = 2$ is considered, as introduced in [57], and the desired trajectory is specified as $[\sin(t), \cos(t)]^\top$. The actuator gain fault is defined as $\theta = 0.5$, and the actuator bias fault is set to $\sin(t)$, with the fault occurring at $t = 3$s. To assist the pendulum system in tracking the desired trajectory, a PID controller is employed with $k_P = 6$, $k_I = 9$, and $k_D = 0.02$. Compared to the fault-

free case in Figure 2.4(a), the actuator output values in Figure 2.4(b) are significantly higher since the gain fault reduces the effectiveness of the control inputs. As illustrated in Figure 2.4(c), the bias fault has a more severe impact on the pendulum system, leading to frequent oscillations in output curves. The actuator output under both actuator gain and bias faults displays even more frequent and severe oscillations than others, which shows in Figure 2.4(d).

Note that this thesis doesn't consider the total actuator outage faults $\theta_i = 0,\ i = 1,2,\cdots,m$ and the partial actuator outage faults $\theta_i = 0,\ i = 1,2,\cdots,n,(n < m)$. Interested readers are referred to some existing studies on [58, 59]. Different from sensor faults, actuator faults can directly hinder the design of model-based controllers and impact the systems stability. To deal with this issue, researchers have designed FTC methods to mitigate and address the influence of unknown actuator faults.

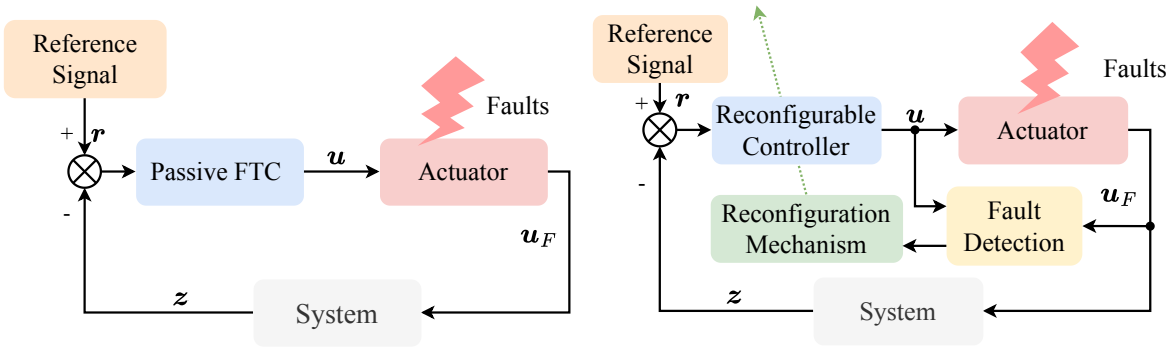

(a) Architecture of a passive FTC.

(b) Architecture of an active FTC.

Figure 2.5: Architecture of two types of FTC.

From the viewpoint of control theory, FTC strategies are commonly classified into two categories: passive FTC (see Figure 2.5(a)) and active FTC [60] (see Figure 2.5(b)). Passive FTC refers to fixed feedback control methods designed to reduce sensitivity to actuator faults. This approach features a simple structure and fast response but tends to be conservative when handling time-varying faults [61]. To overcome these limitations,

an active FTC strategy has been developed. This strategy integrates a fault detection and isolation module with a reconfigurable controller, providing a dynamic mechanism to handle faults. In addition, the active FTC method aims to reallocate control tasks from faulty actuators to healthy actuators [62]. Although active FTC provides greater flexibility and adaptability to handle system faults, it typically involves higher implementation cost and slower response times.

To improve the performance of both passive FTC and active FTC, researchers have integrated adaptive control methods into these frameworks [63] to build upon adaptive FTC control methods. Such methods can adjust controller parameters and compensate for the influence of faults, while also providing greater robustness against model uncertainty. As a result, adaptive FTC has attracted considerable research attention.

2.2.2 Adaptive FTC

The primary goal of adaptive FTC strategies is to maintain system stability despite the presence of model uncertainty and actuator faults [64–69]. As stated in [64], Khalili et al. employed radial basis function neural networks (RBFNNs) to approximate model uncertainties, and a distributed adaptive FTC framework was introduced to ensure the stability of uncertain multi-agent systems (MASs). Similarly, Wang et al. [65] utilized RBFNNs combined with a backstepping technique to design finite-time adaptive FTC schemes capable of handling actuator faults. In [66], Yang et al. developed a distributed adaptive controller incorporating both RBFNNs and predefined-time techniques to stabilize switched odd-rational-power MASs. A different approach was proposed in [67], where a parameter estimator was designed to identify uncertain parameters, and event-triggered adaptive FTC methods were used to guarantee stability in nonlinear systems. Addressing unknown nonlinearities, actuator saturation, and faults, Wang et al. [68] presented an event-triggered adaptive saturated FTC strategy. Wu et al. [69] focused

on the tracking control problem of nonaffine uncertain systems with actuator faults, where an event-triggered adaptive fuzzy output feedback FTC method was proposed.

In addition, some researchers have explored adaptive FTC approaches to compensate for unknown actuator faults. Furthermore, some researchers have designed adaptive fault-tolerant controller to compensate for the actuator faults [70–73]. As stated in [70], the authors designed a RBFNN to compensate for actuator gain faults, an observer to handle external disturbances, and a fault-tolerant controller to guarantee the system stability. Deng et al. [73] explored the consensus problem of heterogeneous MASs under actuator faults and network denial-of-service by leveraging an adaptive fault-tolerant resilient controller. However, the above adaptive FTC techniques on handling model uncertainty struggle with imperfect observations and observation noise in some case. To overcome this, few authors have studied GP-based adaptive FTC methods [74] to deal with model uncertainty and actuator bias faults.

Since the primary goal of FTC is to maintain stability of systems subject to faults, rather than explicitly guaranteeing safety, recent studies have focused on safety-critical control methods for autonomous systems, such as control barrier functions (CBFs).

2.3 Control Barrier Functions

Safety is a fundamental requirement for autonomous systems such as UAVs and UGVs. To address this, CBF methods have been proposed.

2.3.1 Fundamental Concepts

This subsection begins with the forward set invariance, which is the fundamental concept of safety. Consider the following control affine systems:

$$\dot{\boldsymbol{x}} = \boldsymbol{f}(\boldsymbol{x}) + \boldsymbol{g}(\boldsymbol{x})\boldsymbol{u}, \tag{2.13}$$

where $\boldsymbol{f}:\mathbb{R}^n\to\mathbb{R}^n$ and $\boldsymbol{g}:\mathbb{R}^n\to\mathbb{R}^{n\times m}$ respectively denote drift and gain dynamics, and both them are locally Lipschitz. $\boldsymbol{x}\in\mathbb{R}^n$ stands for the system state. Control input is defined as $\boldsymbol{u}\subset\mathbb{U}\in\mathbb{R}^m$. $\mathbb{U}$ represents the compact sets of control input.

Definition 2.3.1 (Forward Invariant [21]). *If there exists a set $\mathscr{A}$ and for every $\boldsymbol{x}_0\in\mathscr{A}$, there exists a trajectory $\boldsymbol{x}:I(\boldsymbol{x}_0)\to\mathbb{R}^n$ with $\boldsymbol{x}(0)=\boldsymbol{x}_0$ satisfying $\boldsymbol{x}(t)\in\mathscr{A}$, then this set $\mathscr{A}$ is said to be forward invariant. If the set $\mathscr{A}$ is forward invariant, then system* (2.13) *is safe with respect to the set $\mathscr{A}$.*

Assume that the set $\mathscr{A}$ is defined as

$$\begin{aligned}\mathscr{A}&=\{\boldsymbol{x}\in\mathbb{R}^n:h(\boldsymbol{x})\geqslant 0\},\\ \partial\mathscr{A}&=\{\boldsymbol{x}\in\mathbb{R}^n:h(\boldsymbol{x})=0\},\\ \mathrm{Int}(\mathscr{A})&=\{\boldsymbol{x}\in\mathbb{R}^n:h(\boldsymbol{x})>0\},\end{aligned}\tag{2.14}$$

where $h:\mathbb{R}^n\to\mathbb{R}$ is a continuously differentiable function. $\partial\mathscr{A}$ and $\mathrm{Int}(\mathscr{A})$ stand for the interior and boundary of set $\mathscr{A}$.

Before providing the definition of CBFs, we first introduce the concept of an extended class $\mathscr{K}$ function, defined as follows:

Definition 2.3.2 (Extended Class $\mathscr{K}$ Function [18]). *If a continuous function $\alpha:(-b,a)\to(-\infty,\infty)$ is strictly increasing and $\alpha(0)=0$, then this function α is said to be extended class $\mathscr{K}$ for some $a,b>0$.*

Definition 2.3.3 (Reciprocal CBFs [18]). *Consider system* (2.13)*, and provided a set $\mathscr{A}\subset\mathbb{R}^n$ defined by* (2.14) *for a continuously differentiable function $h:\mathbb{R}^n\to\mathbb{R}$. A continuously differentiable function $B:\mathrm{Int}(\mathscr{A})$ is said to be a reciprocal CBFs, if there exists three class*

$\mathcal{K}$ functions α_1, α_2, and α_3 such that

$$\frac{1}{\alpha_1(h(\boldsymbol{x}))} \leqslant B(\boldsymbol{x}) \leqslant \frac{1}{\alpha_2(h(\boldsymbol{x}))},$$

$$\sup_{\boldsymbol{u}\in\mathbb{U}} \left\{L_f B(\boldsymbol{x}) + L_g B(\boldsymbol{x})\boldsymbol{u} - \alpha(h(\boldsymbol{x}))\right\} \leqslant 0, \forall \boldsymbol{x} \in \mathrm{Int}(\mathscr{A}), \tag{2.15}$$

where $L_f B(\boldsymbol{x})$ and $L_g B(\boldsymbol{x})$ represent the Lie derivatives of $B(\boldsymbol{x})$ with respect to the vector fields $\boldsymbol{f}$ and $\boldsymbol{g}$, respectively.

Definition 2.3.4 (Zeroing CBFs [18])**.** *Consider system* (2.13)*, and provided a set $\mathscr{A} \subset \mathbb{R}^n$ defined by* (2.14) *for a continuously differentiable function $h : \mathbb{R}^n \to \mathbb{R}$, then the function h is said to be a zeroing CBFs defined on a set $\mathbb{D}$ with $\mathscr{A} \subseteq \mathbb{D} \subset \mathbb{R}^n$, if there exists an extended class $\mathcal{K}$ function α such that*

$$\sup_{\boldsymbol{u}\in\mathbb{U}} \left\{L_f h(\boldsymbol{x}) + L_g h(\boldsymbol{x})\boldsymbol{u} + \alpha(h(\boldsymbol{x}))\right\} \geqslant 0, \quad \forall \boldsymbol{x} \in \mathbb{D}, \tag{2.16}$$

where $L_f h(\boldsymbol{x})$ and $L_g h(\boldsymbol{x})$ represent the Lie derivatives of $h(\boldsymbol{x})$ with respect to the vector fields $\boldsymbol{f}$ and $\boldsymbol{g}$, respectively.

It is worth noticing that defining h on a set $\mathbb{D}$ larger than $\mathbb{C}$ allows one to account for the effects of model perturbations [75]. To show the mechanism of zeroing CBFs (see Figure 2.6), a linear function with positive coefficient γ is leveraged as $\alpha(\cdot) : \alpha(h(\boldsymbol{x})) = \gamma h(\boldsymbol{x})$, and γ serves as a decay rate of a lower bound of $h(\boldsymbol{x})$.

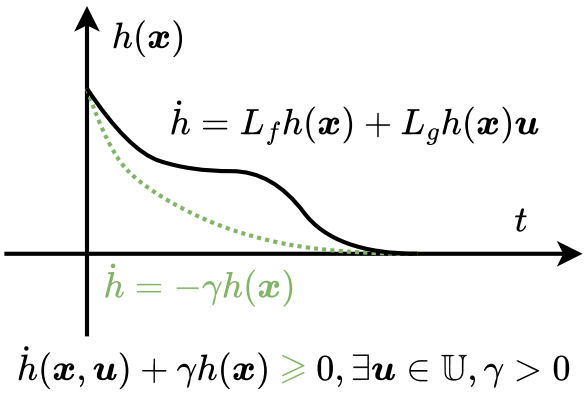

Figure 2.6: Mechanism of zeroing CBFs.

This chapter introduces two types of CBFs, but the thesis mainly focuses on the second type of CBF, namely, the zeroing CBF. While CBFs offer formal safety guarantees for autonomous systems, their effectiveness heavily depends on the accuracy of the system model. In practice, model uncertainty poses significant challenges for the design of CBF-based controllers. To overcome this limitation, researchers have developed uncertainty-aware CBF approaches that integrate robust design techniques or uncertainty estimates into the framework.

2.3.2 Uncertainty-Aware CBFs

Model uncertainty in autonomous systems is non-ignorable due to inherent randomness or noise and a lack of knowledge or understanding within systems. Given this, researchers extend CBFs to robust CBFs [76–79], adaptive CBFs [80–83], and learning-based CBFs [84–86]. As stated in [76], the authors designed robust control Lyapunov function (CLF) and robust CBF methods to stability and safety of systems with drift uncertainty. Buch et al. [77] studied the influence of sector-bounded uncertainties for true system models and designed a second-order cone program (SOCP)-based controller with robust CBFs. However, the SOCP may cause the feasible issue for the design of CBF and CLF-based controllers. For addressing this issue, Cohen et al. [78] developed a duality-based approach for robust CBF and robust CLF under drift and gain uncertainties. However, the above methods are conservative when facing higher bounds of uncertainty. To overcome this, adaptive CBF methods are proposed [80–83]. As stated in [80], the authors designed online estimation methods to address parameter uncertainty and developed robust adaptive CBF methods to ensure the safety of uncertain systems. For reducing the influences of model uncertainty, Wang et al. [81] explored finite-time convergence techniques to estimate uncertain system parameters and integrated this methods into CBF frameworks. In [83], the authors presented adaptive esti-

mator to handle matched and mismatched uncertainties as well as respectively studied the CBFs and HOCBFs. In addition, some researchers have used learning-based methods to handle model uncertainty. As stated in [86], Taylor et al. developed an episodic learning framework for CBFs to mitigate the influences of model uncertainty. However, the above methods on adaptive and learning-based CBFs still struggle to handle imperfect measurements and observation noise. To address these challenges, researchers have explored the GP-based CBFs to ensure the safety of uncertain systems.

Research on GP-based CBFs can be categorized into two directions: modelling system uncertainty [87–91] and modelling uncertain terms in the CBF constraints [34, 92, 93]. As stated in [87], Emam et al. proposed a GP-based framework to learn both additive and multiplicative disturbances in system dynamics and designed a robust CBF controller to ensure safety under uncertainty. To model unknown system dynamics, Long et al. [90] developed a probabilistic CLF-CBF approach using matrix-valued GP regression, providing both stability and safety guarantees under worst-case uncertainty. In [93], Wang et al. investigated a GP-based CBF method and Bayesian optimization to optimize the safe control performance by modelling uncertainty within the CBF constraints. Nevertheless, the aforementioned CBF methods can lose their effectiveness when applied to systems with high relative degrees.

For example, consider the following ACC system [94]:

$$\underbrace{\begin{bmatrix} \dot{v} \\ \dot{d} \end{bmatrix}}_{\dot{\boldsymbol{x}}} = \underbrace{\begin{bmatrix} -\frac{Fr}{m} \\ v_0 - v \end{bmatrix}}_{\boldsymbol{f}(\boldsymbol{x})} + \underbrace{\begin{bmatrix} \frac{1}{m} \\ 0 \end{bmatrix}}_{\boldsymbol{g}(\boldsymbol{x})} u, \tag{2.17}$$

where m is the mass of the ego vehicle and its rolling resistance can be represented as $Fr = f_0 + f_1 v + f_2 v^2$. Parameters v, d, and v_0 stand for the velocity of ego vehicle, the distance between ego vehicle and its preceding vehicle, and the velocity of its preceding vehicle. The CBF is set as $h(\boldsymbol{x}) = d - d_{\text{safe}}$ that has relative degree two (i.e., $r = 2$). The

corresponding CBF constraint can be obtained as below:

$$\underbrace{v_0 - v}_{L_f h(\boldsymbol{x})} + \underbrace{0}_{L_g h(\boldsymbol{x})} \times u + \underbrace{d - d_{\text{safe}}}_{\alpha(\boldsymbol{x})} \geqslant 0. \tag{2.18}$$

Note that $L_g h(\boldsymbol{x}) = 0$ in (2.18), the safe control input u cannot guarantee the safety of autonomous systems. Given this, HOCBFs have been proposed to address this issue.

2.4 High-Order Control Barrier Functions

In practical applications, nonlinear systems with high relative degrees are common, such as the serial spring-mass system (relative degree six) and the two-link pendulum with elastic actuators (relative degree four) [95]. Since zeroing CBFs are limited in handling such systems, researchers have proposed HOCBFs to investigate the safety systems with higher relative degrees. This section presents the fundamental concepts of HOCBFs and reviews recent advances in uncertainty-aware HOCBF methods.

2.4.1 Fundamental Concepts

This subsection begins with the definitions of the class $\mathcal{K}$ function and relative degree.

Definition 2.4.1 (Class $\mathcal{K}$ function [96])**.** *If a continuous function $\alpha : [0, a) \to [0, \infty), a > 0$ is strictly increasing and $\alpha(0) = 0$, then this function α is said to be class $\mathcal{K}$.*

Definition 2.4.2 (Relative Degree [96])**.** *If a scalar function $h : \mathbb{R}^n \to \mathbb{R}$ is r-times continuously differentiable at $\boldsymbol{x}$, and if $L_g L_f^j h(\boldsymbol{x}) = 0, \forall 1 \leqslant j < r-1$ and $L_g L_f^{r-1} h(\boldsymbol{x}) \neq 0$ in a region $\mathbb{D}$, then the function h is said to have relative degree $r \in \mathbb{N}$ for all $x \in \mathbb{D}$.*

Consider a state constraint set of the form as follows:

$$\mathcal{A}_0 = \{\boldsymbol{x} \in \mathbb{R}^n | h(\boldsymbol{x}) \geqslant 0\}, \tag{2.19}$$

where function h has the same meaning defined in (2.14).

To obtain an effective control input, we need to compute the derivative of h along the system (2.13) until the control input appears. Then, one considers the collection of functions

$$\begin{aligned}
&\beta_0(\boldsymbol{x}) = h(\boldsymbol{x}),\\
&\beta_i(\boldsymbol{x}) = h^i(\boldsymbol{x}) = \dot{\beta}_{i-1}(\boldsymbol{x}) + \alpha_i(\beta_{i-1}(\boldsymbol{x})), \quad \forall i \in \{1,2,\dots,r-1\},\\
&\beta_r(\boldsymbol{x},\boldsymbol{u}) = h^r(\boldsymbol{x},\boldsymbol{u}) = \dot{\beta}_{r-1}(\boldsymbol{x},\boldsymbol{u}) + \alpha_r(\beta_{r-1}(\boldsymbol{x})),
\end{aligned} \tag{2.20}$$

where each $\alpha_i(\cdot) \in \mathscr{K}$, and each β_i for $i \in \{0,1,\cdots,r-1\}$ is dependent of $\boldsymbol{u}$ for all $\boldsymbol{x} \subset \mathbb{D}$.

Correspondingly, a sequence of sets $\mathscr{A}_i,\ i \in \{0,1,\cdots,r\}$ can be defined as the zero superlevel set of β_i :

$$\begin{aligned}
\mathscr{A}_i &= \{\boldsymbol{x} \in \mathbb{R}^n : \beta_i(\boldsymbol{x}) \geqslant 0\},\\
\partial\mathscr{A}_i &= \{\boldsymbol{x} \in \mathbb{R}^n : \beta_i(\boldsymbol{x}) = 0\},\\
\mathrm{Int}(\mathscr{A}_i) &= \{\boldsymbol{x} \in \mathbb{R}^n : \beta_i(\boldsymbol{x}) > 0\}.
\end{aligned} \tag{2.21}$$

Definition 2.4.3 (HOCBFs [22])**.** *Denote $h : \mathbb{R}^n \to \mathbb{R}$ have relative degree $r \in \mathbb{N}$ for system* (2.13) *satisfying* (2.20) *and a sequence of sets $\mathscr{A}_i$ satisfying* (2.21)*. If there exist a sequence of class $\mathscr{K}$ functions $\alpha_i(\cdot), i \in \{0,1,\cdots,r\}$ such that*

$$\sup_{\boldsymbol{u}\in\mathbb{U}} \underbrace{\left\{L_f\beta_{r-1}(\boldsymbol{x}) + L_g\beta_{r-1}(\boldsymbol{x})\boldsymbol{u} + \alpha_r(\beta_{r-1}(\boldsymbol{x}))\right\}}_{\beta_r(\boldsymbol{x},\boldsymbol{u}) = h^r(\boldsymbol{x},\boldsymbol{u})} \geqslant 0, \forall \boldsymbol{x} \in \mathscr{A}_1 \bigcap \mathscr{A}_2 \bigcap \cdots, \bigcap \mathscr{A}_r, \tag{2.22}$$

then function h is said to be a candidate HOCBF of the relative degree r for system (2.13)*, where $L_f\beta_{r-1}(\boldsymbol{x}) = L_f h(\boldsymbol{x}) + \sum_{i=1}^{r-1} L_f^i(\alpha_{r-i} \circ \beta_{r-i-1})(\boldsymbol{x})$ and $L_g\beta_{r-1}(\boldsymbol{x}) = L_g L_f^{r-1} h(\boldsymbol{x})$.*

Note that CBFs can be viewed as a special case of HOCBFs when the relative degree is one. In addition, if a sequence of class $\mathscr{K}$ functions are selected as $\alpha_i(h(\boldsymbol{x})) = k_i h(\boldsymbol{x})$ with $k_i > 0, i = \{0,\cdots,r\}$, the HOCBF formulation reduces to an exponential CBF. Compared to CBFs, HOCBFs are more sensitive since each $\beta_i(\boldsymbol{x})$ needs to be non-negative.

Furthermore, each class $\mathcal{K}$ function $\alpha_i(h(\boldsymbol{x}))$ can be chosen from various forms, such as the a quadratic function $\alpha_i(h(\boldsymbol{x})) = h^2(\boldsymbol{x})$, a linear function $\alpha_i(h(\boldsymbol{x})) = k_i h(\boldsymbol{x})$, and a square root function $\alpha_i(h(\boldsymbol{x})) = \sqrt{h(\boldsymbol{x})}$. Nevertheless, the design of HOCBF-based controllers still rely on accurate system models. Given this, some researchers study uncertainty-aware HOCBF methods that integrate robust design techniques or uncertainty estimates into HOCBF frameworks.

2.4.2 Uncertainty-Aware High-Order CBFs

Compared to CBFs, the HOCBFs are easily affected by model uncertainty. For example, consider the following systems with model uncertainty:

$$\dot{\boldsymbol{x}} = \hat{\boldsymbol{f}}(\boldsymbol{x}) + \boldsymbol{g}(\boldsymbol{x})\boldsymbol{u}, \tag{2.23}$$

where $\hat{\boldsymbol{f}}(\boldsymbol{x}) \in \mathbb{R}^n$ denotes the partially known drift systems. $\boldsymbol{g}(\boldsymbol{x})$ and $\boldsymbol{u}$ have the same meanings as those defined in system (2.13).

Firstly, denote a function $h(\boldsymbol{x})$ satisfying Definition 2.3.4, then one obtains the following CBF constraint with the respect to system (2.23):

$$\sup_{\boldsymbol{u}\in\mathbb{U}} \left\{ L_{\hat{f}} h(\boldsymbol{x}) + L_g h(\boldsymbol{x})\boldsymbol{u} + \alpha(h(\boldsymbol{x})) \right\} \geqslant 0, \quad \forall \boldsymbol{x} \in \mathbb{D}, \tag{2.24}$$

Then, assume the system (2.23) have relative degree r and, define a new $\Gamma(\boldsymbol{x})$ satisfying Definition 2.4.3, the HOCBF constraint can be written as follows:

$$\sup_{\boldsymbol{u}\in\mathbb{U}} \left\{ \underbrace{L_{\hat{f}} h(\boldsymbol{x}) + \sum_{i=1}^{r-1} L_{\hat{f}}^i (\alpha_{r-i} \circ \beta_{r-i-1})(\boldsymbol{x})}_{L_{\hat{f}}\beta_{r-1}(\boldsymbol{x})} + \underbrace{L_g L_{\hat{f}}^{r-1} h(\boldsymbol{x})}_{L_g\beta_{r-1}(\boldsymbol{x})} \boldsymbol{u} + \alpha_r(\beta_{r-1}(\boldsymbol{x})) \right\} \geqslant 0, \tag{2.25}$$

for all $\boldsymbol{x} \in \mathbb{D}$.

According to (2.24) and (2.25), it can be observed that the drift uncertainty in system (2.23) only influences the term $L_{\hat{f}} h(\boldsymbol{x})$ in CBF constraint (2.24). However, in HOCBF

constraint (2.25), the drift uncertainty affects not only the term $L_{\hat{f}}\beta_{r-1}(\boldsymbol{x})$ but also the term $L_g L_{\hat{f}}^{r-1}h(\boldsymbol{x})$. To overcome these limitations, some authors have explored robust exponential CBFs [97, 98], learning-based exponential CBFs [84, 99, 100], and concurrent learning-based HOCBFs [101]. As stated in [97], Chinelato et al. developed the robust exponential CBF framework to ensure the safety of uncertain systems. In contrast, Seiler et al. [98] considered the influences of unmodelled dynamics including unknown actuator dynamics and time delays and designed robust CBF methods with integral quadratic constraints to handle them. In [100], the authors leveraged neural networks techniques to approximate the exponential CBF constraint including uncertain terms. Wang et al. [101] studied the safety-critical tracking control problem for uncertain systems by using a concurrent learning method to learn the HOCBF constraint under uncertainty. Furthermore, some researchers assume that the model uncertainty follows a structure similar to that defined in Definition 2.4.2 and is matched with the control input. Therefore, the term $L_g L_{\hat{f}}^{r-1}h(\boldsymbol{x})$ can be replaced by the term $L_g L_f^{r-1}h(\boldsymbol{x})$ in the HOCBF constraint. However, the above robust exponential CBF methods in [97, 98] and the assumption stated in [101] remain conservative in some cases. The learning-based exponential CBF and HOCBF methods in [84, 99–101] face more challenges when dealing with imperfect state measurements and observation noise. To address the above issues, very few researchers have explored the GP-based HOCBF methods [38]. Nevertheless, the HOCBF approaches still struggle to guarantee the safety of uncertain systems in the presence of unknown actuator faults.

CHAPTER 3

PROBABILISTIC MODEL-BASED FAULT-TOLERANT CONTROL FOR UNCERTAIN NONLINEAR SYSTEMS

This chapter is based on the paper titled "Probabilistic model-based fault-tolerant control for uncertain nonlinear systems," IEEE Transactions on Cybernetics, vol. 55, no. 4, pp. 1838-1847, April 2025.

To address RQ1 and achieve RO1, this chapter proposes two probabilistic model-based adaptive FTC methods for faulty systems with unknown dynamics. We study GP regression in two cases: an offline learning-based control method and an event-triggered online data-driven modelling method, to learn unknown system dynamics. Considering the computational complexity of GP regression in practical applications, we discuss the case of computational delays in real-time predictions. Moreover, four theoretical criteria are developed to ensure the probabilistic stability of closed-loop systems. Finally, numerical simulations validate the effectiveness of proposed control methods and demonstrate their competitiveness compared to existing approaches.

The structure of this chapter is outlined as follows. Section 3.1 reviews the related literature pertinent to this work, while Section 3.2 presents the necessary background

and preliminaries. The core contributions of this chapter are detailed in Sections 3.3 and 3.4. Section 3.5 provides numerical examples to validate the proposed approaches. The chapter is concluded in Section 3.6. Additionally, an overview of two methods developed in this chapter is illustrated in Figure 3.1.

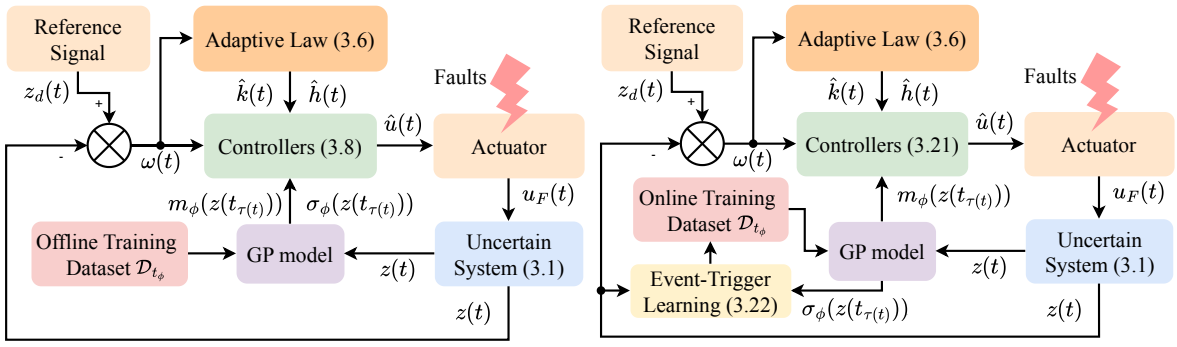

(a) Offline learning-based control.

(b) Online learning-based control.

Figure 3.1: An overview of two probabilistic adaptive FTC methods.

3.1 Introduction

FTC is a specialized strategy designed to ensure fail-safe operation in real-time conditions when components in a system fail or become faulty [12]. Adaptive control, known for its ability to deal with model uncertainty, control failures, and environmental disturbances [10], has recently been combined with FTC methods to enhance system reliability [5, 65, 102–107]. To tackle unknown actuator faults, adaptive fault-tolerant controllers have been designed for uncertain nonlinear systems by using the backstepping technique [65, 102–104]. Moreover, the reinforcement learning strategy has been used to enhance adaptive FTC methods to deal with actuator faults [5, 105]. In [106], Qiu et al. extended FTC to adaptive fuzzy control for uncertain stochastic nonlinear systems. However, the FTC strategies often depend on conservative assumptions or non-robust methods to handle model uncertainty. For instance, results in [5, 102, 103] as-

sume known bounds for model uncertainty, while others [65, 104–107] employ adaptive NN methods to approximate unknown system dynamics. Despite their utility, the conservative assumptions in [5, 102, 103] may limit applicability in certain cases. Similarly, adaptive NN techniques in [65, 104–107] face challenges in approximating unknown dynamics when dealing with imperfect measurements and limited data.

Recently, the GP modelling method has gained attention for dynamic systems modelling due to its inherent advantages in handling model uncertainty. As a nonparametric approach, it offers flexibility and robustness in dealing with uncertain systems [108]. Given this, GP-based control strategies have been used in uncertain nonlinear systems [28–36, 88]. As stated in [28, 29, 33, 36], the GP-based feedback linearization controllers have been designed to study tracking control problems. Furthermore, researchers have also extended GP-based control to the CBFs [34, 35, 88], adaptive sliding-mode control [30], MPC [31], and RL [32]. To improve the data efficiency and decrease the computational time of GP regression, event-triggered sampling strategies [28, 29, 36] and the active basis vector method [30] have been leveraged to limit the size of the training dataset. However, the computational time required for GP regression cannot be ignored when collecting training data in online learning. In real-time control tasks, predictions need to be generated at each updated time to model unknown dynamics based on GP regression, making it essential to account for the computational delays associated with this process. However, only a few studies have focused on this aspect [109]. Furthermore, results in [28–36, 88] mainly investigate tracking control problems without faults and face challenges when dealing with unknown actuator faults. Therefore, we aim to extend existing works to GP-based adaptive FTC strategies in this chapter.

3.2 Preliminaries

This section introduces some notations, uncertain control-affine systems, fault modeling, and corresponding control objectives, along with some necessary assumptions.

3.2.1 Notations

Let $\mathbb{R} = (-\infty, +\infty), \mathbb{R}_{0,+} = [0, +\infty), \mathbb{R}_{+} = (0, +\infty), \mathbb{R}^n$ be n-dimensional Euclidean space, and $\mathbb{R}^{n\times m}$ be the space of $n \times m$ real matrices. $\mathbb{N}$ and $\mathbb{N}_0$ indicate all natural numbers without and with zero. I_n stands for the $n \times n$ real identity matrix. $\|\cdot\|$ refers to the Euclidean norm. $|\cdot|$ presents the absolute value. $\Pr\{\cdot\}$ means probability of an event. $z^{[p]}$ implies the p-th measurement of the state vector z. $z^{(n)}$ indicates the n-th derivation. $\mathbb{X}$ represents the compact set. $\emptyset$ stands fo the empty set. Given matrix Ψ, $\lambda_{\min}(\Psi)$ and $\lambda_{\max}(\Psi)$ refer to its minimum and maximum eigenvalues. $\det(\Psi)$ represents the determinant of matrix Ψ.

3.2.2 Problem Formulation

Consider a single-input nonlinear system expressed in the controllability canonical form as follows [29]:

$$\begin{aligned} \dot{z}_i(t) &= z_{i+1}(t), \quad i = 1, 2, \cdots, n-1, \\ \dot{z}_n(t) &= f(z(t)) + g(z(t))u(t), \; z_0 = z(0), \end{aligned} \tag{3.1}$$

where $z(t) = [z_1(t), z_2(t), \cdots, z_n(t)]^\top \in \mathbb{X} \subseteq \mathbb{R}^n$ refers to the state variable. $u(t) \in \mathbb{R}$ denotes the control input. Note that functions $f(\cdot)$ and $g(\cdot)$ may not be fully known for real systems. Then, the following assumption is made:

Assumption 3.2.1 (System Dynamics [96, 110])**.** *The function $f(\cdot) : \mathbb{X} \to \mathbb{R}$ is unknown but is Lipschitz continuous on the compact domain $\mathbb{X}$ with a Lipschitz constant L_f, satisfying $|f(z(t)) - f(z^*(t))| \leqslant L_f \|z(t) - z^*(t)\|$ for all $z(t), z^*(t) \in \mathbb{X}$. The function $g(z(t)) : \mathbb{X} \to \mathbb{R}$ is known and satisfies $g(z(t)) \neq 0$ for all $z(t) \in \mathbb{R}^n$, with $|g(z(t))| \leqslant \bar{g}$, where $\bar{g}$ is a constant.*

Remark 3.2.1. *This chapter assumes the $g(\cdot)$ is known, which helps guarantee global controllability and facilitates the design of a controller for system* (3.1)*, but it restricts the system class. Interested readers are referred to [111] for studies on systems with unknown dynamics $g(\cdot)$.*

Assumption 3.2.2 (Measurable State)**.** *Suppose that availability noise measurements satisfy* $y^{[\phi]} = f(z(t_\phi)) + d^{[\phi]}$ *at arbitrary time instances* $t = t_\phi$ *with* $\phi \in \mathbb{N}_0$*, and noise* $d^{[\phi]} \sim \mathcal{N}(0, \sigma_n^2)$ *is assumed Gaussian independent and identically distributed. Then, a training dataset can be defined as follows:*

$$\mathscr{D}_{t_\phi} = \left\{ z^{[p]}, y^{[p]} \right\}_{p=1}^{N_\phi}.$$

where ϕ *indicates an index of the number of collected noisy data, while* $N_\phi \in \mathbb{N}_0$ *means the current number of collected noisy data. Note that dataset* $\mathscr{D}_{t_\phi}$ *can be updated as* $\mathscr{D}_{t_{\phi+1}}$ *when new data is collected at* $t = t_{\phi+1}$*.*

Supposing that the function f satisfies Assumptions 2.1.1 and 3.2.2, its posterior mean m_ϕ and standard deviation σ_ϕ on state z can be obtained based on the dataset $\mathscr{D}_{t_\phi}$. Moreover, the SE function defined in (2.5) is adopted in this chapter.

3.2.3 Fault Modeling

This chapter focuses on actuator bias faults caused by wear-and-tear factors in system components [6]. Such faults may degrade control performance and pose significant threats to system stability, as detailed below:

$$u_F(t) = \hat{u}(t) + \Delta h(t), \quad \forall t \geqslant t_F, \tag{3.2}$$

where $\hat{u}(t)$ stands for the control input that needs to be designed. $\Delta h(t) \in \mathbb{R}$ refers to an unknown time-varying bias fault. t_F represents an unknown time-instant of fault occurrence and $u(t) = u_F(t)$ if $t \geqslant t_F$.

Assumption 3.2.3 (Fault Bound [112])**.** *Actuator bias fault* $\Delta h(t)$ *is unknown time-varying but bounded function which satisfies* $|\Delta h(t)| \leqslant \bar{h}$ *and* $0 < \bar{h} < +\infty$*, where parameter* $\bar{h}$ *is a known finite constant.*

Remark 3.2.2. *As stated in equation* (2.12)*, actuator faults are commonly divided into bias faults and gain faults. Considering the limitations of the proposed methods, this chapter preliminarily focuses on addressing the challenges posed by unknown system dynamics and bias faults. The general fault model will be considered in future studies.*

Assumption 3.2.4 (Desired Trajectory)**.** *In this chapter, desired trajectory* $z_d^\star(t)$ *fulfills* $z_d^\star(t) = [z_d(t), \dot{z}_d(t), \cdots, z_d^{(n-1)}(t)]^\top \in \mathbb{R}^n$*, where* $z_d(t)$ *and its first n derivations are bounded and known, satisfying* $\bar{z}_{d_n} \geqslant \left| z_d^{(n)}(t) \right|$*,* $\bar{z}_d^\star = \sup_{t \in \mathbb{R}_{0,+}} \|z_d^\star(t)\|$*.*

In what follows, we define a tracking error between the state of nonlinear system (3.1) and the desired trajectory's state as $\omega_i(t) = z_i(t) - z_d^{(i-1)}(t), i = 1,2,\cdots,n$ with $\omega(t) = [\omega_1(t),\omega_2(t),\cdots,\omega_n(t)]^\top \in \mathbb{R}^n$. Based on system (3.1), the dynamics of the error system are defined as follows:

$$\begin{aligned} \dot{\omega}_i(t) &= z_{i+1}(t) - z_d^{(i)}(t), \quad i = 1,2,\cdots,n-1, \\ \dot{\omega}_n(t) &= f(z(t)) + g(z(t))u(t) - z_d^{(n)}(t). \end{aligned} \tag{3.3}$$

When $t \geqslant t_F$, error system (3.3) can be rewritten as follows:

$$\dot{\omega}(t) = A\omega(t) + B\left(f(z(t)) + g(z(t))u_F(t) - z_d^{(n)}(t)\right). \tag{3.4}$$

where $A = \begin{bmatrix} \bar{0} & I_{n-1} \\ 0 & 0 \end{bmatrix}_{n\times n}$, $B = \begin{bmatrix} 0_{n-1} \\ 1 \end{bmatrix}_{n\times 1}$, and $\bar{0} = 0 \times I_{n-1}$.

3.2.4 Control Objectives

This chapter aims to propose novel offline and online learning-based adaptive FTC strategies for uncertain nonlinear system (3.1) subject to fault model (3.2), with the goal of achieving the following control objectives:

- **Unknown dynamics fitting.** The proposed two learning strategies can fit the unknown dynamics of systems and generate probabilistic models to facilitate the design of adaptive fault-tolerant controllers.
- **Unknown fault compensation.** The designed control strategies should effectively compensate for an unknown actuator fault, reducing its influence on the system state.
- **Desired state tracking.** System (3.1) can track desired trajectory $z_d^\star(t)$. The condition $\lim_{t\to+\infty} \|z(t) - z_d^\star(t)\| \leqslant \bar{\omega}$ holds for any initial condition $z(0)$, where $0 < \bar{\omega} \in \mathbb{R}_+$ is the upper bound of the tracking error.

3.3 Offline Learning-Based Adaptive FTC

This section presents the design and theoretical analysis of an offline learning-based adaptive FTC method. Subsection 3.3.1 designs an adaptive fault-tolerant controller with delayed predictions. Subsection 3.3.2 analyzes the probabilistic stability and derives a probabilistic bound for the derivatives of the system state.

3.3.1 Learning-Based FTC with Delayed GP Predictions

This subsection designs a probabilistic model-based adaptive fault-tolerant controller for system (3.4), based on dataset $\mathscr{D}_{t_\phi}$ in Assumption 3.2.2, leading to the following representation:

$$\begin{aligned}
\hat{u}(t) &= g^{-1}(z(t))(\hat{u}_1(t)+\hat{u}_2(t)),\\
\hat{u}_1(t) &= -\hat{k}(t)\omega^\top(t)\Upsilon B - \frac{\hat{h}^2(t)\omega^\top(t)\Upsilon B}{\hat{h}(t)|\omega^\top(t)\Upsilon B|+\delta(t)},\\
\hat{u}_2(t) &= -\hat{f}_\phi(z(t)) - \bar{\beta}\sigma_\phi(z(t))
\end{aligned} \tag{3.5}$$

with the corresponding adaptive law:

$$\dot{\hat{k}}(t) = k_1\left(\omega^\top(t)\Upsilon B\right)^2,\ \dot{\hat{h}}(t) = h_1\left|\omega^\top(t)\Upsilon B\right|, \tag{3.6}$$

where $\hat{k}(t)\in\mathbb{R}$ is the time-varying gain with an initial positive value. $\hat{h}(t)\in\mathbb{R}$ implies the estimation of the unknown actuator fault with initial $0<\hat{h}(0)\in\mathbb{R}$. Parameters k_1 and h_1 are positive constants. $0<\delta(t)\in\mathbb{R}$ denotes a uniformly continuous function satisfying $\lim_{T\to\infty}\int_0^T\delta(\zeta)d\zeta\leqslant\bar{\delta}<+\infty$. $\hat{f}_\phi(z(t)),\sigma_\phi(z(t))$, and $\bar{\beta}$ are posterior mean, posterior variance, and the upper bound of the gain parameter, as defined in Assumption 3.2.2. The positive matrix Υ needs to be designed, as determined by the following equation:

$$\Upsilon A + A^\top\Upsilon - 2\Upsilon BB^\top\Upsilon = -Q \tag{3.7}$$

for any positive definite matrix Q.

Predictions for new test data based on GP regression depend on training data. Nevertheless, real-time control of uncertain systems requires generating predictions at every time instant, making the computational time of GP regression non-negligible in practical applications. Moreover, for online learning-based control, the updated time of the data-driven model should also be considered if new data is collected, which will be discussed later. Given this, we should leverage delayed values $m_\phi(z(t_{\tau(t)}))=\hat{f}_\phi(z(t))$ and $\sigma_\phi(z(t_{\tau(t)}))=\sigma_\phi(z(t))$ in practice. Here, $t_{\tau(t)}$ is the last model evaluation time, and $\alpha(\cdot):\mathbb{R}\to\mathbb{R}$ defines the overall computational time as follows:

$$t_{k+1}=t_k+\alpha(t_k),\ \ \tau(t)=\underset{k\in\mathbb{N}}{\operatorname{argmax}}\, t_{k+1}<t$$

with the discrete-time $t_k,\forall k\in\mathbb{N},t_0=0$, and Figure 3.2 shows the illustration of learning-based control with delayed GP predictions. Note that overall computational time is

unequal in different time instants. This overall computational time contains the computational time for predictions generated at every time instant in the case of offline learning-based control (as discussed in Section 3.3), and the time for data-driven model updates as well as predictions generated in the case of online learning-based control (as explored in Section 3.4). Moreover, this chapter assumes that transmission time delays are absent.

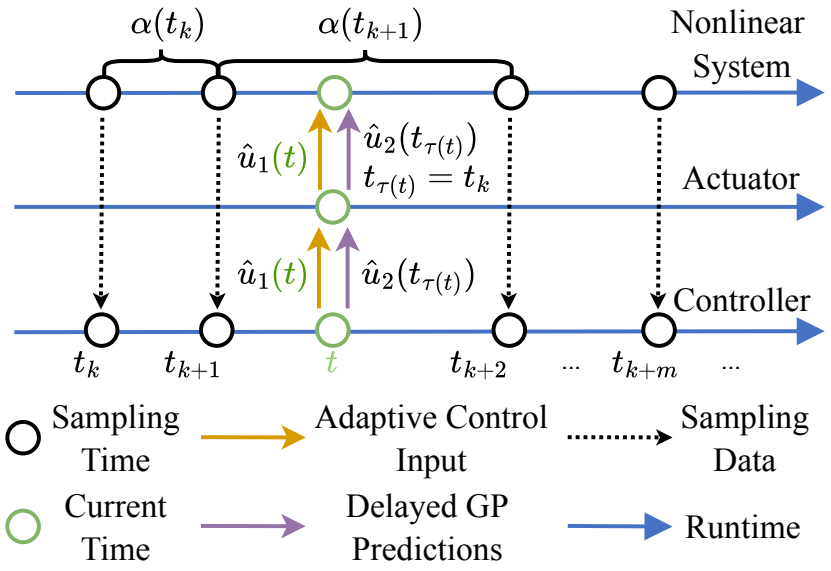

Figure 3.2: Illustration of the offline learning-based control with delayed GP predictions. This approach requires the collection of offline training data before operation.

Then, controller (3.5) can be rewritten as follows:

$$\begin{aligned}
\hat{u}(t) &= g^{-1}(z(t))(\hat{u}_1(t) + \hat{u}_2(t)), \\
\hat{u}_1(t) &= -\hat{k}(t)\omega^\top(t)\Upsilon B - \frac{\hat{h}^2(t)\omega^\top(t)\Upsilon B}{\hat{h}(t)|\omega^\top(t)\Upsilon B| + \delta(t)}, \\
\hat{u}_2(t) &= \hat{u}_2(t_{\tau(t)}) = -m_\phi(z(t_{\tau(t)})) - \bar{\beta}\sigma_\phi(z(t_{\tau(t)})).
\end{aligned} \tag{3.8}$$

To determine the worst-case influences of computational time $\alpha(\cdot)$ for tracking accuracy, the following assumption is given:

Assumption 3.3.1 (Computational Time Bound [109])**.** *The overall computational time $\alpha(t)$ has a constant bound $0 < \bar{\alpha} \in \mathbb{R}_+$, and its induced time delay affects the posterior mean and variance.*

3.3.2 Stability Analysis

This subsection establishes sufficient conditions to ensure the probabilistic stability of system (3.4) and the probabilistic boundedness of the system state's derivation.

Theorem 3.3.1 (Probabilistic Stability)**.** *Suppose that computational time bound $\bar{\alpha}$ fulfills $\bar{\alpha} < 1/L_f$ and the derivations of the system state $\|\dot{z}(t)\|$ has a probabilistic bound $\tilde{\mathcal{Z}}$. Under Assumptions 2.1.1, 3.2.1-3.3.1, tracking error $\omega(t)$ is bounded by*

$$\|\omega(t)\| \leqslant \bar{\omega} = \frac{4\lambda_{\max}(\Upsilon)L_f\tilde{\mathcal{Z}}\bar{\alpha}}{\lambda_{\min}(Q)},\ \forall t \in \mathbb{R}_{0,+}$$

with a high probability $1-\varrho$ based on controller (3.8)*.*

Proof. Considering the following Lyapunov functional for error system (3.4) as follows:

$$V(t) = \omega^\top(t)\Upsilon\omega(t) + \frac{\left(\hat{k}(t)-\bar{k}\right)^2}{k_1} + \frac{\left(\hat{h}(t)-h^*\right)^2}{h_1}, \tag{3.9}$$

where parameters $\bar{k}$ and h^* will be designed later.

Accordingly, it is deduced from (3.9) that

$$\begin{aligned}\dot{V}(t) = {} & \omega^\top(t)\left(\Upsilon A + A^\top\Upsilon\right)\omega(t) + 2\omega^\top(t)\Upsilon B\Big(f(z(t)) - f(z(t_{\tau(t)})) + f(z(t_{\tau(t)})) - m_\phi(z(t_{\tau(t)}))\\ & - \bar{\beta}\sigma_\phi(z(t_{\tau(t)})) + g(z(t))\Delta h(t) - z_d^{(n)}(t) - \hat{k}(t)\omega^\top(t)\Upsilon B - \frac{\hat{h}^2(t)\omega^\top(t)\Upsilon B}{\hat{h}(t)|\omega^\top(t)\Upsilon B| + \delta(t)}\Big)\\ & + 2\hat{k}(t)\left(\omega^\top(t)\Upsilon B\right)^2 - 2\bar{k}\left(\omega^\top(t)\Upsilon B\right)^2 + 2\hat{h}(t)\left|\omega^\top(t)\Upsilon B\right| - 2h^*\left|\omega^\top(t)\Upsilon B\right|.\end{aligned} \tag{3.10}$$

Based on Assumptions 2.1.1 and 3.2.4, we obtain

$$\omega^\top(t)\Upsilon B\left(g(z(t))\Delta h(t) - z_d^{(n)}(t)\right) \leqslant \left(\bar{g}\bar{h} + \bar{z}_{d_n}\right)\left|\omega^\top(t)\Upsilon B\right|. \tag{3.11}$$

According to Lemma 2.1.1, one gets

$$|f(z(t_{\tau(t)})) - m_\phi(z(t_{\tau(t)}))| \leqslant \bar{\beta}\sigma_\phi(z(t_{\tau(t)})). \tag{3.12}$$

Considering the Lipschitz continuity of $f(\cdot)$ in Assumptions 3.2.1 and 3.3.1, along with using the mean value theorem and the probabilistic state changing rate $\|\dot{z}(t)\|$, we have

$$\begin{aligned} f(z(t)) - f(z(t_{\tau(t)})) &\leqslant L_f\|z(t) - z(t_{\tau(t)})\|\\ &\leqslant L_f\tilde{\mathcal{Z}}\left|t - t_{\tau(t)}\right|\\ &\leqslant 2L_f\tilde{\mathcal{Z}}\bar{\alpha}. \end{aligned} \tag{3.13}$$

Choosing $\bar{k}$ to be sufficiently large such that $\bar{k} \geqslant 1$, then it follows from (3.7) that

$$\Upsilon A + A^{\top}\Upsilon - 2\bar{k}\Upsilon BB^{\top}\Upsilon \leqslant -Q. \tag{3.14}$$

Letting $h^* = \left(\bar{g}\bar{h} + \bar{z}_{d_n}\right)$, and substituting (3.11), (3.12), (3.13), and (3.14) into (3.10), one proves that

$$\dot{V}(t) \leqslant -\omega^{\top}(t)Q\omega(t) + 4L_f\tilde{\mathcal{Z}}\bar{\alpha}\left(\omega^{\top}(t)\Upsilon B\right) + \frac{2\hat{h}(t)\left|\omega^{\top}(t)\Upsilon B\right|\delta(t)}{\hat{h}(t)|\omega^{\top}(t)\Upsilon B| + \delta(t)}. \tag{3.15}$$

By using the definition of adaptive law (3.6), $\|B\| = 1$, as well as $0 < \hat{h}(0) \in \mathbb{R}$, one yields $\frac{\hat{h}(t)|\omega^{\top}(t)\Upsilon B|\delta(t)}{\hat{h}(t)|\omega^{\top}(t)\Upsilon B| + \delta(t)} \leqslant \delta(t)$, then it derives from (3.15) that

$$\dot{V}(t) \leqslant -\|\omega(t)\|\left(\lambda_{\min}(Q)\|\omega(t)\| - 4\lambda_{\max}(\Upsilon)L_f\tilde{\mathcal{Z}}\bar{\alpha}\right) + 2\delta(t),$$

and then one obtains

$$V(t) + \int_0^T \hat{Q}(\zeta)\|\omega(\zeta)\|d\zeta \leqslant V(0) + 2\bar{\delta},$$

where $\hat{Q}(\zeta) = \lambda_{\min}(Q)\|\omega(\zeta)\| - 4\lambda_{\max}(\Upsilon)L_f\tilde{\mathcal{Z}}\bar{\alpha}$. If $\|\omega(t)\| > \frac{4\lambda_{\max}(\Upsilon)L_f\tilde{\mathcal{Z}}\bar{\alpha}}{\lambda_{\min}(Q)}$, we can derive that $V(t) \leqslant V(0) + 2\bar{\delta}$. Then, $\omega(t), \hat{k}(t)$, and $\hat{h}(t)$ are bounded. By using Barbalat's Lemma, one proves that the tracking error fulfills

$$\lim_{t\to+\infty} \hat{Q}(t)\|\omega(t)\| = 0$$

within the high probability $1-\varrho$, that is $\lim_{t\to+\infty}\|\omega(t)\| = \frac{4\lambda_{\max}(\Upsilon)L_f\tilde{\mathcal{Z}}\bar{\alpha}}{\lambda_{\min}(Q)}$, then the bound of tracking error can be obtained in Theorem 3.3.1. This proof is completed. ■

The state changing rate for system (3.1) based on controller (3.8) is probabilistic bounded shown as follows:

Lemma 3.3.1 (Probabilistic Bound)**.** *Suppose that the computational time bound $\bar{\alpha}$ fulfills $\bar{\alpha} < 1/L_f$. Under Assumptions 2.1.1, 3.2.1-3.3.1, $\|\dot{z}(t)\|$ has a probabilistic bound as*

$$\tilde{\mathcal{Z}} = \frac{1}{1 - L_f\bar{\alpha}}\left[\left(\|A\| + \hat{\bar{k}}\|\Upsilon\|\right)\sup_{z\in\mathbb{X}}\|z(t)\| + \bar{\Upsilon}\right]$$

for all $z(t) \in \mathbb{X}$ with the high probability $1-\varrho$, where $\bar{\Upsilon} = \hat{\bar{k}}\|\Upsilon\|\bar{z}_d^{\star} + \hat{\bar{h}} + \bar{g}\bar{h}$.

Proof. Substituting the controller (3.8) into system (3.1), system (3.1) can be rewritten as

$$\begin{aligned}\dot{z}(t) = Az(t) + B\Bigg(f(z(t)) - m_\phi(z(t_{\tau(t)})) - \bar{\beta}\sigma(z(t_{\tau(t)})) - \hat{k}(t)\omega^\top(t)\Upsilon B \\ - \frac{\hat{h}^2(t)\omega^\top(t)\Upsilon B}{\hat{h}(t)|\omega^\top(t)\Upsilon B| + \delta(t)} + g(z(t))\Delta h(t)\Bigg).\end{aligned} \tag{3.16}$$

Then, adopting the Lemma 2.1.1, $\|B\| = 1$, the proof of Theorem 3.3.1, the norm of $\dot{z}(t)$ is bounded by

$$\begin{aligned}\|\dot{z}(t)\| \leqslant \|A\|\|z(t)\| + L_f\|z(t) - z(t_{\tau(t)})\| + \hat{k}(t)\|\Upsilon\|(\|z(t)\| \\ + \|z_d^\star(t)\|) + \bar{g}\bar{h} + \frac{\hat{h}^2(t)|\omega^\top(t)\Upsilon B|}{\hat{h}(t)|\omega^\top(t)\Upsilon B| + \delta(t)}.\end{aligned} \tag{3.17}$$

Based on the proof of Theorem 3.3.1 and the definitions of adaptive gains (3.5) and laws (3.6), we can derive that $\hat{k}(t)$ and $\hat{h}(t)$ are positive and bounded with finite constant. Assume that the upper bounds of $\hat{k}(t)$ and $\hat{h}(t)$ are $\hat{\bar{k}}$ and $\hat{\bar{h}}$. Then, according to $\delta(t)$ defined in (3.5), one has $\frac{\hat{h}^2(t)|\omega^\top(t)\Upsilon B|}{\hat{h}(t)|\omega^\top(t)\Upsilon B| + \delta(t)} < \hat{h}(t) \leqslant \hat{\bar{h}}$.

The supremum of $\|\dot{z}(t)\|$ over $t \in \mathbb{R}_{0,+}$ is bounded by

$$\begin{aligned}\sup_{t\in\mathbb{R}_{0,+}} \|\dot{z}(t)\| \leqslant \left(\|A\| + \hat{\bar{k}}\|\Upsilon\|\right) \sup_{t\in\mathbb{R}_{0,+}} \|z(t)\| + \hat{\bar{h}} + \bar{g}\bar{h} \\ + L_f\bar{\alpha} \sup_{t\in\mathbb{R}_{0,+}} \left\|z(t) - z(t_{\tau(t)})\right\| + \hat{\bar{k}}\|\Upsilon\|\bar{z}_d^\star.\end{aligned} \tag{3.18}$$

Moreover, by using the mean value theorem on $\|z(t) - z(t_{\tau(t)})\|$, we can obtain

$$\begin{aligned}\sup_{t\in\mathbb{R}_{0,+}} \left\|z(t) - z(t_{\tau(t)})\right\| &= \sup_{\substack{t^*\in(t_{\tau(t)},t)\\ t\in\mathbb{R}_{0,+}}} \left\|\dot{z}(t^*)(t - t_{\tau(t)})\right\| \\ &\leqslant \sup_{\substack{t^*\in(t_{\tau(t)},t)\\ t\in\mathbb{R}_{0,+}}} \|\dot{z}(t^*)\| \left|t - t_{\tau(t)}\right| \\ &\leqslant \bar{\alpha} \sup_{\substack{t^*\in(t_{\tau(t)},t)\\ t\in\mathbb{R}_{0,+}}} \|\dot{z}(t^*)\|.\end{aligned} \tag{3.19}$$

Additionally, one gets $\sup\limits_{\substack{t^*\in(t_{\tau(t)},t)\\ t\in\mathbb{R}_{0,+}}} \|\dot{z}(t^*)\| \leqslant \sup\limits_{t\in\mathbb{R}_{0,+}} \|z(t)\|$ and $\sup\limits_{t\in\mathbb{R}_{0,+}} \|z(t)\| = \sup\limits_{z\in\mathbb{X}} \|z(t)\|$.

Based on the above equations, we can derive that

$$(1 - L_f\bar{\alpha}) \sup_{t\in\mathbb{R}_{0,+}} \|\dot{z}(t)\| \leqslant \left(\|A\| + \hat{\bar{k}}\|\Upsilon\|\right) \sup_{z\in\mathbb{X}} \|z(t)\| + \hat{\bar{k}}\|\Upsilon\|\bar{z}_d^\star + \hat{\bar{h}} + \bar{g}\bar{h}. \tag{3.20}$$

Considering that $z(t) \in \mathbb{X}$, where $\mathbb{X}$ is a compact set, it is reasonable to assume that $\sup_{z\in\mathbb{X}} \|z(t)\|$ is bounded. Moreover, since $\hat{\bar{k}}\|\Upsilon\|\bar{z}_d^\star, \hat{\bar{h}}$, and $\bar{g}\bar{h}$ are bounded, the upper bound of $\|\dot{z}(t)\|$ exists if $\bar{\alpha} < 1/L_f$. Therefore, the expression for the upper bound $\tilde{\mathcal{Z}}$ provided in Theorem 3.3.1 is derived. ■

The existence of the tracking error bound in Theorem 3.3.1 is determined by the finite predictable changing of the state, as reflected by the bounded state-changing rate $\|\dot{z}(t)\|$. Furthermore, the tracking error bound in Theorem 3.3.1 is influenced by the computational time of GP regression. Since the predictions need to be generated at every time instant in real-time control, the number of offline collected training data plays an important role in computational time. However, it remains challenging to decide how much data should be collected. Therefore, to improve the data efficiency and decrease the computational time, we further design an online learning-based adaptive FTC strategy based on the event-triggered strategy.

Remark 3.3.1. *This chapter addresses the challenges of model uncertainties and unknown actuator faults by leveraging GP-based adaptive FTC strategies. Unlike existing results on adaptive NN techniques for model approximation [65, 104–107], our approach effectively handles imperfect measurements and limited data. Moreover, non-ignorable computational delays are considered during real-time predictions, thereby enhancing the practical applicability of GP regression compared to prior works [28–36].*

3.4 Event-triggered Online Learning Strategy

This section provides the design and theoretical analysis of online learning-based adaptive FTC methods. Subsection 3.4.1 introduces the event-triggered model update strategy, while Subsection 3.4.2 establishes two sufficient conditions to ensure the proposed online method.

3.4.1 Event-triggered Model Update Strategy

As online data collection increases, the computational time of GP regression is affected, and the accuracy of system modelling may degrade due to inefficient or redundant data. To address this issue, we propose an event-triggered strategy to maintain data efficiency during updates to the probabilistic system model, thereby improving prediction perfor-

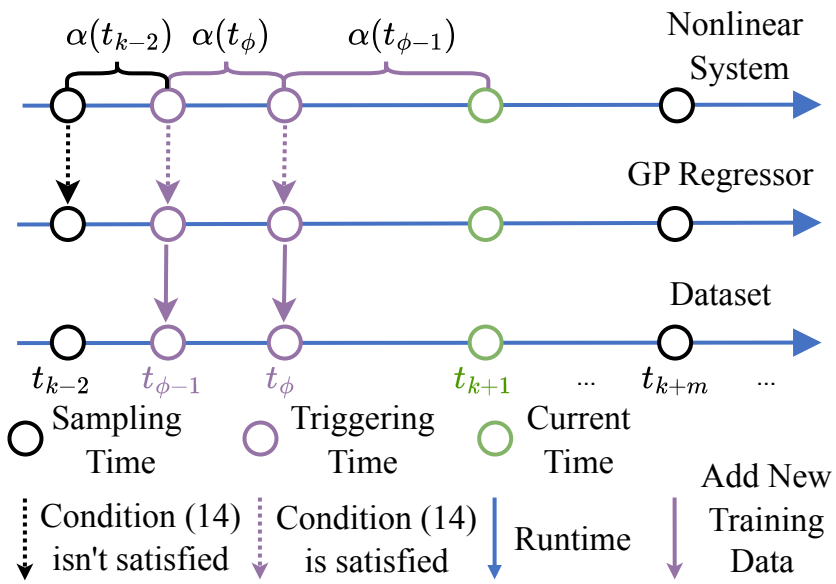

Figure 3.3: Mechanism of the event-triggered online learning strategy under delayed GP predictions. This method collects training data during real-time control.

mance. The controller is designed as follows:

$$\begin{aligned}\hat{u}(t) &= g^{-1}(z(t))(\hat{u}_1(t)+\hat{u}_2(t)),\\ \hat{u}_1(t) &= -\hat{k}(t)\omega^\top(t)\Upsilon B - \frac{\hat{h}^2(t)\omega^\top(t)\Upsilon B}{\hat{h}(t)|\omega^\top(t)\Upsilon B|+\delta(t)},\\ \hat{u}_2(t) &= \hat{u}_2(t_{\tau(t)}) = -m_\phi(z(t_{\tau(t)})).\end{aligned} \tag{3.21}$$

Then, we introduce an event-triggered online learning strategy that ensures the data $z^{[\phi+1]}$ and $y^{[\phi+1]}$ is incorporated into the dataset $\mathscr{D}_\phi$ at time $t_{\phi+1}$ according to the following condition:

$$t_{\phi+1} = \min\left\{t_k \geqslant t_\phi + \alpha(t_\phi) | \bar{\beta}\sigma_\phi(z(t_k)) \geqslant \vartheta(t_k,\bar{\omega},\bar{\alpha})\right\}, \tag{3.22}$$

where $t_k = 1,2,\cdots$. $t_{\phi+1}$ and t_ϕ are next and latest triggering times, respectively. $\vartheta(t_k,\bar{\omega},\bar{\alpha})$ is a trigger threshold function. To enhance understanding, we provide a figure to illustrate the mechanism of the event-triggered online learning strategy under delayed GP predictions (see Figure 3.3).

Remark 3.4.1 (Zeno Behavior Excluded)**.** *Compared to [29, 36], condition* (3.22) *cannot be evaluated at arbitrary times $t \in \mathbb{R}_{0,+}$, as we also consider the computational time required for the GP predictions. Given this, a minimal inter-event time $\Delta t^\phi_{\min} \geqslant \alpha(t_\phi) > 0$*

exists due to $t_{\phi+1} - t_\phi \geqslant \alpha(t_\phi)$*. Practically, all computations are started at discrete time* t_k*, such that the trigger condition has only access to* $z(t_k)$*, but new GP prediction* $m_\phi(\cdot)$ *are available earliest at* $t_k + \alpha(t_k)$*.*

3.4.2 Stability Analysis

In this subsection, we aim to develop two theoretical conditions that ensure the event-triggered strategy for updating the model. To proceed, we first propose a necessary lemma as follows:

Lemma 3.4.1 (Posterior Standard Deviation Bound)**.** *For the posterior variance function* $\sigma_N^2(\cdot)$ *defined in* (2.3) *and the SE function defined in* (2.5)*, if there are* N *training data points in dataset* $\mathscr{D}_N$*, then the following inequality holds at the test input* $z^\star$*:*

$$\sigma_N(z^\star) \leqslant \sqrt{\sigma_f^2 - \frac{\sum_{p=1}^{N} k(z^{[p]}, z^\star)^2}{N\sigma_f^2 + \sigma_n^2}}. \tag{3.23}$$

Proof. If there exists N training data at test input $z^\star$, then according to (2.3) and (2.5), we can obtain

$$\begin{aligned}
\sigma_N^2(z^\star) &= k^\star - \boldsymbol{k}^\top (\boldsymbol{K} + \sigma_n^2 I_N)^{-1} \boldsymbol{k} \\
&= \sigma_f^2 - \boldsymbol{k}^\top (\boldsymbol{K} + \sigma_n^2 I_N)^{-1} \boldsymbol{k} \\
&\leqslant \sigma_f^2 - \|\boldsymbol{k}\|^2 \lambda_{\min}\left((\boldsymbol{K} + \sigma_n^2 I_N)^{-1}\right) \\
&= \sigma_f^2 - \frac{\sum_{p=1}^{N} k(z^{[p]}, z^\star)^2}{\lambda_{\max}(\boldsymbol{K}) + \sigma_n^2} \\
&\leqslant \sigma_f^2 - \frac{\sum_{p=1}^{N} k(z^{[p]}, z^\star)^2}{N\sigma_f^2 + \sigma_n^2},
\end{aligned} \tag{3.24}$$

where the last inequality uses the Gershgorin circle theorem and $\boldsymbol{K}_{(p,q)} = k\left(z^{[p]}, z^{[q]}\right) \leqslant \sigma_f^2, p, q \in \{1, 2, \cdots, N\}$.

Therefore, one concludes that posterior standard deviation $\sigma_N(\cdot)$ satisfies $\sigma_N(z^\star) \leqslant \sqrt{\sigma_f^2 - \frac{\sum_{p=1}^{N} k(z^p, z^\star)^2}{N\sigma_f^2 + \sigma_n^2}}$. ■

Then, we develop the following theoretical condition:

Theorem 3.4.1 (Event-triggered Condition)**.** *Assume that the computational time bound $\bar{\alpha}$ fulfills $\bar{\alpha} < 1/L_f$ and select $\bar{\omega} \geqslant 2\left(\tilde{\mathcal{Z}} + \tilde{\mathcal{Z}}_d^\star\right)\bar{\alpha} + 4\eta L_f \tilde{\mathcal{Z}}\bar{\alpha} + \bar{\beta}\bar{\sigma}_\phi(z(t_k))$. Under Assumptions 2.1.1, 3.2.1-3.3.1, event-triggered threshold function* (3.22) *satisfies*

$$\vartheta(t_k, \bar{\omega}, \bar{\alpha}) = \frac{1}{2\eta}\left[\max(\|\omega(t_k)\|, \bar{\omega}) - 2\left(\tilde{\mathcal{Z}} + \tilde{\mathcal{Z}}_d^\star\right)\bar{\alpha}\right] - 2L_f\tilde{\mathcal{Z}}\bar{\alpha}, \tag{3.25}$$

where $\bar{\sigma}_\phi(z(t_k))$ indicates the upper bound of posterior standard deviation $\sigma_\phi(z(t_k))$ with

$$\bar{\sigma}_\phi(z(t_k)) = \begin{cases} \sigma_f, & \text{if } \mathscr{D}_\phi = \emptyset, \\ \sqrt{\sigma_f^2 - \dfrac{\sum_{p=1}^{N_\phi} k(z^{[p]}, z(t_k))^2}{N_\phi\sigma_f^2 + \sigma_n^2}}, & \text{if } \mathscr{D}_\phi \neq \emptyset, \end{cases} \tag{3.26}$$

$\eta = \frac{\lambda_{\max}(\Upsilon)}{\lambda_{\min}(Q)}, \tilde{\mathcal{Z}}_d^\star \geqslant \|\dot{z}_d^\star(t)\|, \forall t \in \mathbb{R}_{0,+}$. The tracking error is bounded by $\bar{\omega}$ with the high probability $1-\rho$.

Proof. The proof is separated into the discussion of two different cases at time $t_{\tau(t)}$. Firstly, we consider the case with $\|\omega(t_{\tau(t)})\| > 2(\tilde{\mathcal{Z}} + \tilde{\mathcal{Z}}_d^\star)\bar{\alpha} + 4\eta L_f\tilde{Z}\bar{\alpha} + 2\eta\bar{\beta}\sigma_\phi(z(t_{\tau(t)}))$. In what follows, we can have

$$\begin{aligned} \|\omega(t)\| &\geqslant \|\omega(t_{\tau(t)})\| - \|\omega(t) - \omega(t_{\tau(t)})\| \\ &\geqslant \|\omega(t_{\tau(t)})\| - \left(\|z(t) - z(t_{\tau(t)})\| + \|z_d^\star(t) - z_d^\star(t_{\tau(t)})\|\right) \\ &\geqslant \|\omega(t_{\tau(t)})\| - 2\left(\tilde{\mathcal{Z}} + \tilde{\mathcal{Z}}_d^\star\right)\bar{\alpha}. \end{aligned} \tag{3.27}$$

Via controller (3.21) and (3.27), $\dot{V}(t)$ can be rewritten as

$$\dot{V}(t) \leqslant -\lambda_{\min}(Q)\|\omega(t)\|\left(\hat{w}(t_{\tau(t)}) - 2\eta\bar{\beta}\sigma_\phi(z(t_{\tau(t)}))\right) + 2\delta(t), \tag{3.28}$$

where $\eta = \frac{\lambda_{\max}(\Upsilon)}{\lambda_{\min}(Q)}, \hat{w}(t_{\tau(t)}) = \|\omega(t_{\tau(t)})\| - 2\left(\tilde{\mathcal{Z}} + \tilde{\mathcal{Z}}_d^\star\right)\bar{\alpha} - 4\eta L_f\tilde{Z}\bar{\alpha}$, and then the convergence of $\|\omega(t)\|$ can be obtained according to the proof of Theorem 3.3.1.

If the tracking error at $t_{\tau(t)}$ fulfills $\bar{\omega} \leqslant \|\omega(t_{\tau(t)})\| \leqslant 2\left(\tilde{\mathcal{Z}} + \tilde{\mathcal{Z}}_d^\star\right)\bar{\alpha} + 4\eta L_f\tilde{Z}\bar{\alpha} + 2\eta\bar{\beta}$ $\sigma_\phi(z(t_{\tau(t)}))$, then condition (3.22) is triggered since

$$\bar{\beta}\sigma_\phi(z(t_{\tau(t)})) \geqslant \vartheta(t_{\tau(t)}, \bar{\omega}, \bar{\alpha}),$$

where threshold function $\vartheta(t_{\tau(t)}, \bar{\omega}, \bar{\alpha}) = \frac{1}{2\eta}\left[\|\omega(t_{\tau(t)})\| - 2\left(\tilde{\mathcal{Z}} + \tilde{\mathcal{Z}}_d^\star\right)\bar{\alpha}\right] - 2L_f\tilde{\mathcal{Z}}\bar{\alpha}$, and new observations $z^{[\phi+1]}, y^{[\phi+1]}$ are added in the training dataset. With the increase of training data, we can obtain standard deviation $\sigma_{\phi+1} < \sigma_\phi$ [11, 43]. According to Lemma 3.4.1 and [29], one derives that $\sigma_\phi \leqslant \bar{\sigma}_\phi$, where $\bar{\sigma}_\phi = \sqrt{\sigma_f^2 - \frac{\sum_{p=1}^{N_\phi} k(z^{[p]}, z(t_{\tau(t)}))^2}{N_\phi\sigma_f^2 + \sigma_n^2}}$.

Considering that there exists no training data in dataset $\mathscr{D}_\phi$ before condition (3.22) is triggered, we obtain

$$\bar{\sigma}_\phi(z(t_{\tau(t)})) = \begin{cases} \sigma_f, & \text{if } \mathscr{D}_\phi = \emptyset, \\ \sqrt{\sigma_f^2 - \dfrac{\sum_{p=1}^{N_\phi} k(z^{[p]}, z(t_{\tau(t)})^2}{N_\phi \sigma_f^2 + \sigma_n^2}}, & \text{if } \mathscr{D}_\phi \neq \emptyset. \end{cases}$$

After training data is collected and the model is updated, the convergence of $\|\omega(t)\|$ can be derived by

$$\dot{V}(t) \leqslant -\lambda_{\min}(Q)\|\omega(t)\| \left(\hat{w}(t_{\tau(t)}) - 2\eta\bar{\beta}\bar{\sigma}_\phi(z(t_{\tau(t)}))\right) + 2\delta(t). \tag{3.29}$$

Therefore, we can conclude that the proposed event-triggered strategies (3.22) and (3.25) can guarantee the convergence of the tracking error when $\|\omega(t)\| \geqslant \bar{\omega}$. ■

Condition (3.25) cannot guarantee arbitrarily small tracking error bounds due to the delayed effects of model updating. Despite this limitation, triggered condition (3.25) ensures that smaller tracking error bounds can be achieved through more frequent model updates. Furthermore, Theorem 3.4.1 offers an effective approach for determining the error bound $\bar{\omega}$.

Remark 3.4.2. *Compared to offline learning-based control, online learning-based control offers improved fitting performance for unknown system dynamics but may incur higher computational time due to frequent model updates. However, obtaining accurate and efficient training data can be challenging in practical applications due to inefficient sampling or the high cost of simulation. Therefore, this section further investigates the event-triggered online learning method.*

3.5 Numerical Simulations

This section presents numerical simulations to validate the effectiveness and competitiveness of the proposed control methods in trajectory tracking, fitting unknown dynamics, and compensating for unknown actuator faults.

3.5.1 Simulation Setup

We aim to validate the theoretical results and proposed control methods, namely offline learning-based adaptive FTC (`GP-AFTC`) and event-triggered data-driven adaptive FTC

(ET-DDAFTC), through two examples. Additionally, we analyze the impact of computational delay $\alpha(t)$ on learning-based control by considering four different cases of computational delays for each example. Furthermore, our control methods are compared with two existing works: the NN-based finite-time adaptive FTC method (NN-FTAFTC) [65] and the event-triggered data-driven control method (ET-DDC) [29].

To investigate the influence of the computational delay $\alpha(t)$ for tracking errors, we suppose that $\alpha(t) = \bar{\alpha}$ and respectively select $\bar{\alpha} = 0.01\text{s}, 0.1\text{s}, 0.5\text{s}, 1\text{s}$.

Consider a pendulum system with $n = 2$ with control input as follows [57]:

$$\begin{aligned} \dot{z}_1(t) &= z_2(t) \\ \dot{z}_2(t) &= -\frac{g}{l}\sin(z_1(t)) - \frac{b}{ml^2}z_2(t) + \frac{1}{ml^2}u(t), \end{aligned} \tag{3.30}$$

where unknown dynamic $f(z(t)) = -\frac{g}{l}\sin(z_1(t)) - \frac{b}{ml^2}z_2(t)$ satisfies Assumption 3.2.1. $g(z(t)) = \frac{1}{ml^2}$. m represents the mass of this system. l is the pendulum length. g indicates gravitational acceleration. b refers to the coefficient of friction. Then, we choose $m = 0.1\text{kg}$, $l = 1\text{m}$, $b = 0.1\text{kg} * \text{m}^2/\text{s}$, and $g = 9.8\text{m}^2/\text{s}$, selecting the initial state of system (3.30) as $z_0 = [3,2]^\top$ and denoting desired trajectory $z_d^\star(t) = [z_d(t), \dot{z}_d(t)]^\top$ with $z_d(t) = \sin(t)$. Moreover, the actuator bias fault can be considered as follows:

$$u_F(t) = \hat{u}(t) + \Delta h(t), \quad \forall t \geqslant t_F,$$

where we assume that system (3.30) suffers from bias faults $\Delta h(t) = 0.5\cos(t), t \in [1\text{s}, 7.5\text{s})$ and $\Delta h(t) = 0.3\cos(t), t \in [7.5\text{s}, 15\text{s})$. Then, we set $k_1 = 6$ and $h_1 = 2$ for the adaptive law and choose $\delta(t) = \exp(-0.3t)$ for the controller. The hyperparameters are initialized as $\sigma_f = 1$ and $l = 1$ in SE function (2.5).

According to above-mentioned system parameters as well as selecting $Q = 5 * I_2$, and solving condition (3.7), matrix Υ can be obtained as $\Upsilon = \begin{bmatrix} 6.3884 & 1.5811 \\ 1.5811 & 2.0202 \end{bmatrix}$.

3.5.2 Simulation Results

3.5.2.1 Offline Learning-based AFTC

Collecting training data: Assume that there aren't any faults occurring during this period, and we design a PD controller as $u_{\text{collect}}(t) = -k_P\omega_1(t) - k_D\omega_2(t)$ with control gains $k_P = 7$ and $k_D = 5$ selected according to [113]. System (3.30) is initialized 3 times, where its initial values are randomly selected from the interval $[-5,5] \times [-5,5]$ based

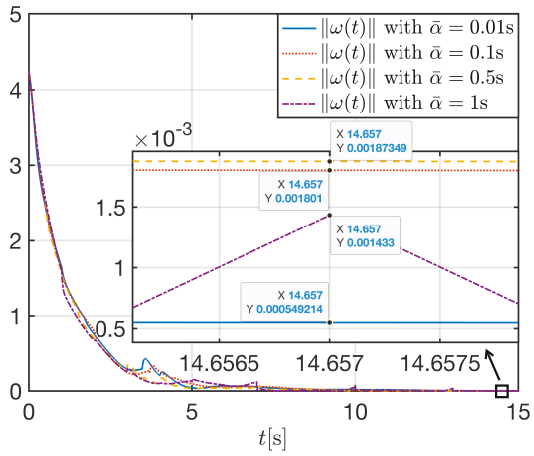

(a) Profiles of the norms of tracking errors.

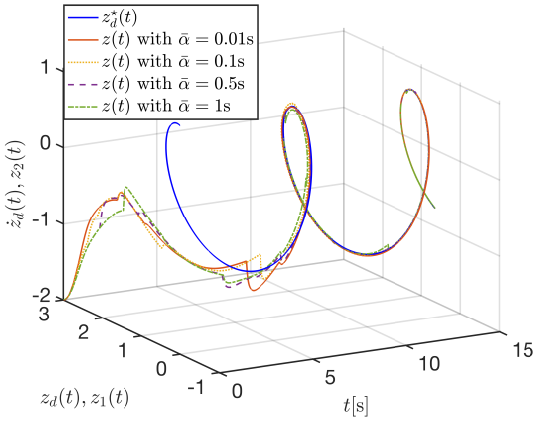

(b) Profiles of system states.

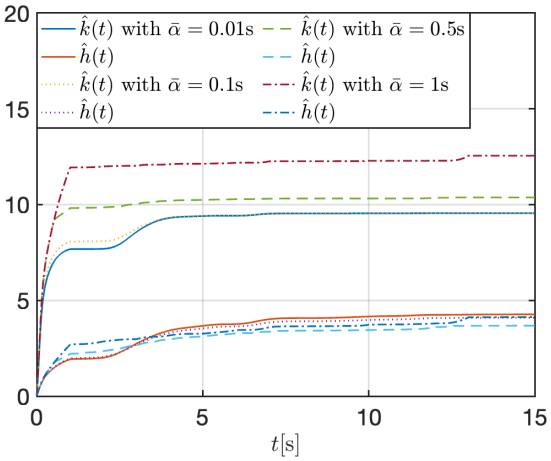

(c) Profiles of adaptive laws.

Figure 3.4: Simulation results of offline learning-based adaptive FTC.

on a uniform distribution, and $t^c_{\max} = 4$s with a sampled time step of 0.1s, resulting in a training dataset $\mathscr{D}_{t^c_{\max}}$. Observations of $f(z(t))$ are perturbed with $\mathcal{N}(0, \sigma_n^2)$ with $\sigma_n = 0.1$. Then, we choose $\bar{\beta} = 2$ and apply posterior mean $\mu_{t^c_{\max}}(\cdot)$ and variance $\sigma_{t^c_{\max}}(\cdot)$ generated in each time instant for controller (3.8). Furthermore, different computational delays are respectively testified.

As shown in Figure 3.4(a), $\|\omega(t)\|$ increases with the rise in computational delays, and this figure also demonstrates that the error bound $\bar{\omega}$ in Theorem 3.3.1 increases with the rise in computational delays. Although $\|\omega(t)\|$ is influenced by computational delays as shown in Figure 3.4(a), the error remains small subject to actuator faults based on controller (3.8). Figure 3.4(b) illustrates the evolutions of desired trajectory $z_d^\star(t)$ and system state $z(t)$ with different computational delays, and system state $z(t)$ generally approaches desired trajectory $z_d^\star(t)$ based on controller (3.8). In Figure 3.4(c), the values of $\hat{k}(t)$ and $\hat{h}(t)$, respectively, converge to bounded positive values, and their bounded values increase with the rise in computational delays. Given this, one concludes that offline-based controller (3.8) ensures system (3.30) track the desired trajectory under unknown system dynamics and actuator faults.

3.5.2.2 Event-triggered Data-driven AFTC

Event-triggered model updating: We select the same parameters values as those used in Section 3.5.1: $\bar{\beta}$ for condition (3.22) and $\bar{\sigma}_\phi$ based on (3.26) for error bound $\bar{\omega}$ for condition (3.25) with $\bar{\omega} = 2\left(\tilde{\mathcal{Z}} + \tilde{\mathcal{Z}}_d^\star\right)\bar{\alpha} + 4\eta L_f \tilde{\mathcal{Z}}\bar{\alpha} + \bar{\beta}\bar{\sigma}_\phi$.

Then, generated posterior means and variances in each time instant are respectively applied in controller (3.21) and event-triggered condition (3.22). Moreover, their performance is demonstrated under different computational delays. Figure 3.5(a) shows that $\|\omega(t)\|$ remains bounded based on controller (3.21). Compared to offline learning scenarios at equivalent time instants, $\|\omega(t)\|$ shown in Figure 3.5(a), is smaller for computation times of 0.5s and 1s, but larger for computation times of 0.01s and 0.1s. The reason is that error bound $\bar{\omega}$ obtained in Theorem 3.4.1 is different from error bound $\bar{\omega}$ derived in Theorem 3.3.1 for different computation times. As shown in Figure 3.5(b), controller (3.21) can also assist system (3.30) in tracking the desired trajectory, and one observes that online-based controller (3.21) have a better performance than offline-based controller (3.8) during the initial phase of the simulation. In Figure 3.5(c), one finds that adaptive gains $\hat{k}(t)$ can converge lower bounded positive values than in Figure 3.4(c) but the values of $\hat{h}(t)$ remain similar. As depicted in Figure 3.5(d), one observes that new

data collection mainly occurs before 12s, and the number of data collected in different computational delays respectively is 15 in $\bar{\alpha} = 0.01$s, 8 in $\bar{\alpha} = 0.1$s, 6 in $\bar{\alpha} = 0.5$s, and 5 in $\bar{\alpha} = 1$s, which is less than 120 offline training data.

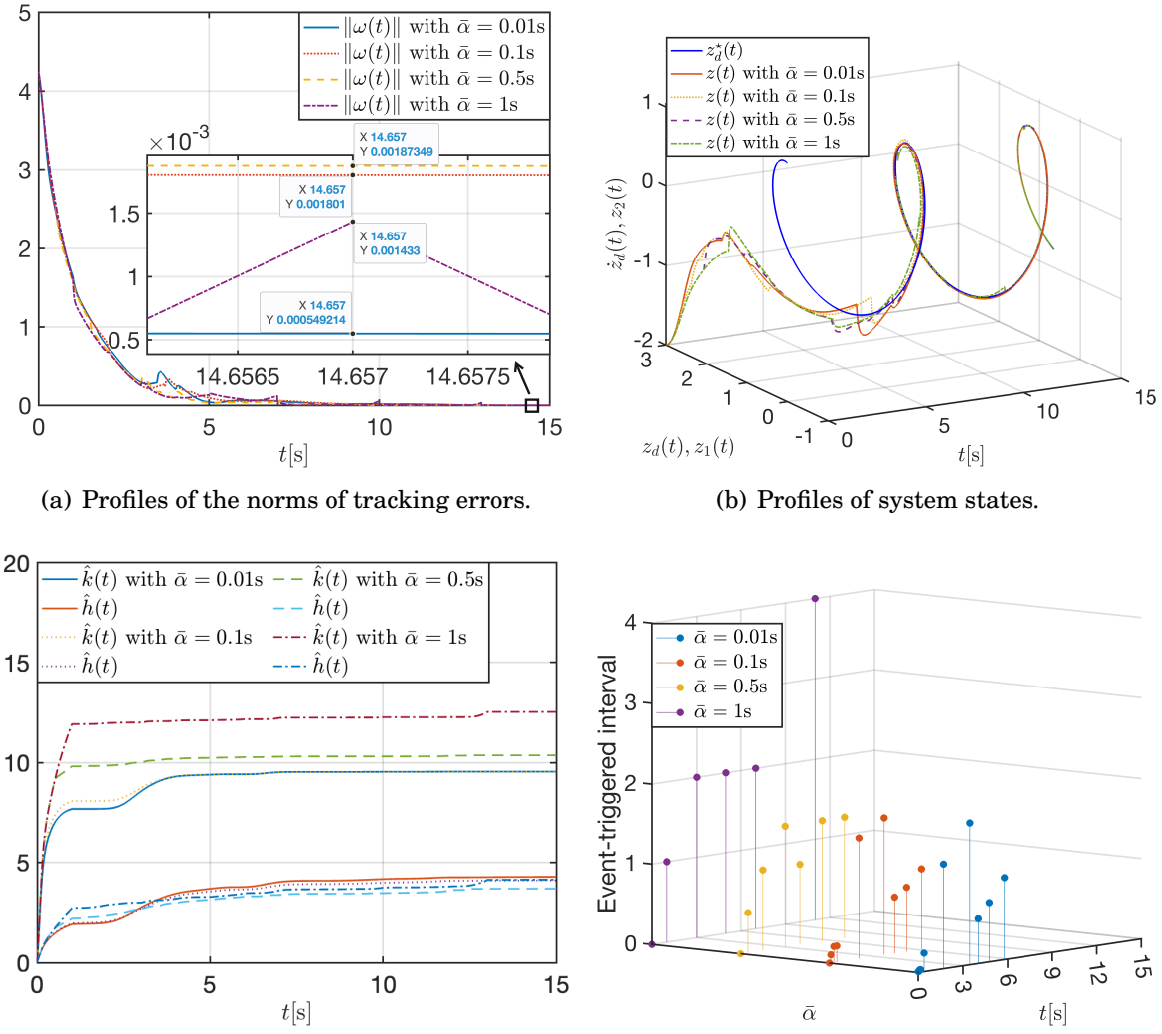

(a) Profiles of the norms of tracking errors.

(b) Profiles of system states.

(c) Profiles of adaptive laws.

(d) Event-triggered strategy.

Figure 3.5: Simulation results of event-triggered data-driven adaptive FTC.

Therefore, we can conclude that online learning-based adaptive fault-tolerant controller (3.21) can assist system (3.30) in tracking the desired trajectory under both unknown system dynamics and actuator faults.

3.5.2.3 Performance Comparisons

Comparisons with [65] and [29]: We illustrate the competitiveness of proposed control strategies in this chapter through comparisons with the findings presented NN-FTAFTC in [65] and ET-DDC in [29]. For fair comparisons, we maintain identical system parameters and actuator fault values, adopt the same controller parameters used in Sections 3.5.2.1 and 3.5.2.2. Controller parameters are selected from [65] and [29], and take computational delay $\bar{\alpha} = 0.01$s. Moreover, some of the parameters for the NN in [65] are chosen from [104]. Note that this section only concentrates on the comparisons of the control performance. As shown in Figure 3.6(a), $\|\omega(t)\|$ under NN-FTAFTC has the fastest convergence speed but has a worse convergence performance compared to other methods. Although ET-DDC is not an FTC method, it contributes to the convergence of $\|\omega(t)\|$ to a small value in Figure 3.6(a), as actuator bias faults may be treated as data noise through online data collection. As depicted in Figure 3.6(a), $\|\omega(t)\|$ can be converges to small values under ET-DDAFTC and GP-AFTC. In certain instances, ET-DDAFTC helps $\|\omega(t)\|$ converge smaller values than GP-AFTC. Figure 3.6(b) shows the evolution of system state $z(t)$ under different control methods and desired trajectory $z_d^\star(t)$. GP-AFTC and NN-FTAFTC have worse control performance at the beginning of the simulation. Therefore, one concludes that ET-DDAFTC and GP-AFTC of this chapter show better control performance than NN-FTAFTC in [65] and ET-DDC in [29].

Comparisons between online and offline learning: Although tracking error bound $\bar{\omega}$ under offline learning is lower than under online learning from theoretical analysis, opposite phenomena may exist in the simulation. To further explore the reason, we take four different types of offline collection data and show control performance compared with online learning. We set $\bar{\alpha} = 0.01$s and four different initialization times, namely $2, 3, 4$, and 6, along with the collect time $t_{\max}^c$ respectively set to 6s, 4s, 3s, and 2s. The total number of training data is fixed at 120 for each of these four collections. As depicted in Figure 3.6(c), tracking error $\omega(t)$ exhibits the worst convergence performance among all methods based on offline dataset 4, and online collection can assist $\|\omega(t)\|$ in keeping smaller values at most simulation times. The differences in the tracking errors among offline datasets 1, 2, and 3, as shown in Figure 3.6(c), are not significant. Figure 3.6(d) illustrates the evolution of system state $z(t)$ and desired trajectory $z_d^\star(t)$. However, the online collection exhibits poor tracking performance during the first 5s of the simulation, while the convergence of $z(t)$ is comparable for offline datasets 1 and 2, as shown in Figure 3.6(d). Offline datasets 3 and 4 demonstrate worse tracking performance, with

offline dataset 4 performing the worst among all datasets. Based on these simulation results, we conclude that longer collection times are beneficial for GP−AFTC, whereas increasing initialization times may not provide significant advantages for offline learning. While the event-triggered online collection achieves better tracking performance, it does not guarantee smaller error bounds.

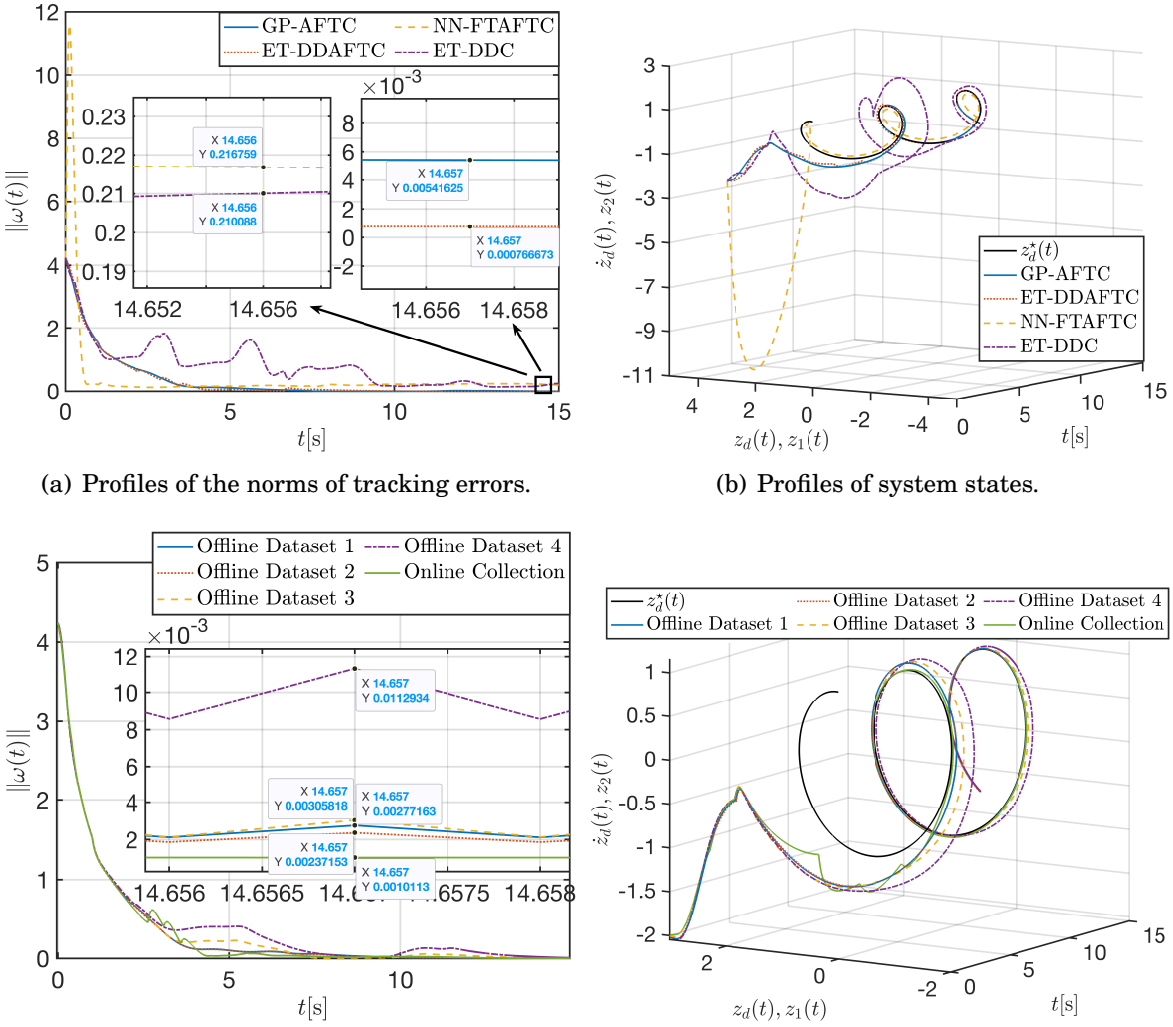

(a) Profiles of the norms of tracking errors.

(b) Profiles of system states.

(c) Profiles of tracking errors.

(d) Profiles of system states.

Figure 3.6: Comparative results of control performance among offline and online methods, NN−FTAFTC, and ET−DDC.

Remark 3.5.1. *From theoretical analysis, tracking error bounds under offline learning are smaller than under online learning. However, opposite phenomena may occur in the simulation. The main reason is that the direct impact of data efficiency on controllers is*

not explicitly reflected in theoretical results. Therefore, event-triggered online collection can help controllers achieve better performance in practical applications compared to offline training data collection.

Remark 3.5.2 (Limitation)**.** *While GP−AFTC and ET−DDAFTC methods have shown potential for addressing unknown actuator bias faults and system dynamics, they also have several limitations. Firstly, we consider unknown dynamics in drift dynamics, but input gain dynamics are assumed to be known. However, input gain dynamics are commonly unknown in some cases. Additionally, we investigate the case of unknown actuator bias faults but do not address unknown actuator gain faults. Actuator gain faults should not be ignored. Therefore, future research should focus on more general nonlinear systems with unknown drift and gain dynamics, exploring methods to deal with both unknown gain and bias faults.*

3.6 Conclusion

In this chapter, we have proposed two GP-based adaptive FTC methods to address actuator faults and model uncertainties. We have considered the impact of computational delays and developed four probabilistic theoretical conditions to ensure the validity of the proposed control methods. Finally, numerical simulations have demonstrated the effectiveness and competitiveness of theoretical results and control strategies.

CHAPTER 4

LEARNING-BASED FAULT-TOLERANT CONTROL WITH HIGH-ORDER CONTROL BARRIER FUNCTIONS

This chapter is based on the paper titled "Learning-Based Fault-Tolerant Control with High-Order Control Barrier Functions," IEEE Transactions on Automation Science and Engineering, vol. 22, pp. 14689-14698, 2025.

To deal with RQ2 and achieve RO2, this chapter proposes a novel probabilistically fault-tolerant safe control framework that integrates GP regression, the FTC strategy, and the HOCBF method. To handle inherent uncertainty, we adopt a probabilistic method that combines CLF with HOCBF using GP regression. Building on this foundation, we design a fault-tolerant GP-based CLF-HOCBF method to address unknown actuator faults. Furthermore, we establish two theoretical criteria to ensure the probabilistic safety and stability of the proposed control framework. To validate our method, we implement it in the autonomous driving simulator CARLA, demonstrating its effectiveness and competitiveness compared to existing approaches.

This chapter is structured as follows. Section 4.1 reviews related work closely associated with the topic of this study. Section 4.2 outlines the essential background and

preparatory material. The principal findings of this chapter are detailed in Sections 4.3 and 4.4. Section 4.5 illustrates the two proposed approaches through numerical simulations. The chapter concludes with a summary provided in Section 4.6. Moreover, an overview of the methods developed in this chapter is depicted in Figure 4.1.

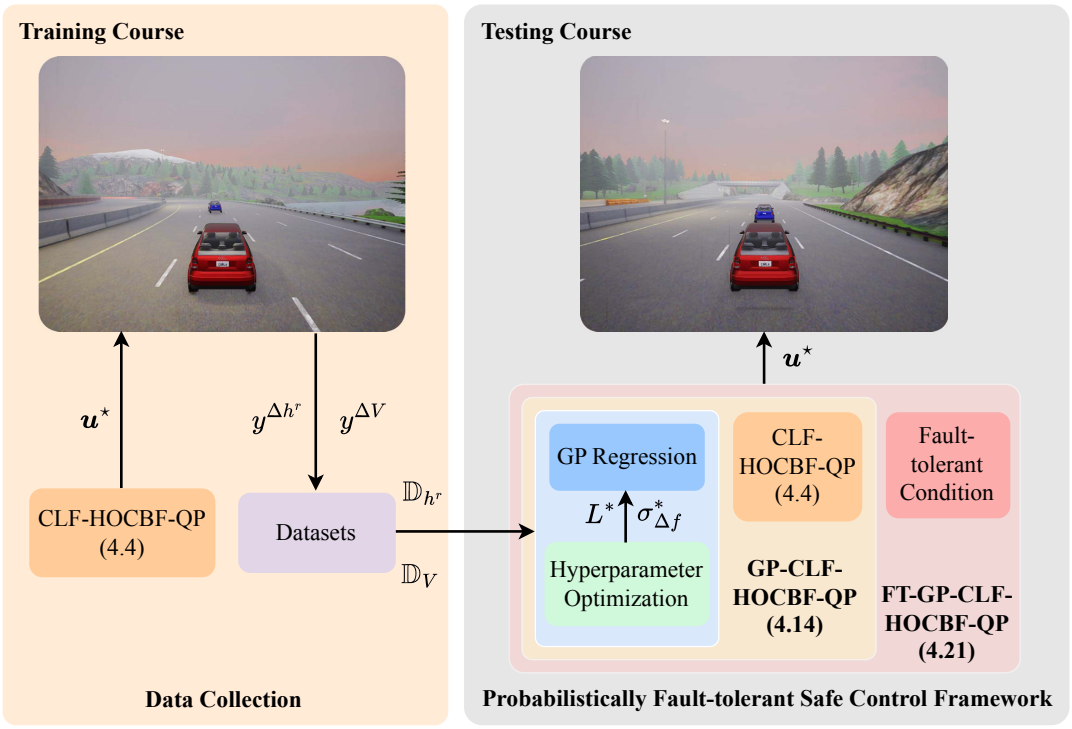

Figure 4.1: An overview of a probabilistically fault-tolerant safe control framework. In this framework, GP regression is applied to model uncertain constraints, and the fault-tolerant condition is designed to enhance the performance of systems subject to unknown actuator bias faults.

4.1 Introduction

As a powerful theoretical tool for synthesizing controllers that guarantee the safety of dynamical systems, the CBF method has garnered considerable attention and has been applied in areas such as autonomous driving and bipedal walking [21]. To handle model uncertainty, researchers have proposed various extensions, including the adaptive CBF

method [80, 81], RL-based CBF method [84], and robust CBF method [79], among others. As stated in [81], the authors exploited a robust-adaptive CBF method to ensure the safety of nonlinear systems and estimated unstructured parametric uncertainties using the dynamic regressor extension and mixing method. Lopez et al. [80] developed a robust adaptive CBF framework and dealt with structured parametric uncertainties based on an adaptive data-driven strategy and a set membership identification method. In [84], the authors used RL to estimate model uncertainty and designed an RL-CLF-CBF method to guarantee the safety of the system. By using the episodic learning framework, Taylor et al. [79] investigated a learning-based CBF method to deal with model uncertainty. Note that the above studies rely on accurate output measurements and will be disturbed by imperfect measurements. Given this, scholars further leveraged GP regression to fit model uncertainty [34, 37]. As stated in [34], the authors used GP regression to establish a GP-CLF-CBF method to handle model uncertainty. Mestres et al. [37] further explored the safety stabilization of systems and studied regularity properties of various controllers fulfilling the constraints of GP-CLF and GP-CBF. Unlike the aforementioned methods [79–81, 84], GP regression can generate a probabilistic method to fit model uncertainty and exhibit the robustness against measurement noise.

However, the above CBF methods are only suitable for systems with a relative degree of one. To overcome this limitation, a HOCBF method has been proposed, which can be applied to control systems with arbitrary relative degrees, extending its applicability to a wide range of robotic systems. Researchers have further developed the robust adaptive HOCBF method [114] and the GP-based HOCBF approach [25, 38] to handle model uncertainty. As stated in [114], the authors used a concurrent learning method to approximate structured uncertainties and proposed a robust adaptive CLF-HOCBF quadratic programming (CLF-HOCBF-QP) method. Aali et al. [38] designed the GP-based HOCBF approach to handle model uncertainty. In [25], the authors proposed a

sparse GP techique for HOCBF frameworks in the presence of model uncertainty. Different from model uncertainty, faults pose potential threaten to systems, as their occurrence is random. Therefore, researchers studied FTC to handle faults [115]. To ensure the safety of faulty systems, scholars designed a fault-tolerant safety-critical control method [27, 116]. To mitigate the influence of actuator gain faults in safety-critical systems, Dong et al. [27] presented a fault-tolerant HOCBF method based on the robust method. As stated in [116], the authors proposed a fault-tolerant neural CBF method to tackle sensor faults and attacks. However, the above studies [27, 116] only consider the case of faults. Therefore, this chapter aims to develop a GP-based CLF-HOCBF-QP method with fault tolerance to address model uncertainty and unknown actuator bias faults, ensuring the safety of faulty systems.

4.2 Background and Preliminaries

4.2.1 Notations and Definitions

Throughout this chapter, $\mathbb{R}$ denotes the set of real numbers. $\mathbb{R}^+$ stands for the set of positive real numbers. $\mathbb{R}^n$ refers to n-dimensional Euclidean space, and $\mathbb{R}^{n\times m}$ stands for the space of $n \times m$ real matrices. $\Pr\{\cdot\}$ is probability of an event. $\|\cdot\|$ is the Euclidean norm. $|\cdot|$ presents absolute value.

Consider the following nonlinear control affine system:

$$\dot{\boldsymbol{x}} = \boldsymbol{f}(\boldsymbol{x}) + \boldsymbol{g}(\boldsymbol{x})\boldsymbol{u}, \tag{4.1}$$

where $\boldsymbol{x} \in \mathbb{R}^n$ and $\boldsymbol{u} \in \mathbb{R}^m$ refer to the state of the system and control input, respectively. $\boldsymbol{f}(\boldsymbol{x}) : \mathbb{R}^n \to \mathbb{R}^n$ and $\boldsymbol{g}(\boldsymbol{x}) : \mathbb{R}^n \to \mathbb{R}^{n\times m}$ stand for the drift dynamic and input dynamic, and both $\boldsymbol{f}(\boldsymbol{x})$ and $\boldsymbol{g}(\boldsymbol{x})$ are locally Lipschitz continuous. In practical applications, control input should be constrained and satisfied $\boldsymbol{u} \in \mathbb{U}$, in which $\mathbb{U}$ is a compact set.

Definition 4.2.1 (CLF [21])**.** *If there exist a differentiable continuously positive definite function $V : \mathbb{R}^n \to \mathbb{R}^+$ and a class $\mathcal{K}$: function $\xi(\cdot)$ such that*

$$\inf_{u\in\mathbb{U}} \left\{ L_f V(\boldsymbol{x}) + L_g V(\boldsymbol{x})\boldsymbol{u} - \xi(V(\boldsymbol{x})) \right\} \leqslant 0, \tag{4.2}$$

for all $\boldsymbol{x} \in \mathcal{D}$, then function V is said to be CLF on set $\mathcal{D}$.

4.2.2 High-Order CBFs

Above Definition 2.3.4 can provide a safety guarantee for system (4.1) based on a function h. Note that the feasibility and efficiency of this definition depends on $L_f h(\boldsymbol{x})\boldsymbol{u} \neq 0$. However, as stated in [94], the control input $\boldsymbol{u}$ does not appear due to $L_f h(\boldsymbol{x})\boldsymbol{u} = 0$ as defined by (2.16). To address this issue, this section further introduces HOCBFs. Assume that a function h satisfies Definition 2.4.2, one derives

Definition 4.2.2 (HOCBF [94, 117])**.** *Define a sequence of functions $\beta_i(\boldsymbol{x})$ satisfying $\beta_0(\boldsymbol{x}) = h(\boldsymbol{x}), \beta_i(\boldsymbol{x}) = \dot{\beta}_{i-1}(\boldsymbol{x}) + \alpha_i(\beta_{i-1}(\boldsymbol{x})), i \in \{1, \cdots, r-1\}$, and $\beta_r(\boldsymbol{x}, \boldsymbol{u}) = \dot{\beta}_{r-1}(\boldsymbol{x}, \boldsymbol{u}) + \alpha_r(\beta_{r-1}(\boldsymbol{x}))$, where $\alpha_i(\cdot)$ is a sequence of class $\mathcal{K}$ functions. Let $\mathscr{A}_i$ be a sequence of sets defined as $\mathscr{A}_i = \{\boldsymbol{x} \in \mathbb{R}^n : \beta_{i-1}(\boldsymbol{x}) > 0\}$. Then, the function $h : \mathbb{R}^n \to \mathbb{R}$ is said to be a candidate HOCBF of relative degree r for system* (4.1) *on an open set $\hat{\mathscr{A}}$ satisfying $\bigcap_{i=1}^{r} \mathscr{A}_i \subset \hat{\mathscr{A}}$, if there exists a sequence of functions $\alpha_i(\cdot)$ and function h has relative degree r on some nonempty $\mathbb{X} \subseteq \hat{\mathscr{A}}$ such that*

$$\sup_{\boldsymbol{u} \in \mathbb{U}} \underbrace{\left\{ L_f \beta_{r-1}(\boldsymbol{x}) + L_g \beta_{r-1}(\boldsymbol{x})\boldsymbol{u} + \alpha_r(\beta_{r-1}(\boldsymbol{x})) \right\}}_{\beta_r(\boldsymbol{x}, \boldsymbol{u})} \geqslant 0, \forall \boldsymbol{x} \in \hat{\mathscr{A}}, \tag{4.3}$$

where $L_f \beta_{r-1}(\boldsymbol{x}) = L_f^r h(\boldsymbol{x}) + \sum_{i=1}^{r-1} L_f^i(\alpha_{r-i} \circ \beta_{r-i-1})(\boldsymbol{x})$ and $L_g \beta_{r-1}(\boldsymbol{x}) = L_g L_f^{r-1} h(\boldsymbol{x})$.

To design a safe controller for system (4.1), the constraints of CLF and HOCBF are integrated into a QP problem as follows:

CLF-HOCBF-QP:

$$\boldsymbol{u}^\star = \arg \min_{u \in \mathbb{U}, \delta \in \mathbb{R}} \frac{1}{2} \boldsymbol{u}^\top H \boldsymbol{u} + F^\top \boldsymbol{u}, \tag{4.4a}$$

$$\text{s.t. } L_f V(\boldsymbol{x}) + L_g V(\boldsymbol{x})\boldsymbol{u} + \xi(V(\boldsymbol{x})) \leqslant \delta, \tag{4.4b}$$

$$L_f \beta_{r-1}(\boldsymbol{x}) + L_g \beta_{r-1}(\boldsymbol{x})\boldsymbol{u} + \alpha_r(\beta_{r-1}(\boldsymbol{x})) \geqslant 0, \tag{4.4c}$$

---

where H and F indicate weighting matrices with appropriate dimension; the vector $\boldsymbol{u} = [\boldsymbol{u}^\top, \delta]^\top$ contains the control input $\boldsymbol{u}$ and slack variable δ; the variable δ is exploited to relax the CLF constraint, aiming to provide preference to safety over stability under the presence of conflict.

4.3 Probabilistic CLF-HOCBF-QP

This section focuses on the design and theoretical analysis of a probabilistically safe control method.

4.3.1 Problem Formulation

In this chapter, we refer to system (4.1) as the normal model and consider the following nonlinear control affine system with unknown dynamics as the true system:

$$\dot{\boldsymbol{x}} = \boldsymbol{f}(\boldsymbol{x}) + \Delta\boldsymbol{f}(\boldsymbol{x}) + \boldsymbol{g}(\boldsymbol{x})\boldsymbol{u}, \tag{4.5}$$

where $\Delta\boldsymbol{f}(\boldsymbol{x}) \in \mathbb{R}^n$ represents the unknown modelling error. System state $\boldsymbol{x}$ and system dynamics $\boldsymbol{f}, \boldsymbol{g}$. Control input $\boldsymbol{u}$ have the same definitions in system (4.1).

Assumption 4.3.1 (Model Uncertainty [114])**.** *Assume that the unknown modelling error $\Delta\boldsymbol{f}(\boldsymbol{x})$ is structured and there exists a set $\mathbb{X}' \subseteq \hat{\mathscr{A}}$ such that $L_{\Delta f}L_f^j h(\boldsymbol{x}) = 0, \forall 1 \leqslant j < r-1$ and $L_{\Delta f}L_f^{r-1}h(\boldsymbol{x}) \neq 0$ hold for all $\boldsymbol{x} \in \mathbb{X}'$.*

Based on Assumption 4.3.1, the r-th derivatives of $\tilde{h}$ and the derivatives of $\tilde{V}$ for system (4.5) can be expressed as follows:

$$\begin{aligned} \dot{\tilde{V}}(\boldsymbol{x},\boldsymbol{u}) =& L_f V(\boldsymbol{x}) + L_{\Delta f} V(\boldsymbol{x}) + L_g V(\boldsymbol{x}) u, \\ \tilde{h}^r(\boldsymbol{x},\boldsymbol{u}) =& L_f^r h(\boldsymbol{x}) + L_{\Delta f} L_f^{r-1} h(\boldsymbol{x}) + L_g L_f^{r-1} h(\boldsymbol{x}) u + S(h(\boldsymbol{x})) + \alpha_r(\beta_{r-1}(\boldsymbol{x})), \end{aligned} \tag{4.6}$$

where $S(h(\boldsymbol{x})) = \sum_{i=1}^{r-1} L_f^i(\alpha_{r-i} \circ \beta_{r-i-1})(\boldsymbol{x})$.

Remark 4.3.1 (Limitations)**.** *The above assumption requires that the model uncertainty in system* (4.5) *will appear with control input in r-th order derivatives of $\tilde{h}$, thus avoiding the analytical difficulties associated with formulating affine constraints on $\boldsymbol{u}$. Additionally, some physical systems fulfil with this assumption, such as Lagrangian mechanical systems. Considering that this chapter mainly studies how to guarantee the safety of a faulty system with model uncertainty, we preliminarily explore the case of the drift uncertainty with this assumption. Interested readers are referred to [25, 38] for more general cases on GP-based HOCBF conditions.*

The nominal system of their values are given by

$$\begin{aligned} \dot{V}(\boldsymbol{x},\boldsymbol{u}) =& L_f V(\boldsymbol{x}) + L_g V(\boldsymbol{x})\boldsymbol{u}. \\ h^r(\boldsymbol{x},\boldsymbol{u}) =& L_f^r h(\boldsymbol{x}) + L_g L_f^{r-1} h(\boldsymbol{x})\boldsymbol{u} + S(h(\boldsymbol{x})) + \alpha_r(\beta_{r-1}(\boldsymbol{x})), \end{aligned} \tag{4.7}$$

We define functions $\Delta V(\boldsymbol{x})$ and $\Delta h^r(\boldsymbol{x})$ to represent errors between (4.6) and (4.7) as follows:

$$\Delta V(\boldsymbol{x}) = \dot{\tilde{V}}(\boldsymbol{x},\boldsymbol{u}) - \dot{V}(\boldsymbol{x},\boldsymbol{u}), \Delta h^r(\boldsymbol{x}) = \tilde{h}^r(\boldsymbol{x},\boldsymbol{u}) - h^r(\boldsymbol{x},\boldsymbol{u}).$$

Note that uncertainty $\Delta h^r(\boldsymbol{x})$ and $\Delta V(\boldsymbol{x})$ are scalar values. This approach is more effective than directly learning vector-valued unknown dynamics. For true system (4.5), optimization problem (4.4a) can be rewritten as follows:

$$\boldsymbol{u}^\star = \arg\min_{\boldsymbol{u}\in\mathbb{U},\delta\in\mathbb{R}} \frac{1}{2}\boldsymbol{u}^\top H\boldsymbol{u} + F^\top \boldsymbol{u}, \tag{4.8a}$$

$$\text{s.t. } \dot{V}(\boldsymbol{x},\boldsymbol{u}) + \Delta V(\boldsymbol{x}) + \xi(V(\boldsymbol{x})) \leqslant \delta, \tag{4.8b}$$

$$h^r(\boldsymbol{x},\boldsymbol{u}) + \Delta h^r(\boldsymbol{x}) \geqslant 0. \tag{4.8c}$$

4.3.2 Design of the GP-CLF-HOCBF Method

To fit $\Delta V(\boldsymbol{x})$ and $\Delta h^r(\boldsymbol{x})$ using GP regression, we make the following assumption, which is commonly used in estimation.

Assumption 4.3.2 (Measurable Variables [35])**.** *It is assumed that the system state $\boldsymbol{x}$ is fully observable, and that $\tilde{V}(\boldsymbol{x})$, $\tilde{h}^{r-1}(\boldsymbol{x})$, the first derivative of $V(\boldsymbol{x},\boldsymbol{u})$, and r-th derivative of $h(\boldsymbol{x},\boldsymbol{u})$ can be computed and estimated.*

Based on Assumption 4.3.2, we can approximately measure $\Delta V(\boldsymbol{x})$ and $\Delta h^r(\boldsymbol{x})$ by collecting trajectories from true system (4.5), resulting in the following measurements [34]:

$$\begin{aligned}
\Delta\tilde{V}_j &= \frac{\tilde{V}(\boldsymbol{x}(t+\Delta t)) - \tilde{V}(\boldsymbol{x}(t))}{\Delta t} - \dot{V}(\boldsymbol{x}_j,\boldsymbol{u}_j), \\
\Delta\tilde{h}^r_j &= \frac{\tilde{h}^{r-1}(\boldsymbol{x}(t+\Delta t)) - \tilde{h}^{r-1}(\boldsymbol{x}(t))}{\Delta t} - h^r(\boldsymbol{x}_j,\boldsymbol{u}_j),
\end{aligned} \tag{4.9}$$

where $j = 1,2,\cdots,N$ is the index of collected data. The state $\boldsymbol{x}_j = (\boldsymbol{x}(t+\Delta t) + \boldsymbol{x}(t))/2$ represents the mean of the state during $[t, t+\Delta t)$ and $\boldsymbol{u}_j$ indicates the control input in the same interval. Δt refers to the sampling interval. $\Delta\tilde{V}$ and $\Delta\tilde{h}^r$ denote the approximate measurements.

Considering the influences of the approximation errors and measurement noise, we assume availability of the measurements $y_j^{\Delta V} = \Delta\tilde{V}_j + d_j^{\Delta V}$ and $y_j^{\Delta h^r} = \Delta\tilde{h}^r_j + d_j^{\Delta h^r}$, where $d_j^{\Delta V} \sim \left(0, \sigma^2_{v,n}\right)$ and $d_j^{\Delta h^r} \sim \left(0, \sigma^2_{h,n}\right)$ stand for the approximation errors and measurement

noises. Then, we respectively define datasets for $\Delta V(\boldsymbol{x})$ and $\Delta h^r(\boldsymbol{x})$ as $\mathbb{D}_V = \left\{\boldsymbol{x}_j, y_j^{\Delta V}\right\}_{j=1}^N$ and $\mathbb{D}_{h^r} = \left\{\boldsymbol{x}_j, y_j^{\Delta h^r}\right\}_{j=1}^N$.

Remark 4.3.2. *For practical applications, we collect only the system state $x(t)$ using a sensor at each sampling time. The terms $\Delta\tilde{V}_j$ and $\Delta\tilde{h}_j^r$ are computed by the computation module. Since approximation errors and measurement noise exist, we assume that the measurements are given by $y_j^{\Delta V} = \Delta\tilde{V}_j + d_j^{\Delta V}$ and $y_j^{\Delta h^r} = \Delta\tilde{h}_j^r + d_j^{\Delta h^r}$.*

Based on Assumptions 2.1.1, 4.3.1, and 4.3.2, the posterior means and variances of the uncertain terms $\Delta V(\boldsymbol{x})$ and $\Delta h^r(\boldsymbol{x})$ are denoted by $m_V(\boldsymbol{x})$, $\sigma_V(\boldsymbol{x})$, and $m_{h^r}(\boldsymbol{x})$, $\sigma_{h^r}(\boldsymbol{x})$, respectively, and are obtained using the datasets $\mathbb{D}_V$ and $\mathbb{D}_{h^r}$. Furthermore, the SE function defined in (2.5) is employed in this chapter.

Then, the definition of GP-CLF is shown as follows:

Definition 4.3.1 (GP-CLF [34])**.** *For a valid CLF as defined in Definition 4.2.1, and under Assumptions 2.1.1 and 4.3.2, as well as Lemma 2.1.1, the function V is said to be GP-CLF on the set $\mathscr{D}$ for system* (4.5) *if there exists a class $\mathcal{K}$ function $\xi(\cdot)$ such that*

$$\sup_{\boldsymbol{u}\in\mathbb{U}}\left\{L_f V(\boldsymbol{x}) + L_g V(\boldsymbol{x})\boldsymbol{u} + m_V(\boldsymbol{x}) + \psi\sigma_V(\boldsymbol{x}) + \xi(V(\boldsymbol{x}))\right\} \leqslant \delta, \forall \boldsymbol{x} \in \mathscr{D} \tag{4.10}$$

with the high probability $1-\rho$, where $m_V(\boldsymbol{x})$ and $\sigma_V(\boldsymbol{x})$ are posterior mean and standard deviation of $\Delta V(\boldsymbol{x})$.

Inspired by [34], the following theorem can be obtained:

Theorem 4.3.1 (GP-HOCBF)**.** *Provided Assumptions 2.1.1, 4.3.1, and 4.3.2 hold and based on Lemma 2.1.1, for a valid HOCBF defined in Definition 4.2.2, a function h is said to be GP-HOCBF for system* (4.5) *if there exist a set of class $\mathcal{K}$ functions $\alpha_r(\cdot)$ such that*

$$\sup_{\boldsymbol{u}\in\mathbb{U}}\left\{L_f^r h(\boldsymbol{x}) + L_g L_f^{r-1} h(\boldsymbol{x})\boldsymbol{u} + S(h(\boldsymbol{x})) + m_{h^r}(\boldsymbol{x}) - \psi\sigma_{h^r}(\boldsymbol{x})\right\} \geqslant -\alpha_r(\beta_{r-1}(\boldsymbol{x})), \forall \boldsymbol{x} \in \mathbb{X} \tag{4.11}$$

with the high probability $1-\rho$, where $m_{h^r}(\boldsymbol{x})$ and $\sigma_{h^r}(\boldsymbol{x})$ represent posterior mean and standard deviation of $\Delta h^r(\boldsymbol{x})$.

Proof. Based on Assumption 2.1.1 and Lemma 2.1.1, each of the following inequalities holds with a probability of at least $1-\rho$ for a given dataset $\mathbb{D}_{h^r} = \left\{\boldsymbol{x}_j, y_j^{\Delta h^r}\right\}_{j=1}^N$ and

$\forall \boldsymbol{x} \in \hat{\mathscr{A}}$:

$$\left| m_{h^r}(\boldsymbol{x}) - \Delta h^r(\boldsymbol{x}) \right| \leqslant \psi \sigma_{h^r}(\boldsymbol{x}),$$

then we can derive that

$$\begin{aligned} -\psi \sigma_{h^r}(\boldsymbol{x}) &\leqslant m_{h^r}(\boldsymbol{x}) - \Delta h^r(\boldsymbol{x}) \leqslant \psi \sigma_{h^r}(\boldsymbol{x}) \\ m_{h^r}(\boldsymbol{x}) - \psi \sigma_{h^r}(\boldsymbol{x}) &\leqslant \Delta h^r(\boldsymbol{x}) \leqslant m_{h^r}(\boldsymbol{x}) + \psi \sigma_{h^r}(\boldsymbol{x}). \end{aligned}$$

According to (4.4c), we can derive that

$$\tilde{h}^r(\boldsymbol{x}, \boldsymbol{u}) = h^r(\boldsymbol{x}, \boldsymbol{u}) + \Delta h^r(\boldsymbol{x}). \tag{4.12}$$

Since $\Delta h^r(\boldsymbol{x})$ is unknown, if we have $h^r(\boldsymbol{x}, \boldsymbol{u}) + \Delta h^r(\boldsymbol{x}) \geqslant 0$, then function h is a valid HOCBF for true system (4.5).

When (4.11) is satisfied, there is

$$\sup_{\boldsymbol{u} \in \mathbb{U}} \left\{ h^r(\boldsymbol{x}, \boldsymbol{u}) + m_{h^r}(\boldsymbol{x}) - \psi \sigma_{h^r}(\boldsymbol{x}) \right\} \geqslant 0. \tag{4.13}$$

Therefore, one obtains that h is a valid GP-HOCBF for true system (4.5). ■

Incorporating (4.10) and (4.11) into the optimization problem (4.8a), a novel GP-based CLF-HOCBF-QP can be derived as

---

GP-CLF-HOCBF-QP:

$$\boldsymbol{u}^\star = \arg \min_{\boldsymbol{u} \in \mathbb{U}, \delta \in \mathbb{R}} \frac{1}{2} \boldsymbol{u}^\top H \boldsymbol{u} + F^\top \boldsymbol{u}, \tag{4.14a}$$

$$\text{s.t. } \dot{V}(\boldsymbol{x}, \boldsymbol{u}) + m_V(\boldsymbol{x}) + \psi \sigma_V(\boldsymbol{x}) + \xi(V(\boldsymbol{x})) \leqslant \delta, \tag{4.14b}$$

$$h^r(\boldsymbol{x}, \boldsymbol{u}) + m_{h^r}(\boldsymbol{x}) - \psi \sigma_{h^r}(\boldsymbol{x}) \geqslant 0, \tag{4.14c}$$

Note that proposed GP-CLF-HOCBF-QP (4.14) does not require knowledge of the dynamics of true system (4.5) since uncertainty are fitted using GP regression.

4.4 Probabilistically Fault-Tolerant Safe Control

This section proposes a probabilistically fault-tolerant safe control strategy and establishes its theoretical conditions.

4.4.1 Modelling of Faults

This chapter investigates unknown actuator bias faults that are induced by the component torn-and-worn factors [61]. These faults can lead to decreased control performance and pose a threat to system safety, as detailed below:

$$\boldsymbol{u}_F = \boldsymbol{u}^\star + \Delta\boldsymbol{u}_F, \quad \forall t \geqslant t_F, \tag{4.15}$$

where $\Delta\boldsymbol{u}_F \in \mathbb{R}^m$ is an unknown time-varying actuator bias fault; $0 < t_F \in \mathbb{R}$ indicates an unknown time-instant of fault occurrence; the control input $\boldsymbol{u} = \boldsymbol{u}_F$ if $t \geqslant t_F$.

Incorporating (4.15) into (4.5), we can derive that

$$\dot{\boldsymbol{x}} = \boldsymbol{f}(\boldsymbol{x}) + \Delta\boldsymbol{f}(\boldsymbol{x}) + \boldsymbol{g}(\boldsymbol{x})(\boldsymbol{u}^\star + \Delta\boldsymbol{u}_F), \text{if } t \geqslant t_F. \tag{4.16}$$

Assumption 4.4.1 (Fault Bound [118])**.** *Actuator bias fault $\Delta\boldsymbol{u}_F$ is unknown time-varying but bounded function which fufills $\|\Delta\boldsymbol{u}_F\| \leqslant \Delta\boldsymbol{u}_F^{\max}$ with $0 < \Delta\boldsymbol{u}_F^{\max} < +\infty$. Parameter $\Delta\boldsymbol{u}_F^{\max}$ is a known constant.*

Remark 4.4.1. *Unlike general control methods, FTC aims to maintain the performance of faulty systems at an acceptable level. However, FTC methods do not strictly guarantee safety. Therefore, ensuring the safety of faulty systems before they are handled by a safety engineer is crucial. To address this issue, this chapter proposes a fault-tolerant GP-HOCBF approach to enhance safety.*

4.4.2 Theoretical Analysis and Strategy Design

This subsection establishes two sufficient conditions for probabilistic fault-tolerant constraints as follows:

Theorem 4.4.1 (Fault-tolerant GP-CLF)**.** *According to Definition 4.3.1 and Assumption 4.4.1, the function V is said to be fault-tolerant GP-CLF if the following inequality holds:*

$$\sup_{\boldsymbol{u}\in\mathbb{U}} \left\{L_f V(\boldsymbol{x}) + L_g V(\boldsymbol{x})\boldsymbol{u} + m_V(\boldsymbol{x}) + \psi\sigma_V(\boldsymbol{x}) + \xi(V(\boldsymbol{x}))\right\} \leqslant \delta - \|L_g V(\boldsymbol{x})\|\Delta\boldsymbol{u}_F^{\max}, \tag{4.17}$$

for all $\boldsymbol{x} \in \mathscr{D}$ with the high probability $1-\varrho$.

Proof. Calculate the Lie derivative of $V(\boldsymbol{x})$ along system (4.16), we can derive that

$$\begin{aligned}\dot{V}(\boldsymbol{x}) &= L_f V(\boldsymbol{x}) + L_{\Delta f} V(\boldsymbol{x}) + L_g V(\boldsymbol{x})\boldsymbol{u} + L_g V(\boldsymbol{x})\Delta\boldsymbol{u}_F \\ &\leqslant L_f V(\boldsymbol{x}) + m_V(\boldsymbol{x}) + \psi\sigma_V(\boldsymbol{x}) + L_g V(\boldsymbol{x})\boldsymbol{u} + L_g V(\boldsymbol{x})\Delta\boldsymbol{u}_F \\ &\leqslant L_f V(\boldsymbol{x}) + m_V(\boldsymbol{x}) + \psi\sigma_V(\boldsymbol{x}) + L_g V(\boldsymbol{x})\boldsymbol{u} + \left\|L_g V(\boldsymbol{x})\right\| \Delta\boldsymbol{u}_F^{\max} \\ &\leqslant -\xi(V(\boldsymbol{x})) + \delta, \end{aligned} \tag{4.18}$$

for all $\boldsymbol{x} \in \mathscr{D}$ with the high probability $1-\rho$. ■

Theorem 4.4.2 (Fault-tolerant GP-HOCBF)**.** *Based on Theorem 4.3.1 and Assumption 4.4.1, the function h is said to be fault-tolerant GP-HOCBF (FT-GP-HOCBF) for system* (4.16) *if there exist a set of class $\mathcal{K}$ functions $\alpha_i(\cdot)$ such that*

$$\begin{aligned}&\sup_{\boldsymbol{u}\in\mathbb{U}} \left\{L_f^r h(\boldsymbol{x}) + L_g L_f^{r-1} h(\boldsymbol{x})\boldsymbol{u} + S(h(\boldsymbol{x})) + m_{h^r}(\boldsymbol{x}) - \psi\sigma_{h^r}(\boldsymbol{x})\right\} \\ &\geqslant -\alpha_r(\beta_{r-1}(\boldsymbol{x})) + \left\|L_g L_f^{r-1} h(\boldsymbol{x})\right\| \Delta\boldsymbol{u}_F^{\max}, \end{aligned} \tag{4.19}$$

for all $\boldsymbol{x} \in \mathbb{X}$ with the high probability $1-\rho$.

Proof. The Lie derivative of $\beta_{r-1}(\boldsymbol{x})$ along the vector field of system (4.16) is

$$\begin{aligned}\dot{\beta}_{r-1}(\boldsymbol{x}) &= L_f \beta_{r-1}(\boldsymbol{x}) + L_{\Delta f}\beta_{r-1}(\boldsymbol{x}) + L_g \beta_{r-1}(\boldsymbol{x})\boldsymbol{u} + L_g \beta_{r-1}(\boldsymbol{x})\Delta\boldsymbol{u}_F \\ &= L_f^r h(\boldsymbol{x}) + S(h(\boldsymbol{x})) + L_{\Delta f} L_f^{r-1} h(\boldsymbol{x}) + L_g L_f^{r-1} h(\boldsymbol{x})\boldsymbol{u} + L_g L_f^{r-1} h(\boldsymbol{x})\Delta\boldsymbol{u}_F \\ &\geqslant L_f^r h(\boldsymbol{x}) + S(h(\boldsymbol{x})) + m_{h^r}(\boldsymbol{x}) - \psi\sigma_{h^r}(\boldsymbol{x}) + L_g L_f^{r-1} h(\boldsymbol{x})\boldsymbol{u} + L_g L_f^{r-1} h(\boldsymbol{x})\Delta\boldsymbol{u}_F \\ &\geqslant L_f^r h(\boldsymbol{x}) + S(h(\boldsymbol{x})) + m_{h^r}(\boldsymbol{x}) - \psi\sigma_{h^r}(\boldsymbol{x}) + L_g L_f^{r-1} h(\boldsymbol{x})\boldsymbol{u} - \left\|L_g L_f^{r-1} h(\boldsymbol{x})\right\| \Delta\boldsymbol{u}_F^{\max} \\ &\geqslant -\alpha_r(\beta_{r-1}(\boldsymbol{x})), \end{aligned} \tag{4.20}$$

for all $\boldsymbol{x} \in \mathbb{X}$ with the high probability $1-\rho$. ■

Combining (4.17) and (4.19) into the optimization problem (4.8a), an FT-GP-CLF-HOCBF-QP can be obtained as follows:

FT-GP-CLF-HOCBF-QP:

$$\boldsymbol{u}^\star = \arg\min_{u\in\mathbb{U},\delta\in\mathbb{R}} \frac{1}{2}\boldsymbol{u}^\top H\boldsymbol{u} + F^\top\boldsymbol{u}, \tag{4.21a}$$

$$\text{s.t. (4.17) and (4.19)} \tag{4.21b}$$

Equation (4.21) will be implemented when system actuator bias faults are detected by fault detection modules. To mitigate the influence of faulty data, no new data will be received after the fault occurrence. This chapter primarily focuses on the design of fault-tolerant safety-critical control methods rather than fault diagnosis techniques.

Remark 4.4.2. *Since the design of the HOCBF method heavily relies on an accurate system model, the model uncertainty and unknown system faults may influence the effectiveness of the HOCBF, reducing its reliability. Given this, we develop a novel safe control method that integrates the HOCBF method and GP regression into the FTC framework.*

4.4.3 Probabilistically Fault-Tolerant Safe Control Algorithm

To clarify the proposed FT-GP-CLF-HOCBF method, we develop a probabilistically fault-tolerant safe control algorithm, presented in Algorithm 4.1. The safe control input $\boldsymbol{u}^\star$ is utilized to mitigate the impact of actuator bias faults after fault detection.

Algorithm 4.1: Probabilistically Fault-Tolerant Safe Control

Data: $\mathscr{D} = \{X, Y\}$ sampled from a training course;
Input: Observation $\boldsymbol{x}$, parameter ψ, and optimal hyperparameters $L^*, \sigma^*_{\Delta f}$;
Output: Control input $\boldsymbol{u}$;

```
while the system is operational do
    Receive observation x;
    Compute posterior means m_V(x), m_{h^r}(x) and standard deviations
      σ_V(x), σ_{h^r}(x);
    Compute the stability constraint terms: V(x), L_f V(x), L_g V(x), and the safety
      constraint terms: β_{r-1}(x), L_f^r h(x), S(h(x)), L_g L_f^{r-1} h(x);
    if a fault has been detected then
        Compute (4.21) to obtain safe control input u*;
    else
        Compute (4.14) to obtain safe control input u*;
```

Remark 4.4.3. *This chapter proposes an FT-GP-CLF-HOCBF method to deal with model uncertainty and unknown actuator bias faults. Compared to existing works on fault diagnosis [119] and FTC [6, 120–122], the proposed control framework is designed to handle both model uncertainty and faults while ensuring system safety. Furthermore, we extend the study of the HOCBF method [25, 38, 114] to incorporate fault tolerance, thereby enhancing their practical applicability in safety-critical systems.*

4.5 Numerical Example

In this section, we validate the GP-CLF-HOCBF and FT-GP-CLF-HOCBF methods within the autonomous driving simulator CARLA [123]. We aim to develop learning-based fault-tolerant HOCBF methods that ensure a faulty vehicle with model uncertainty maintaining a safe distance from its preceding vehicle until it can be handled by a safety engineer. To evaluate the competitiveness of the FT-GP-CLF-HOCBF method, we compare it to existing work on HOCBF methods.

4.5.1 Experiment Setup

We implement GP regression using scikit-learn [124], and the QP is based on the solver for convex optimization in [125]. Then, we consider a scenario where an ego vehicle is required to maintain a safe distance from its preceding vehicle, namely, ACC with collision avoidance. We define the state variable is $\boldsymbol{x} = [v, d]^\top \in \mathbb{R}^2$, and the vector $\boldsymbol{u} = [u, \delta]^\top \in \mathbb{R}^2$, where v refers to the velocity of the ego vehicle and d is the distance between the preceding vehicle and the ego vehicle. The variable u indicates the control input of the ego vehicle and parameter δ stands for a slack variable. The ACC model can be represented as follows [94]:

$$\begin{bmatrix} \dot{v} \\ \dot{d} \end{bmatrix} = \begin{bmatrix} -\frac{Fr}{m} \\ v_0 - v \end{bmatrix} + \begin{bmatrix} \frac{1}{m} \\ 0 \end{bmatrix} u, \tag{4.22}$$

where m stands for the mass of the ego vehicle and its rolling resistance can be represented as $Fr = f_0 + f_1 v + f_2 v^2$. We set $m = 1650, f_0 = 2, f_1 = 5$, and $f_2 = 3$. Note that the steering and throttle commands of the preceding vehicle and steering command of the ego vehicle are calculated based on the standard kinematic bicycle model and PID controllers [86]. The control input of the ego vehicle is determined by solving QP problem, and this control input is then converted into the throttle command.

In this experiment, the control target is to reach the desired speed $v_d = 18$m/s while maintaining a safe distance 10m with respect to the preceding vehicle. According to these, we design a CLF as $V(\boldsymbol{x}) = (v - v_d)^2$ and a CBF as $h(\boldsymbol{x}) = d - 10$ that has relative degree two (i.e., $r = 2$). We set the initial state $\boldsymbol{x}_0 = [0, 31.14]^\top$, weighted matrices $H = \text{diag}\left[\frac{2}{m^2}, 2\right]$ and $F = \left[\frac{-2Fr}{m^2}, 0\right]$.

Considering that the effects of model uncertainty $\Delta f(\boldsymbol{x})$, the state $\boldsymbol{x}$ is converted into $\hat{\boldsymbol{x}} = [v - 2, d]^\top$. According to measurements $y_j^{\Delta V}$ and $y_j^{\Delta h^r}$, we aim to learn $\Delta V(\boldsymbol{x})$ and

$\Delta h^r(\boldsymbol{x})$ by using GP regression, optimizing the kernels' hyperparameters for improved fitting performance.

Remark 4.5.1 (Feasibility and Safety Considerations [126])**.** *The proposed QP-based controller may still encounter feasibility and safety issues in extreme test cases. For instance, if the initial distance between the leading vehicle and the ego vehicle is small while the desired speed is high, maintaining safety could be challenging. However, the ego vehicle can always decelerate safely to zero velocity, as the maximum braking force is constrained by $u \leqslant u_{\max}$. This results in the following hybrid braking controller:*

$$u = \begin{cases} u^\star, & \text{if } u^\star \text{ exists,} \\ -u_{\max}\dfrac{v}{\|v\|}, & \text{if } u^\star \text{ does not exist, and } \|v\| \neq 0, \\ 0, & \text{if } u^\star \text{ does not exist, and } \|v\| = 0. \end{cases}$$

4.5.2 Experiment Results

Building on the simulation cases from [94], we consider three types of class $\mathcal{K}$ functions (linear, quadratic, and square root functions) as defined in Definition 4.2.2 to construct a HOCBF with $r = 2$ for the safety constraint as follows:

Form 1: Both α_1 and α_2 are linear:

$$\begin{aligned} \beta_1(\boldsymbol{x}) &= \dot{h}(\boldsymbol{x}) + \alpha_1(h(\boldsymbol{x})) \\ \beta_2(\boldsymbol{x}) &= \dot{\beta}_1(\boldsymbol{x}) + \alpha_2(\beta_1(\boldsymbol{x})). \end{aligned} \tag{4.23}$$

Form 2: Both α_1 and α_2 are quadratic:

$$\begin{aligned} \beta_1(\boldsymbol{x}) &= \dot{h}(\boldsymbol{x}) + (\alpha_1(h(\boldsymbol{x})))^2 \\ \beta_2(\boldsymbol{x}) &= \dot{\beta}_1(\boldsymbol{x}) + (\alpha_2(\beta_1(\boldsymbol{x})))^2. \end{aligned} \tag{4.24}$$

Form 3: Both α_1 and α_2 are square root:

$$\begin{aligned} \beta_1(\boldsymbol{x}) &= \dot{h}(\boldsymbol{x}) + \sqrt{\alpha_1(h(\boldsymbol{x}))} \\ \beta_2(\boldsymbol{x}) &= \dot{\beta}_1(\boldsymbol{x}) + \sqrt{\alpha_2(\beta_1(\boldsymbol{x}))}. \end{aligned} \tag{4.25}$$

We validate our proposed methods using three types of class $\mathcal{K}$ functions.

4.5.2.1 GP-CLF-HOCBF Method for Forms 1, 2, and 3

In this case, we firstly discuss system (4.22) with the model uncertainty $\Delta f(\boldsymbol{x})$ but without unknown actuator bias faults Δu_F. To collect the necessary data, we begin by running the `CLF-HOCBF-QP` (4.4) until the system violates the safety constraints. We gather training data from a desired trajectory in 'Town 04' of CARLA and demonstrate the test results on another desired trajectory within the same map, as shown in Figure 4.2.

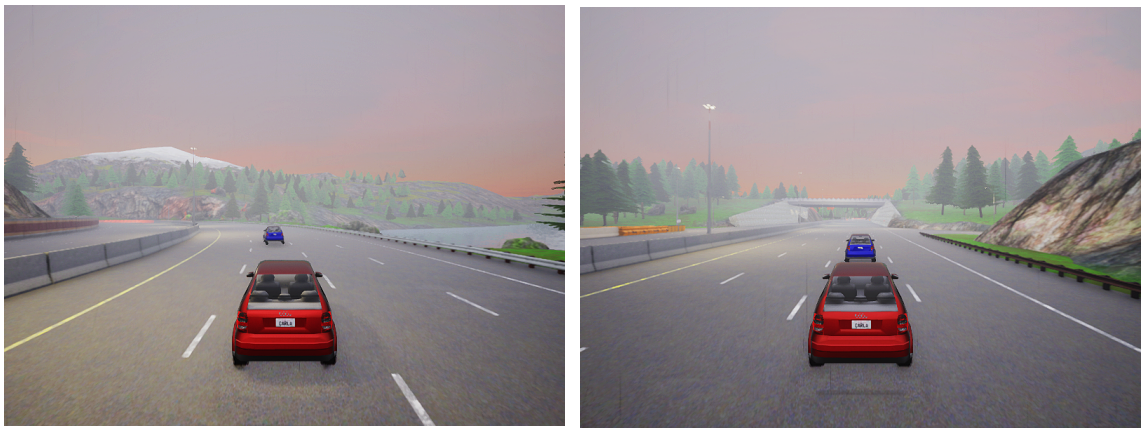

(a) Training course. (b) Test course.

Figure 4.2: Simulation environment in CARLA. The vehicles track the desired trajectories on different courses. Left: The **training course** was generated data to train. Right: An unknown **test course** is tested. Red vehicle is the ego vehicle and blue vehicle is the preceding vehicle.

Then, we select $\psi = 1.2$ and apply the posterior means $m_{h^r}(\boldsymbol{x})$ and $m_V(\boldsymbol{x})$ and the standard deviations $\sigma_{h^r}(\boldsymbol{x})$ and $\sigma_V(\boldsymbol{x})$ generated in each time instant for constraints (4.14c) and (4.14b). The noise for $y_j^{\Delta V}$ and $y_j^{\Delta h^r}$ is set as $d_j^{\Delta V(\boldsymbol{x})} = (0, 0.05)$ and $d_j^{\Delta h^r(\boldsymbol{x})} = (0, 0.05)$, respectively.

As shown in Figure 4.3(a), the velocity curves of the ego vehicle under three types of class $\mathcal{K}$ functions converge to the desired speed for $t \geqslant 2.5$s. After 5s, the velocity curves converge to the velocity of the leading vehicle under three types of class $\mathcal{K}$ functions. With the help of GP regression, all distance curves remain greater than 10m. After 4s, the curve of quadratic form (4.24) decreases more rapidly toward safe distance 10m from the leading vehicle than linear and square root forms ((4.23) and (4.25)). Additionally, that square root form (4.25) is conservative. In Figure 4.3(b), we can observe that the values of $\beta_0(\boldsymbol{x})$ and $\beta_1(\boldsymbol{x})$ are larger than 0. Compared to linear and square root

forms ((4.23) and (4.25)), the curve of quadratic form (4.24) decreases more rapidly and approaches 0.1 more closely after 6s. Given this, one concludes that GP-CLF-HOCBF-QP (4.14) under quadratic form (4.24) more effectively enables system (4.22) to reach desired speed and maintain a safe distance under the case of the model uncertainty $\Delta f(\boldsymbol{x})$.

(a) Profiles of the system state.

(b) Profiles of CBFs.

Figure 4.3: Simulation results of the GP-CLF-HOCBF Method for Forms 1, 2, and 3 (linear, quadratic, and square root class $\mathcal{K}$ functions, respectively).

4.5.2.2 FT-GP-CLF-HOCBF Method for Forms 1, 2, and 3

In this case, we consider system (4.22) with the model uncertainty $\Delta f(\boldsymbol{x})$ and the unknown actuator bias fault Δu_F. We choose $t_F = 0.25$s, $\Delta u_F = |\sin(t)|$, and $\Delta u_F^{\max} = 1$. The actuator bias fault will influences the throttle command of the ego vehicle and threatens the safety of ego vehicle. Furthermore, we select the same parameters in Section 4.5.2.1, and unknown actuator bias fault only occur in the test course.

As shown in Figure 4.4(a), the velocity curves of the ego vehicle under three types of class $\mathcal{K}$ functions are greater than leader's curve when $t \geqslant t_F$, and the results show that actuator bias faults influence the ego vehicle's velocity. However, the distance curve of square root form (4.25) remains above 15m, which is more conservative. The distance curves of linear and quadratic forms ((4.23) and (4.24)) are close to 10m. Compared to square root form (4.25), linear and quadratic forms ((4.23) and (4.24)) more effectively enables ego vehicle to reach the desired speed and maintains a safe distance with its preceding vehicle. In Figure 4.4(b), one observes that the values of $\beta_0(\boldsymbol{x})$ and $\beta_1(\boldsymbol{x})$ under the linear and quadratic forms ((4.23) and (4.24)) remain close to but strictly greater

than 0. Therefore, we can conclude that FT-GP-CLF-HOCBF-QP (4.21) under constraints (4.17) and (4.19) can assist system (4.22) in achieving control objectives under model uncertainty and unknown actuator bias faults, and three types of class $\mathcal{K}$ functions affect the performance of FT-GP-CLF-HOCBF-QP (4.21).

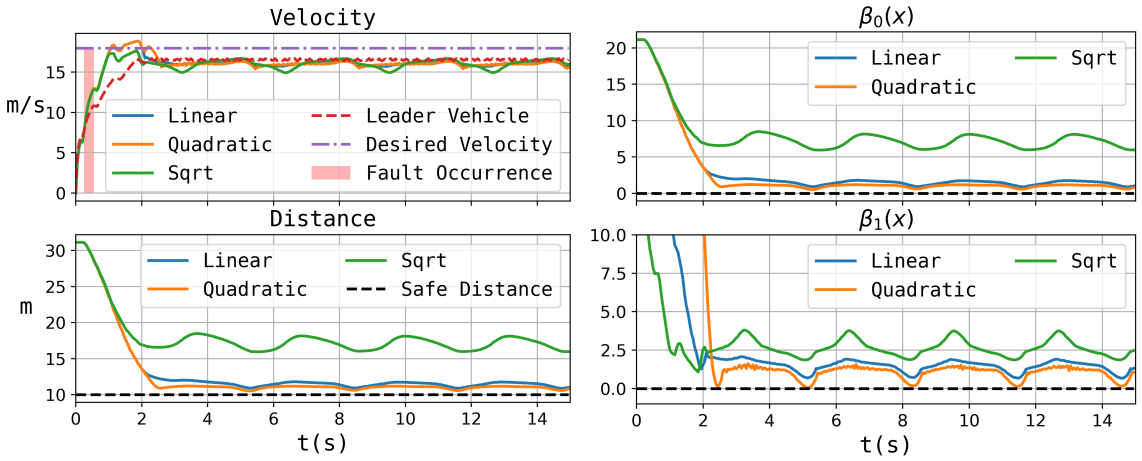

(a) Profiles of the system state.

(b) Profiles of CBF.

Figure 4.4: Simulation results of the FT-GP-CLF-HOCBF Method for Forms 1, 2, and 3 (linear, quadratic, and square root class $\mathcal{K}$ functions, respectively).

4.5.2.3 Performance Comparisons

We illustrate the competitiveness of the proposed FT-GP-CLF-HOCBF in this chapter through comparisons with findings presented GP-HOCBF in [38]. Note that this case only focuses on the comparisons of the safety performance under the linear class $\mathcal{K}$ function.

As shown in Figure 4.5(a), the values of $\beta_0(\boldsymbol{x})$ and $\beta_1(\boldsymbol{x})$ are greater than 0 based on FT-GP-CLF-HOCBF. However, under the GP-HOCBF in [38], $\beta_0(\boldsymbol{x})$ and $\beta_1(\boldsymbol{x})$ exhibit several negative values, indicating that the safety of the system cannot be guaranteed in the presence of unknown actuator bias faults. It is worth noting that, despite these negative values, part of $\beta_0(\boldsymbol{x})$ and $\beta_1(\boldsymbol{x})$ values remain non-negative when using GP-HOCBF. Therefore, we further select smaller values of actuator bias faults $\Delta u_F = 0.5|\sin(t)|$ to investigate the robustness of GP regression. In Figure 4.5(b), the results show that the values of $\beta_0(\boldsymbol{x})$ and $\beta_1(\boldsymbol{x})$ are both greater than 0 on the basis of FT-GP-CLF-HOCBF and GP-HOCBF. Given this, one concludes that our method provides better safety performance compared to GP-HOCBF in [38] when system experiences larger actuator bias faults, while GP-HOCBF remains robustness against smaller actuator bias faults.

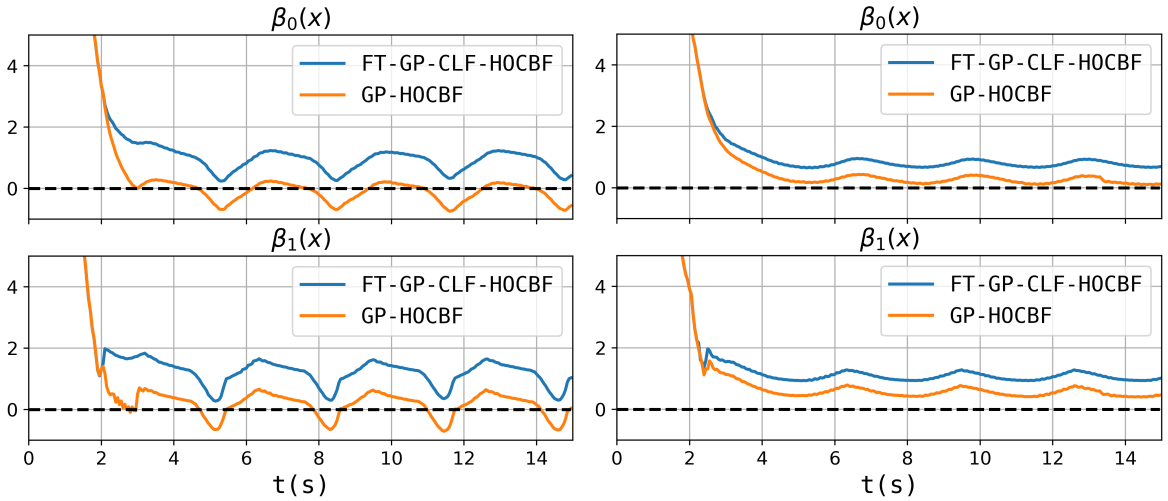

(a) Actuator bias fault case: $\Delta u_F = |\sin(t)|$.

(b) Actuator bias fault case: $\Delta u_F = 0.5|\sin(t)|$.

Figure 4.5: Comparison results of `FT-GP-CLF-HOCBF` and `GP-HOCBF` under two different actuator bias faults.

4.6 Conclusion

In this chapter, we have proposed a fault-tolerant GP-based CLF-HOCBF method to address the issues of model uncertainty and unknown actuator bias faults. We have developed three sufficient conditions to guarantee our proposed methods. Finally, numerical simulations within the autonomous driving simulator CARLA have demonstrated the effectiveness and competitiveness of our theoretical results and control strategy.

There are some limitations in the proposed method that will be addressed in future work. In the current model-based learning framework, only uncertainty in the drift term is considered, while the input dynamics are assumed to be fully known, which may not reflect many real-world systems. Moreover, the method focuses exclusively on unknown actuator bias faults, without taking into account unknown actuator gain faults that are also critical in practice. Lastly, improving the regression accuracy of the Gaussian process model remains an important direction for future investigation.

CHAPTER 5

SAFE LEARNING FOR ADAPTIVE FAULT-TOLERANT CONTROL WITH PROBABILISTIC CONTROL BARRIER FUNCTION

This chapter is based on the paper titled "Safe Learning for Adaptive Fault-Tolerant Control with Probabilistic Control Barrier Functions," IEEE Transactions on Automation Science and Engineering, Under Review.

To deal with RQ3 and achieve RO3, this chapter proposes probabilistically and adaptively safe control frameworks that integrate GPs and online fault estimation into the CBF method, further extending this approach to systems with high relative degrees. To handle model uncertainty, we develop GP-based CBF and HOCBF constraints to ensure the probabilistic safety. In addition, we design an adaptive fault estimator to estimate unknown actuator gain faults. Finally, the proposed methods are validated on an ACC system and a mobile robotic system, demonstrating their effectiveness and superiority in ensuring safety, compared to existing methods.

The structure of this chapter is arranged as follows. Section 5.1 presents a review of related work pertinent to this study. Section 5.2 introduces the essential background

and preliminary concepts. The central results are provided in Sections 5.3 and 5.4. Numerical examples illustrating the two proposed approaches are given in Section 5.5. The chapter concludes with a summary in Section 5.6. Furthermore, the overall framework of the methods introduced in this chapter is shown in Figure 5.1.

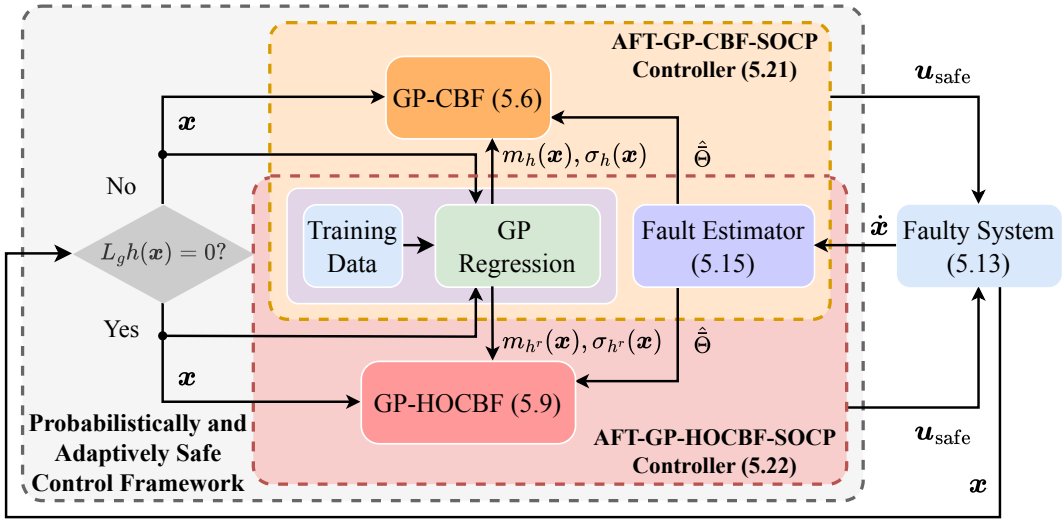

Figure 5.1: An overview of the probabilistically and adaptively safe control framework. According to the structure of $L_g h(\boldsymbol{x})$, the controller switches between CBF and HOCBF constraints. Uncertain terms are modelled using GP regression. Actuator gain faults are estimated based on a fault estimator after the occurrence of faults.

5.1 Introduction

Modern control systems are becoming increasingly complex, integrating more components that make them potentially more vulnerable to unexpected faults, such as actuator faults. To address these challenges, FTC has been developed to maintain the functionality of faulty systems [115]. Building on this foundation, researchers have extended FTC to adaptive FTC [127], learning-based FTC [74], and so on. However, existing FTC methods cannot strictly guarantee safety for faulty systems, posing potentially safe risks in practical applications. Therefore, safe control methods have been developed, including RL [20], MPC [128], and CBF [18]. Given this, researchers have explored the

fault-tolerant RL approach [105], the fault-tolerant MPC approach [129], and the fault-tolerant CBF approach [26]. However, the RL-based FTC method in [105] addressed the issues of actuator gain faults but did not guarantee safety. Xu et al. [129] designed an adaptive estimator to estimate actuator faults and focused only on the stability of closed-loop systems by using the fault-tolerant MPC method. As stated in [26], Hilten proposed the changed fault-tolerant CBF method, but its effectiveness was constrained by the fixed boundaries of the control input. This chapter aims to study *adaptive fault-tolerant safety-critical control* to tackle unknown actuator faults and model uncertainty, guaranteeing the safety of systems.

In practical control tasks, the effectiveness of CBF methods heavily relies on accurate system models, which may not always be available due to model uncertainty [130]. Therefore, researchers have investigated robust CBF [77], robust adaptive CBF [80, 81], and RL-based CBF [84]. However, the robust CBF method in [77] was conservative. The adaptive law designed in [80] may exhibit a slow response due to inappropriate selection of adaptive parameters and was limited by the structure of model uncertainty. As stated in [81, 84], the proposed learning-based methods depended on accurate output measurements and might lose their effectiveness in the presence of observation noise. To deal with the above issues, GP regression has emerged as a promising solution, providing a probabilistic framework to model uncertainty [11]. Recent studies have explored GP-based CBF [34]. Fernando et al. [34] established the probabilistic CLF-CBF method to deal with model uncertainty and ensure the stability and safety of systems. However, the above methods struggle to address both model uncertainty and actuator faults.

Note that the above CBF methods are only suitable for systems with a relative degree of one. To overcome this limitation, the HOCBF has been proposed, which can be applied to control systems with arbitrary relative degrees, extending its applicability to a wide range of robotic systems. Researchers have considered the fault-tolerant

HOCBF method [27] to deal with the system faults and studied robust adaptive HOCBF [114] and GP-based HOCBF [25] methods to tackle model uncertainty. Dong et al. [27] proposed a robust fault-tolerant HOCBF method, which is conservative and may even become unsafe in worst-case fault scenarios. The methods proposed in [25, 114] only addressed model uncertainty and might fail to ensure safety when systems encounter unknown actuator faults. Although very few authors [131] presented a fault-tolerant safe control framework that integrates GP regression and HOCBFs into the FTC framework to ensure probabilistic stability and safety, this method still struggles to address unknown actuator gain faults. To address these challenges, this chapter proposes GP-based CBF and HOCBF methods with the adaptive FTC technique to handle model uncertainty and actuator faults, ensuring the probabilistic safety.

5.2 Preliminaries

5.2.1 Notations and Definition

Let $\mathbb{R}$ be the set of real numbers. $\mathbb{R}^+$ stands for the set of positive real numbers. $\mathbb{R}^n$ refers to $n-$dimensional Euclidean space, and $\mathbb{R}^{n\times m}$ stands for the space of $n\times m$ real matrices. $\Pr\{\cdot\}$ is probability of an event. $\|\cdot\|$ is the Euclidean norm. $|\cdot|$ presents absolute value. $\mathbb{U}$ stands for a control constraint set.

Consider the following nonlinear control-affine systems:

$$\dot{\boldsymbol{x}} = \boldsymbol{f}(\boldsymbol{x}) + \boldsymbol{g}(\boldsymbol{x})\boldsymbol{u}, \tag{5.1}$$

where $\boldsymbol{x} \in \mathbb{R}^n$ and $\boldsymbol{u} = [u_1, u_2, \cdots, u_m]^\top \in \mathbb{U} \subseteq \mathbb{R}^m$ indicate the system state and the control input. The drift dynamics $\boldsymbol{f} : \mathbb{R}^n \to \mathbb{R}^n$ and the input dynamics $\boldsymbol{g} : \mathbb{R}^n \to \mathbb{R}^{n\times m}$ are known and local Lipschitz function in $\boldsymbol{x}$.

5.2.2 High-Order CBFs

Although CBF method in (2.16) can ensure the safety of a system, it loses effectiveness when $L_g h(\boldsymbol{x}) = 0$ in some practical applications. To address this issue, the HOCBF

method is proposed [22]. Before presenting this approach, we first assume the function h fulfilling Definition 2.4.2.

Definition 5.2.1 (HOCBF [22])**.** *Define a set of functions* $\beta_i(\boldsymbol{x}) = \dot{\beta}_{i-1}(\boldsymbol{x}) + \alpha_i(\beta_{i-1}(\boldsymbol{x})), i \in \{1, \cdots, r-1\}$ *with* $\beta_0(\boldsymbol{x}) = h(\boldsymbol{x})$ *and a class of sets* $\mathbb{A}_i = \{\boldsymbol{x} \in \mathbb{R}^n : \beta_i(\boldsymbol{x}) > 0\}$*. If there exist a set of class* $\mathcal{K}$ *functions* $\alpha_i(\cdot)$ *such that*

$$\sup_{\boldsymbol{u} \in \mathbb{U}} \underbrace{\{L_f \beta_{r-1}(\boldsymbol{x}) + L_g \beta_{r-1}(\boldsymbol{x})\boldsymbol{u} + \alpha_r(\beta_{r-1}(\boldsymbol{x}))\}}_{\beta_r(\boldsymbol{x},\boldsymbol{u}) = h^r(\boldsymbol{x},\boldsymbol{u})} \geqslant 0, \tag{5.2}$$

then function $h : \mathbb{R}^n \to \mathbb{R}$ *is said to be a candidate HOCBF of the relative degree* r *for system* (5.1)*, holding for all* $\boldsymbol{x} \in \mathbb{A}$*, where* $L_f \beta_{r-1}(\boldsymbol{x}) = L_f^r h(\boldsymbol{x}) + \sum_{i=1}^{r-1} L_f^i(\alpha_{r-i} \circ \beta_{r-i-1})(\boldsymbol{x})$ *and* $L_g \beta_{r-1}(\boldsymbol{x}) = L_g L_f^{r-1} h(\boldsymbol{x})$*.*

5.3 Probabilistic Safety Constraints

In this sections, we establish probabilistic CBF and HOCBF constraints and develop two theoretical conditions.

5.3.1 Problem Statement

This chapter focuses on nonlinear control-affine systems with model uncertainty, resulting in the following definition:

$$\dot{\boldsymbol{x}} = \boldsymbol{f}(\boldsymbol{x}) + \Delta \boldsymbol{f}(\boldsymbol{x}) + \boldsymbol{g}(\boldsymbol{x})\boldsymbol{u}, \tag{5.3}$$

where $\Delta \boldsymbol{f}(\boldsymbol{x}) : \mathbb{R}^n \to \mathbb{R}^n$ represents the model uncertainty. $\boldsymbol{x}, \boldsymbol{f}(\boldsymbol{x}), \boldsymbol{g}(\boldsymbol{x})$, and $\boldsymbol{u}$ are defined as in (5.1).

Assumption 5.3.1 (Model Uncertainty [114])**.** *Assume that the unknown modelling error* $\Delta \boldsymbol{f}(\boldsymbol{x})$ *is structured and there exists a set* $\mathbb{A}' \subseteq \mathbb{A}$ *such that* $L_{\Delta f} L_f^j h(\boldsymbol{x}) = 0, \forall 1 \leqslant j < r-1$ *and* $L_{\Delta f} L_f^{r-1} h(\boldsymbol{x}) \neq 0$ *hold for all* $\boldsymbol{x} \in \mathbb{A}'$*.*

5.3.2 Probabilistic CBFs

Based on system (5.3), the derivatives of the CBF can be derived as follows:

$$\dot{\tilde{h}}(\boldsymbol{x}, \boldsymbol{u}) = L_f h(\boldsymbol{x}) + L_{\Delta f} h(\boldsymbol{x}) + L_g h(\boldsymbol{x})\boldsymbol{u} + \alpha(h(\boldsymbol{x})). \tag{5.4}$$

Denote $\Delta h(\boldsymbol{x}) = \dot{\tilde{h}}(\boldsymbol{x},\boldsymbol{u}) - \dot{h}(\boldsymbol{x},\boldsymbol{u})$ as error of CBF between nominal system (5.1) and true system (5.3). Inspired by [34], we collect trajectories from true system to fit $\Delta h(\boldsymbol{x})$ by using GP regression with the following measurement:

$$y_j^h = \frac{\left(\tilde{h}(\boldsymbol{x}(t+\Delta t)) - \tilde{h}(\boldsymbol{x}(t))\right)}{\Delta t} - \dot{h}(\boldsymbol{x}_j,\boldsymbol{u}_j) + d_j, \tag{5.5}$$

where $j = 1,2,\ldots,N$ is the index of collected data. The state $\boldsymbol{x}_j = (\boldsymbol{x}(t+\Delta t)+\boldsymbol{x}(t))/2$ is the mean of the state during $[t, t+\Delta t)$ and $\boldsymbol{u}_j$ indicates control input in the same interval. Δt refers to the sampling interval. $d_j \sim \left(0, \sigma_{h,n}^2\right)$ stands for the white measurement noises.

The SE function defined in (2.5) is used in this chapter. Under Assumptions 2.1.1, 4.3.1, and 4.3.2, the posterior mean and variance of the uncertain term $\Delta h(\boldsymbol{x})$ are denoted by $m_h(\boldsymbol{x})$ and $\sigma_h(\boldsymbol{x})$ and are obtained using the dataset $\mathbb{D}_h = \left\{\boldsymbol{x}_j, y_j^h\right\}_{j=1}^N$. This leads to the following lemma:

Lemma 5.3.1 (GP-CBF [34])**.** *According to Lemma 2.1.1 and Assumption 2.1.1, for a valid CBF defined in* (2.16)*, if there exists an extended class $\mathcal{K}$ function α such that*

$$\sup_{\boldsymbol{u}\in\mathbb{U}} \left\{L_f h(\boldsymbol{x}) + L_g h(\boldsymbol{x})\boldsymbol{u} + m_h(\boldsymbol{x}) - \psi\sigma_h(\boldsymbol{x})\right\} \geqslant -\alpha(h(\boldsymbol{x})), \tag{5.6}$$

then the function $h(\boldsymbol{x})$ is said to be GP-CBF for system (5.3) *for all $\boldsymbol{x} \in \mathbb{A}$ with high probability $1-\varrho$.*

5.3.3 Probabilistic High-Order CBFs

Accordingly, if system (5.3) satisfies Assumption 2.1.1, we can obtain the following the r-th derivatives of the HOCBF:

$$\tilde{h}^r(\boldsymbol{x},\boldsymbol{u}) = L_f^r h(\boldsymbol{x}) + L_{\Delta f} L_f^{r-1} h(\boldsymbol{x}) + L_g L_f^{r-1} h(\boldsymbol{x})\boldsymbol{u} + S(h(\boldsymbol{x})) + \alpha_r(\beta_{r-1}(\boldsymbol{x})), \tag{5.7}$$

where $S(h(\boldsymbol{x})) = \sum_{i=1}^{r-1} L_f^i(\alpha_{r-i}\circ\beta_{r-i-1})(\boldsymbol{x})$.

Define $\Delta h^r(\boldsymbol{x}) = \tilde{h}^r(\boldsymbol{x},\boldsymbol{u}) - h^r(\boldsymbol{x},\boldsymbol{u})$ as error of HOCBF between nominal system (5.1) and true system (5.3). Then, one gets the following measurement for GP regression:

$$y_j^{h^r} = \left(\tilde{h}^{r-1}(\boldsymbol{x}(t+\Delta t)) - \tilde{h}^{r-1}(\boldsymbol{x}(t))\right)/\Delta t - h^r(\boldsymbol{x}_j,\boldsymbol{u}_j) + d_j^{h^r},\ d_j^{h^r} \sim (0, \sigma_{h^r,n}^2) \tag{5.8}$$

with collection training dataset $\mathbb{D}_{h^r} = \left\{\boldsymbol{x}_j, y_j^{h^r}\right\}_{j=1}^N$.

Based on Assumptions 2.1.1, 4.3.1, and 4.3.2, the posterior means and variances of the uncertain terms $\Delta V(\boldsymbol{x})$ and $\Delta h^r(\boldsymbol{x})$ are denoted by $m_V(\boldsymbol{x})$, $\sigma_V(\boldsymbol{x})$, and $m_{h^r}(\boldsymbol{x})$, $\sigma_{h^r}(\boldsymbol{x})$,

respectively, and are obtained using the datasets $\mathbb{D}_V$ and $\mathbb{D}_{h^r}$. Furthermore, the SE function defined in (2.5) is employed in this chapter.

Note that the training outputs in (5.5) and (5.8) are computed from the state of the system. In practical applications, the state of the system can be obtained from onboard sensors and used to generate training data. Then, one obtains:

Theorem 5.3.1 (GP-HOCBF)**.** *Provided Assumptions 2.1.1 and 5.3.1 hold and based on Lemma 2.1.1, for a valid HOCBF defined in* (5.2)*, if there exist a set of class $\mathcal{K}$ functions $\alpha_i(\cdot),\ i \in \{0,1,\cdots,r\}$ such that*

$$\sup_{\boldsymbol{u}\in\mathbb{U}} \left\{ L_f^r h(\boldsymbol{x}) + L_g L_f^{r-1} h(\boldsymbol{x})\boldsymbol{u} + S(h(\boldsymbol{x})) + m_{h^r}(\boldsymbol{x}) - \psi\sigma_{h^r}(\boldsymbol{x}) \right\} \geqslant -\alpha_r(\beta_{r-1}(\boldsymbol{x})), \tag{5.9}$$

then the function $h(\boldsymbol{x})$ is said to be GP-HOCBF for system (5.3) *for all $\boldsymbol{x} \in \mathbb{A}$ with high probability $1-\rho$.*

Proof. Based on Assumption 2.1.1 and Lemma 2.1.1, each of the following inequalities hold with a probability of at least $1-\rho$ for a given dataset $\mathbb{D}_{h^r}$ and $\forall \boldsymbol{x} \in \mathbb{A}$:

$$\left| m_{h^r}(\boldsymbol{x}) - \Delta h^r(\boldsymbol{x}) \right| \leqslant \psi\sigma_{h^r}(\boldsymbol{x}),$$

then we can derive that

$$\begin{aligned} -\psi\sigma_{h^r}(\boldsymbol{x}) \leqslant m_{h^r}(\boldsymbol{x}) - \Delta h^r(\boldsymbol{x}) \leqslant \psi\sigma_{h^r}(\boldsymbol{x}), \\ m_{h^r}(\boldsymbol{x}) - \psi\sigma_{h^r}(\boldsymbol{x}) \leqslant \Delta h^r(\boldsymbol{x}) \leqslant m_{h^r}(\boldsymbol{x}) + \psi\sigma_{h^r}(\boldsymbol{x}). \end{aligned}$$

According to (5.2) and (5.7), one obtains that

$$\tilde{h}^r(\boldsymbol{x},\boldsymbol{u}) = h^r(\boldsymbol{x},\boldsymbol{u}) + \Delta h^r(\boldsymbol{x}). \tag{5.10}$$

Since $\Delta h^r(\boldsymbol{x})$ is unknown, if we have $h^r(\boldsymbol{x},\boldsymbol{u}) + \Delta h^r(\boldsymbol{x}) \geqslant 0$, then function h is a valid HOCBF for true system (5.3).

When (5.9) is satisfied, there is

$$\sup_{\boldsymbol{u}\in\mathbb{U}} \{ h^r(\boldsymbol{x},\boldsymbol{u}) + m_{h^r}(\boldsymbol{x}) - \psi\sigma_{h^r}(\boldsymbol{x}) \} \geqslant 0. \tag{5.11}$$

Therefore, one obtains that h is a valid GP-HOCBF for (5.3). ■

5.4 Probabilistically Safe Controllers Under Actuator Faults

5.4.1 Faults Modelling

In practical applications, the actuators of control systems may experience faults induced by the component torn-and-worn factors [6], resulting in the following definition [132]:

$$\boldsymbol{u}_F = \Theta \boldsymbol{u}, \quad t \geqslant t_F, \tag{5.12}$$

where $0 < t_F \in \mathbb{R}$ represents the time of fault occurrence. The matrix Θ =diag$[\theta_1, \cdots, \theta_i, \cdots, \theta_m] \in \mathbb{R}^{m\times m}$ defines the actuation effectiveness parameters with $\theta_i \in (0,1]$. If $\theta_i \in (0,1)$, the actuators exhibit a loss of effectiveness, while $\theta_i = 1$ indicates the fault-free. Note that this chapter assumes no case of $\theta_i = 0$, interested readers are referred to [133] for studies on dynamic redundant actuators.

Substituting (5.12) into (5.3), we can obtain

$$\dot{\boldsymbol{x}} = \boldsymbol{f}(\boldsymbol{x}) + \Delta \boldsymbol{f}(\boldsymbol{x}) + \boldsymbol{g}(\boldsymbol{x})\Theta \boldsymbol{u}, \quad t \geqslant t_F, \tag{5.13}$$

then denote $\bar{\Theta} = [\theta_1, \cdots, \theta_i, \cdots, \theta_m]^\top \in \mathbb{R}^m$ and $\hat{\boldsymbol{u}}$ =diag $[u_1, u_2, \cdots, u_m] \in \mathbb{R}^{m\times m}$, it follows from (5.13) that

$$\dot{\boldsymbol{x}} = \boldsymbol{f}(\boldsymbol{x}) + \Delta \boldsymbol{f}(\boldsymbol{x}) + \boldsymbol{g}(\boldsymbol{x})\hat{\boldsymbol{u}}\bar{\Theta}, \quad t \geqslant t_F. \tag{5.14}$$

5.4.2 Faulty Parameters Estimation

Different from model uncertainty, actuator gain faults occur abruptly and decrease the control performance. Inspired by [134], we propose an online estimator as follows:

$$\begin{aligned} \dot{\hat{\boldsymbol{x}}} &= \boldsymbol{f}(\boldsymbol{x}) + \boldsymbol{g}(\boldsymbol{x})\hat{\boldsymbol{u}}\hat{\bar{\Theta}} + \kappa \boldsymbol{e} + \boldsymbol{\omega}\dot{\hat{\bar{\Theta}}}, \\ \dot{\boldsymbol{\omega}} &= \boldsymbol{g}(\boldsymbol{x})\hat{\boldsymbol{u}} - \kappa \boldsymbol{\omega}, \quad \boldsymbol{\omega}(0) = 0. \end{aligned} \tag{5.15}$$

where $\hat{\boldsymbol{x}} \in \mathbb{R}^n$ is the state of the online estimator. $\hat{\bar{\Theta}} = \left[\hat{\theta}_1, \cdots, \hat{\theta}_i, \cdots, \hat{\theta}_m\right]^\top \in \mathbb{R}^m$ denotes the parameter estimate vector. $\boldsymbol{e} = \boldsymbol{x} - \hat{\boldsymbol{x}}$ stands for the state estimation error. $\boldsymbol{\omega} \in \mathbb{R}^{n\times m}$ represents the output of the filter.

Define the parameter estimation error $\tilde{\bar{\Theta}} = \bar{\Theta} - \hat{\bar{\Theta}}$ and an auxiliary variable $\boldsymbol{\vartheta} = \boldsymbol{e} - \boldsymbol{\omega}\tilde{\bar{\Theta}}$, then one yields

$$\begin{aligned} \dot{\boldsymbol{e}} &= \Delta \boldsymbol{f}(\boldsymbol{x}) + \boldsymbol{g}(\boldsymbol{x})\hat{\boldsymbol{u}}\tilde{\bar{\Theta}} - \kappa \boldsymbol{e} - \boldsymbol{\omega}\dot{\hat{\bar{\Theta}}}, \\ \dot{\boldsymbol{\vartheta}} &= -\kappa \boldsymbol{\vartheta}, \quad \boldsymbol{\vartheta}(0) = \boldsymbol{e}(0). \end{aligned}$$

Lemma 5.4.1 (Adaptive Estimation Laws)**.** *Define a positive gain constant $\eta \in \mathbb{R}$, a matrix $\boldsymbol{Q} \in \mathbb{R}^{n\times n}$, an excitation index $\varsigma(t) = \lambda_{\min}(\boldsymbol{Q}(t))$, and a contraction factor $0 < \varphi(t) = (1+\eta\varsigma(t))^{-1} \leqslant 1$, and consider a Lyapunov function $V(\tilde{\tilde{\Theta}}) = \tilde{\tilde{\Theta}}^\top \tilde{\tilde{\Theta}}$. If the estimator follows the adaptive laws:*

$$\dot{\hat{\tilde{\Theta}}} = \eta \boldsymbol{\omega}^\top (\boldsymbol{e} - \boldsymbol{\vartheta}), \quad \dot{\boldsymbol{Q}} = \boldsymbol{\omega}^\top \boldsymbol{\omega}, \tag{5.16}$$

then online estimator (5.15) *ensures the estimation error norm $\|\tilde{\tilde{\Theta}}\|$ is non-increasing and $V(\tilde{\tilde{\Theta}}(t)) \leqslant \varphi(t) V(\tilde{\tilde{\Theta}}(t_F))$ for $t \geqslant t_F$, where $\lambda_{\min}(\boldsymbol{Q}(t))$ is the minimum eigenvalues of $\boldsymbol{Q}(t)$.*

Proof. With the help of auxiliary variable η and (5.16), we can get

$$\begin{aligned}
\dot{V}(\tilde{\tilde{\Theta}}) \leqslant & -\eta \tilde{\tilde{\Theta}}^\top \boldsymbol{\omega}^\top (\boldsymbol{e} - \boldsymbol{\vartheta}) \\
= & -\eta \tilde{\tilde{\Theta}} \boldsymbol{\omega}^\top \boldsymbol{\omega} \tilde{\tilde{\Theta}} \\
\leqslant & 0.
\end{aligned} \tag{5.17}$$

Furthermore, one derives

$$\begin{aligned}
V(\tilde{\tilde{\Theta}}(t)) = & V(\tilde{\tilde{\Theta}}(t_F)) + \int_{t_F}^{t} \dot{V}(\tilde{\tilde{\Theta}}(s)) ds \\
\leqslant & V(\tilde{\tilde{\Theta}}(t_F)) - \int_{t_F}^{t} \eta \tilde{\tilde{\Theta}}^\top(s) \boldsymbol{\omega}^\top(s) \boldsymbol{\omega}(s) \tilde{\tilde{\Theta}}(s) ds \\
\leqslant & V(\tilde{\Theta}(t_F)) - \eta \lambda_{\min} \left(\int_{t_F}^{t} \boldsymbol{\omega}^\top(s) \boldsymbol{\omega}(s) ds \right) \min_{s\in[t_F,t]} \|\tilde{\Theta}(s)\|^2 \\
\leqslant & V(\tilde{\tilde{\Theta}}(t_F)) - \eta \lambda_{\min}(\boldsymbol{Q}(t)) \min_{s\in[t_F,t]} \|\tilde{\tilde{\Theta}}(s)\|^2. \\
\leqslant & V(\tilde{\tilde{\Theta}}(t_F)) - \eta \varsigma(t) V(\tilde{\tilde{\Theta}}(t)).
\end{aligned} \tag{5.18}$$

Therefore, we conclude that estimation error is non-increasing and convergence. ■

According to Lemma 5.4.1, one obtains that there exists a known estimation error set $\upsilon = \{\hat{\theta}_i \in \mathbb{R} | |\theta_i - \hat{\theta}_i| \leqslant \upsilon^i_{\max}, i = 1,2,\cdots,m\}$ and maximum bound error $\upsilon^i_{\max} \in [0,1]$.

5.4.3 Fault-Tolerant Safety Filter via CBFs

To ensure the safety of systems in the presence of actuator gain faults, we construct an adaptive fault-tolerant GP-CBF second-order cone program (AFT-GP-CBF-SOCP).

For convenience the following derivations, we define $\hat{\Theta} = \text{diag}[\hat{\theta}_1, \cdots, \hat{\theta}_i, \cdots, \hat{\theta}_m] \in \mathbb{R}^{m\times m}$, matrix $\tilde{\Theta} = \text{diag}\left[\tilde{\tilde{\Theta}}\right]$. Then, the following result can be obtained:

Theorem 5.4.1 (AFT-GP-CBF)**.** *According to Lemma 5.3.1, for a valid GP-CBF defined in* (5.6)*, if there exists an extended class $\mathcal{K}$ function α such that*

$$\sup_{\boldsymbol{u}\in\mathbb{U}}\left\{L_f h(\boldsymbol{x})+L_g h(\boldsymbol{x})\hat{\Theta}\boldsymbol{u}+m_h(\boldsymbol{x})-\psi\sigma_h(\boldsymbol{x})+\alpha(h(\boldsymbol{x}))-\|L_g h(\boldsymbol{x})\|\|\boldsymbol{v}_{\max}\|\|\boldsymbol{u}\|\right\}\geqslant 0, \tag{5.19}$$

then the function $h(\boldsymbol{x})$ is said to be AFT-GP-CBF for system (5.13) *for all $\boldsymbol{x}\in\mathbb{A}$ with high probability $1-\rho$, where $\boldsymbol{v}_{\max}=\operatorname{diag}\left[v_{\max}^1,v_{\max}^2,\cdots,v_{\max}^m\right]\in\mathbb{R}^{m\times m}$.*

Proof. Calculate the Lie derivative of $\tilde{h}(\boldsymbol{x},\boldsymbol{u})$ along system (5.3) and according to Lemma 5.3.1, we can derive that

$$\begin{aligned}\dot{\tilde{h}}(\boldsymbol{x},\boldsymbol{u})=&L_f h(\boldsymbol{x})+L_{\Delta f}h(\boldsymbol{x})+L_g h(\boldsymbol{x})\Theta\boldsymbol{u}\\ \geqslant&L_f h(\boldsymbol{x})+m_h(\boldsymbol{x})-\psi\sigma_h(\boldsymbol{x})+L_g h(\boldsymbol{x})\left(\hat{\Theta}+\tilde{\Theta}\right)\boldsymbol{u}\\ \geqslant&L_f h(\boldsymbol{x})+m_h(\boldsymbol{x})-\psi\sigma_h(\boldsymbol{x})+L_g h(\boldsymbol{x})\hat{\Theta}\boldsymbol{u}-\|L_g h(\boldsymbol{x})\|\|\tilde{\Theta}\|\|\boldsymbol{u}\|\\ \geqslant&L_f h(\boldsymbol{x})+L_g h(\boldsymbol{x})\hat{\Theta}\boldsymbol{u}+m_h(\boldsymbol{x})-\psi\sigma_h(\boldsymbol{x})-\|L_g h(\boldsymbol{x})\|\|\boldsymbol{v}_{\max}\|\|\boldsymbol{u}\|\\ \geqslant&-\alpha(h(\boldsymbol{x}))+\|L_g h(\boldsymbol{x})\|\|\boldsymbol{v}_{\max}\|\|\boldsymbol{u}\|\end{aligned} \tag{5.20}$$

for all $\boldsymbol{x}\in\mathbb{A}$ with high probability $1-\rho$. ■

Consider a reference control input $\boldsymbol{u}_{\text{ref}}$ derived by feedback control, PID control, or MPC, we can construct an AFT-GP-CBF-SOCP for system (5.13) as:

$$\boldsymbol{u}_{\text{safe}}=\underset{\boldsymbol{u}\in\mathbb{U}}{\operatorname{argmin}}\|\boldsymbol{u}-\boldsymbol{u}_{\text{ref}}\|^2 \tag{5.21a}$$

$$\text{s.t. } L_f h(\boldsymbol{x})+L_g h(\boldsymbol{x})\hat{\Theta}\boldsymbol{u}+m_h(\boldsymbol{x})-\psi\sigma_h(\boldsymbol{x})\geqslant-\alpha(h(\boldsymbol{x}))+\|L_g h(\boldsymbol{x})\|\|\boldsymbol{v}_{\max}\|\|\boldsymbol{u}\|, \tag{5.21b}$$

where the parameter $\hat{\Theta}$ is updated by (5.16).

5.4.4 Fault-Tolerant Safe Control for High Relative Degrees

In this subsection, we aim to propose an AFT-GP-HOCBF-SOCP for systems with high relative degrees. If system (5.13) fulfills Assumptions 2.1.1 and 5.3.1, one derives the following probabilistically adaptive HOCBF constraint:

Theorem 5.4.2 (AFT-GP-HOCBF)**.** *Based on Theorem 5.3.1, for a valid GP-HOCBF defined in* (5.9)*, if there exist a set of a class $\mathcal{K}$ functions $\alpha_i(\cdot)$, $i\in\{0,1,\cdots,r\}$ such that*

$$\begin{aligned}\sup_{\boldsymbol{u}\in\mathbb{U}}\Big\{&L_f^r h(\boldsymbol{x})+L_g L_f^{r-1}h(\boldsymbol{x})\hat{\Theta}\boldsymbol{u}+S(h(\boldsymbol{x}))+m_{h^r}(\boldsymbol{x})-\psi\sigma_{h^r}(\boldsymbol{x})\\ &+\alpha_r(\beta_{r-1}(\boldsymbol{x}))-\left\|L_g L_f^{r-1}h(\boldsymbol{x})\right\|\|\boldsymbol{v}_{\max}\|\|\boldsymbol{u}\|\Big\}\geqslant 0,\end{aligned} \tag{5.22}$$

then the function $h(\boldsymbol{x})$ is said to be AFT-GP-HOCBF for system (5.13) *for all $\boldsymbol{x} \in \mathbb{A}$ with high probability $1-\rho$.*

Proof. Calculate the r-th Lie derivative of $\tilde{h}(\boldsymbol{x},\boldsymbol{u})$ along system (5.3) and based on Theorem 5.3.1, one obtains that

$$
\begin{aligned}
\tilde{h}^r(\boldsymbol{x},\boldsymbol{u}) =& L_f\beta_{r-1}(\boldsymbol{x}) + L_{\Delta f}\beta_{r-1}(\boldsymbol{x}) + L_g\beta_{r-1}(\boldsymbol{x})\Theta\boldsymbol{u} \\
=& L_f^r h(\boldsymbol{x}) + S(h(\boldsymbol{x})) + L_{\Delta f}L_f^{r-1}h(\boldsymbol{x}) + L_gL_f^{r-1}h(\boldsymbol{x})\left(\hat{\Theta}+\tilde{\Theta}\right)\boldsymbol{u} \\
\geqslant& L_f^r h(\boldsymbol{x}) + S(h(\boldsymbol{x})) + m_h(\boldsymbol{x}) - \psi\sigma_h(\boldsymbol{x}) + L_gL_f^{r-1}h(\boldsymbol{x})\hat{\Theta}\boldsymbol{u} + L_gL_f^{r-1}h(\boldsymbol{x})\tilde{\Theta}\boldsymbol{u} \\
\geqslant& L_f^r h(\boldsymbol{x}) + S(h(\boldsymbol{x})) + m_h(\boldsymbol{x}) - \psi\sigma_h(\boldsymbol{x}) + L_gL_f^{r-1}h(\boldsymbol{x})\hat{\Theta}\boldsymbol{u} - \|L_gL_f^{r-1}h(\boldsymbol{x})\|\|\tilde{\Theta}\|\|\boldsymbol{u}\| \\
\geqslant& L_f^r h(\boldsymbol{x}) + S(h(\boldsymbol{x})) + m_h(\boldsymbol{x}) - \psi\sigma_h(\boldsymbol{x}) + L_gL_f^{r-1}h(\boldsymbol{x})\hat{\Theta}\boldsymbol{u} - \|L_gL_f^{r-1}h(\boldsymbol{x})\|\|\boldsymbol{v}_{\max}\|\|\boldsymbol{u}\| \\
\geqslant& -\alpha_r(\beta_{r-1}(\boldsymbol{x})) + \|L_gL_f^{r-1}h(\boldsymbol{x})\|\|\boldsymbol{v}_{\max}\|\|\boldsymbol{u}\| \qquad (5.23)
\end{aligned}
$$

for all $\boldsymbol{x} \in \mathbb{A}$ with high probability $1-\rho$. ■

In what follows, constraint (5.22) is finally transformed as the following AFT-GP-HOCBF-SOCP for system (5.13):

$$
\begin{aligned}
&\boldsymbol{u}_{\text{safe}} = \underset{\boldsymbol{u}\in\mathbb{U}}{\operatorname{argmin}} \|\boldsymbol{u}-\boldsymbol{u}_{\text{ref}}\|^2 \qquad (5.24a) \\
&\text{s.t. } L_f^r h(\boldsymbol{x}) + L_gL_f^{r-1}h(\boldsymbol{x})\hat{\Theta}\boldsymbol{u} + S(h(\boldsymbol{x})) + m_{h^r}(\boldsymbol{x}) - \psi\sigma_{h^r}(\boldsymbol{x}) \\
&\qquad \geqslant -\alpha_r(\beta_{r-1}(\boldsymbol{x})) + \|L_gL_f^{r-1}h(\boldsymbol{x})\|\|\boldsymbol{v}_{\max}\|\|\boldsymbol{u}\|, \qquad (5.24b)
\end{aligned}
$$

where the parameter $\hat{\Theta}$ is updated by (5.16).

Remark 5.4.1. *While the FTC method is designed to maintain the faulty systems with acceptable performance, it cannot strictly guarantee their safety. To overcome this limitation, this chapter introduces two advanced methods, AFT-GP-CBF and AFT-GP-HOCBF, to address the issues of unknown actuator gain faults and model uncertainty. These methods represent a significant step forward in achieving safety in uncertain systems subject to unknown actuator gain faults.*

5.5 Numerical Example

We respectively evaluate our proposed AFT-GP-CBF and AFT-GP-HOCBF methods on two simulated systems: 1) adaptive cruise control system 2) mobile robotic system.

5.5.1 Adaptive Cruise Control System

This subsection compares our algorithm `AFT-GP-CBF` with four methods: `CBF` method [21] (no learning and no estimation), GP-based CBF method [34] (`GP-CBF`) (no estimation), CBF with gain fault estimation method [134] (`FT-CBF`) (no learning), GP-based robust CBF method with a known lowest bound value [77] (`Robust GP-CBF`) (no estimation). Consider the system dynamics with the model uncertainty as follows [135]:

$$\underbrace{\begin{bmatrix} \dot{p} \\ \dot{v} \\ \dot{z} \end{bmatrix}}_{\dot{\boldsymbol{x}}} = \underbrace{\begin{bmatrix} v \\ -\frac{F_r(v)}{m} \\ v_0 - v \end{bmatrix}}_{\boldsymbol{f}(\boldsymbol{x})} + \underbrace{\begin{bmatrix} 0 \\ -\frac{\Delta F_r(v)}{m} \\ 0 \end{bmatrix}}_{\Delta \boldsymbol{f}(\boldsymbol{x})} + \underbrace{\begin{bmatrix} 0 \\ \frac{1}{m} \\ 0 \end{bmatrix}}_{\boldsymbol{g}(\boldsymbol{x})} u, \tag{5.25}$$

where p, v, and z are defined as position, velocity, and distance between ego vehicle and its preceding vehicle. v_0 represents preceding vehicle's velocity. m is the mass of the ego vehicle. $F_r(v)$ stands for the aerodynamic drag with $F_r(v) = f_0 + f_1 v + f_2 v^2$. We define $\Delta F_r(v)$ as the model uncertainty with $\Delta F_r(v) = \Delta f_0 + \Delta f_1 v + \Delta f_2 v^2$. $u \in \mathbb{R}$ is control input.

Then, we select $m = 1650$kg, $f_0 = 0.1, f_1 = 5, f_2 = 0.25, v_0 = 14$m/s, and set $\boldsymbol{x}(0) = [0, 20, 100]^\top$, model uncertainty $\Delta f_0 = 0.6, \Delta f_1 = 3, \Delta f_2 = 2$. The control input $u \in [u_{\min}, u_{\max}]$ with $u_{\min} = -0.3mg$ and $u_{\max} = 0.3mg$, where $g = 9.81\text{m/s}^2$. Define $h(\boldsymbol{x}) = z - 1.8v - \frac{5(v-v_0)^2}{3g}$. Then, we choose $\boldsymbol{u}_{\text{ref}} = Fr(v)$ in controller (5.21).

To fit the model uncertainty $\Delta F_r(v)$, we exploit the CBF-QP-based controller to collect the system state until $h(\boldsymbol{x}) < 0$, constructing a training data set $\mathbb{D}_h$. Note that no actuator faults occur during the data collection process. We set the parameter $\psi = 0.5$, observation noise $d \sim (0, 0.5)$, kernel lengthscale $l = 1$ and signal variance $\sigma_f^2 = 2$.

Since actuator gain fault θ is unknown with known bound values $\theta \in [0.4, 1]$, we assume that actuator gain fault value $\theta = 0.7$ and a fault occurrence time of $t_F = 6$s, which leads to $u_F = 0.7u$. Additionally, we consider two different initial estimation values: a higher initial value $\hat{\theta}_{\text{higher}}(0) = 0.9$, referred to as the AFT-GP-CBF method with a higher initial value (`HAFT-GP-CBF`), and a lower initial value $\hat{\theta}_{\text{lower}}(0) = 0.5$, referred to as the AFT-GP-CBF method with a lower initial value (`LAFT-GP-CBF`). For the gain fault estimator, we set parameters $\eta = 3$ and $\kappa = 3$.

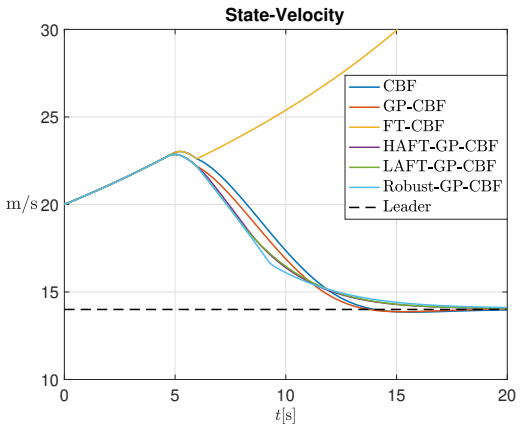

(a) Profiles of the ego vehicle's velocity.

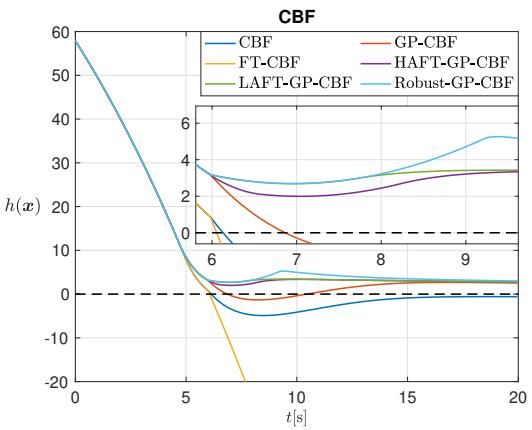

(b) Profiles of different CBFs.

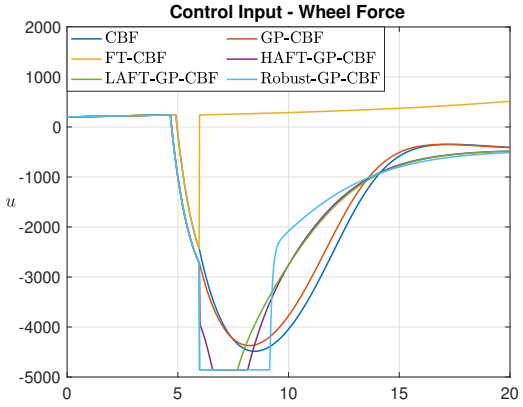

(c) Profiles of control input u.

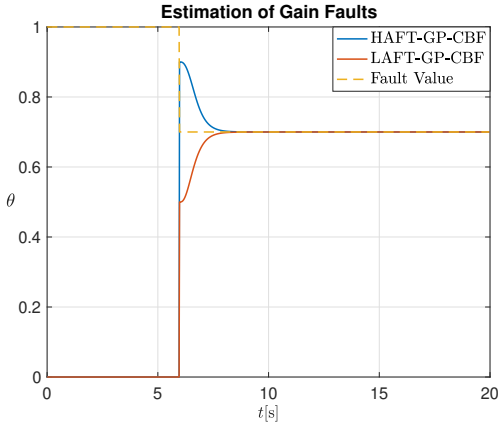

(d) Profiles of fault parameter estimation.

Figure 5.2: Comparative results through the ACC system.

As illustrated in Figure 5.2(a), the value of ego vehicle's velocity based on `FT-CBF` method rapidly increases when $t \geqslant 6$s. Except for the `FT-CBF` method, the velocity of the ego vehicle successfully approaches the leader's velocity when using the other five control methods. In Figure 5.2(b), one observes that the methods of `CBF`, `GP-CBF`, and `FT-CBF` fail to guarantee the safety of the ego vehicle before 7s. Compared with `robust GP-CBF` and `LAFT-GP-CBF` methods, the `HAFT-GP-CBF` method demonstrates reduced conservativeness. The conservativeness of the `Robust GP-CBF` method arises from its consideration of the worst-case scenario for actuator gain faults, while the conservativeness of the `LAFT-GP-CBF` method is due to its lower initial values. After 8s, `LAFT-GP-CBF` method shows lower conservative than `Robust GP-CBF`. Figures 5.2(c) and 5.2(d) display the control input and the estimation of gain faults, showing that the online estimator con-

verges to the gain fault under two different initial values. Therefore, we conclude that our methods, LAFT-GP-CBF and HAFT-GP-CBF, effectively help the ego vehicle maintain a safe distance in the presence of model uncertainty and unknown actuator gain faults while exhibiting reduced conservativeness.

5.5.2 Mobile Robotic System

This subsection aims to compare our algorithms with four methods: HOCBF method [22] (no learning and no estimation), GP-based HOCBF method [25] (GP-HOCBF) (no estimation), HOCBF with gain fault estimation method [134] (FT-HOCBF) (no learning), GP-based robust HOCBF method with a known lowest bound value (Robust GP-HOCBF) (no estimation). Consider the system dynamics with the model uncertainty as follows [114]:

$$\underbrace{\begin{bmatrix}\dot{x}_1\\ \dot{x}_2\\ \dot{x}_3\\ \dot{x}_4\end{bmatrix}}_{\dot{\boldsymbol{x}}} = \underbrace{\begin{bmatrix}x_3\\ x_4\\ 0\\ 0\end{bmatrix}}_{f(\boldsymbol{x})} + \underbrace{\begin{bmatrix}0\\ 0\\ \frac{\Delta x_3}{m}\\ \frac{\Delta x_4}{m}\end{bmatrix}}_{\Delta f(\boldsymbol{x})} + \underbrace{\begin{bmatrix}0 & 0\\ 0 & 0\\ \frac{1}{m} & 0\\ 0 & \frac{1}{m}\end{bmatrix}}_{g(\boldsymbol{x})} \underbrace{\begin{bmatrix}u_1\\ u_2\end{bmatrix}}_{\boldsymbol{u}}, \tag{5.26}$$

where x_1 and x_2 are defined as the position of the mobile robot. x_3 and x_4 represent the velocity of the mobile robot. m is the mass of the mobile robot. We define Δx_3 and Δx_4 as the model uncertainty. u_1 and u_2 are control inputs.

Then, we select $m = 1\text{kg}$, $\boldsymbol{x}(0) = [-3.5, 3.5, 0, 0]^\top$, uncertain terms $\Delta x_3 = 0.1$ and $\Delta x_4 = 0.8$, and the desired state $\boldsymbol{x}_{\text{desired}} = [0,0,0,0]^\top$. The control input $u_1, u_2 \in [u_{\min}, u_{\max}]$ with $u_{\min} = -2.5$ and $u_{\max} = 2.5$. Define $h(\boldsymbol{x}) = (x_1+1)^2 - (x_2-1)^2 - 1$. Then, we choose $\boldsymbol{u}_{\text{ref}} = -K(\boldsymbol{x} - \boldsymbol{x}_{\text{desired}}), K = \begin{bmatrix}1 & 0 & 1 & 0\\ 0 & 1 & 0 & 1\end{bmatrix}^\top$ in controller (5.24).

To fit the model uncertainty $\Delta f(\boldsymbol{x})$, we use HOCBF-QP to collect the system state until either $\beta_0(\boldsymbol{x}) < 0$ or $\beta_1(\boldsymbol{x}) < 0$, thereby constructing the training dataset $\mathbb{D}_{h^r}$. The same kernel and measurement parameters as those described in Section 5.5.1 are used. For this, we set the parameter $\psi = 0.1$.

Suppose actuator gain faults $\theta_1 = 0.7$ and $\theta_2 = 0.6$, with a fault occurrence time of $t_F = 2\text{s}$, resulting in $\boldsymbol{u}_F = \text{diag}[\theta_1, \theta_2]\boldsymbol{u}$. The gain fault boundary is given as $\theta_1, \theta_2 \in [0.35, 1]$. We set initial estimation values: higher initial value $\hat{\Theta}_{\text{higher}}(0) = \text{diag}[0.9, 0.8]$ referred to as the AFT-GP-HOCBF method with a higher initial value (HAFT-GP-HOCBF), and lower initial value $\hat{\Theta}_{\text{lower}}(0) = \text{diag}[0.5, 0.4]$ referred to LAFT-GP-HOCBF. For the gain fault estimator, we set parameters $\eta = 10$ and $\kappa = 1$.

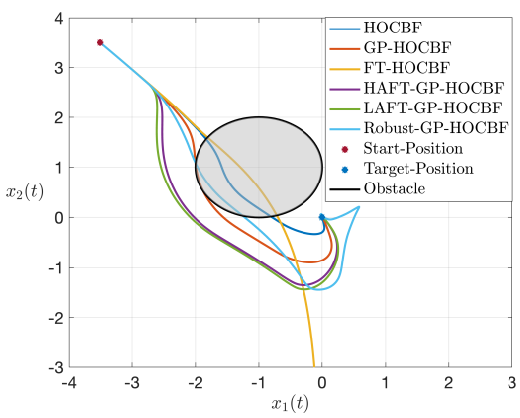

(a) Profiles of the robot's position.

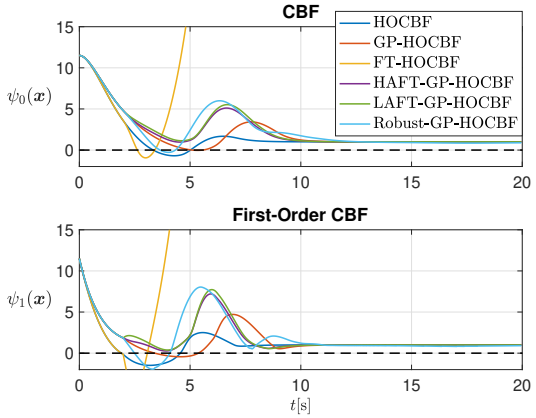

(b) Profiles of HOCBFs.

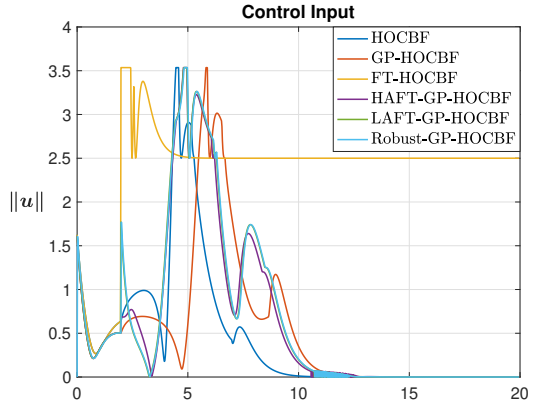

(c) Profiles of control input $\|u\|$.

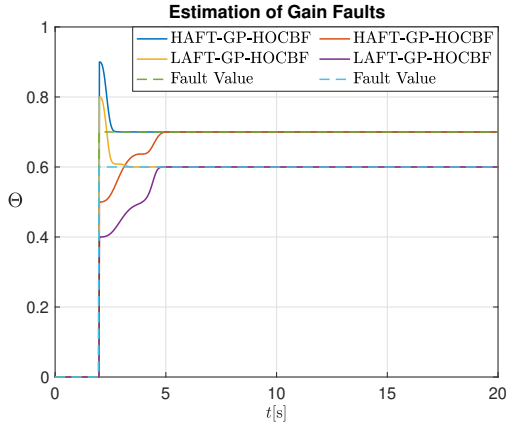

(d) Profiles of fault parameter estimation.

Figure 5.3: Comparative results through the mobile robotic system.

As shown in Figure 5.3(a), the mobile robot is able to reach the target point safely only when the proposed methods, namely `HAFT-GP-HOCBF` and `LAFT-GP-HOCBF`, are applied. This highlights the effectiveness of integrating fault-tolerant mechanisms and GP-based HOCBFs. In Figure 5.3(b), although the `GP-HOCBF` method successfully ensures that $\psi_0(\boldsymbol{x}) \geqslant 0$, it fails to maintain the condition $\psi_1(\boldsymbol{x}) \geqslant 0$, leading to safety violations at the higher-order level. The `FT-HOCBF` method shows instability throughout the simulation, primarily because it considers only actuator faults while neglecting model uncertainty, which plays a critical role in safety-critical systems. Additionally, the `Robust GP-HOCBF` method exhibits noticeable fluctuations during the time interval $t \in [0\text{s}, 10\text{s}]$, suggesting limited robustness under certain conditions. In contrast, both `HAFT-GP-HOCBF` and `LAFT-GP-HOCBF` demonstrate similar and stable performance, effec-

tively maintaining system safety. Figures 5.3(c) and 5.3(d) further illustrate the control input profiles and the gain fault estimation process, showing that the online estimator can accurately converge to the true gain fault values under two different initial conditions. Given this, one concludes that the `HAFT-GP-HOCBF` and `LAFT-GP-HOCBF` methods effectively enable the mobile robot to safely reach the target point in the presence of unknown actuator gain faults and model uncertainty.

5.6 Conclusion

In this chapter, we have proposed two types of probabilistic and adaptive CBF and HOCBF methods to address the challenges posed by unknown actuator gain faults and model uncertainty. By developing a learning-based adaptive fault-tolerant CBF-SOCP and extending it to the HOCBF framework, we have provided two safe control methods for ensuring safety in faulty systems with uncertainty. Two numerical examples have been demonstrated the effectiveness and superiority of our methods, highlighting their potential for application in safety-critical systems such as autonomous vehicles and robotics, compared to existing works.

There are several limitations of our methods which we will study in future research. For instance, in the GP learning for HOCBFs, we assume that model uncertainty is matched, which restricts the allowable structures of unknown model uncertainty. Moreover, we only consider uncertain drift dynamics while ignoring uncertain gain dynamics. In future, we will investigated safety-critical control for systems with uncertain drift and gain dynamics by using the GP regression.

CHAPTER 6

PROBABILISTICALLY SAFE FAULT-TOLERANT CONTROL USING LEARNING-BASED HIGH-ORDER CONTROL BARRIER FUNCTIONS

This chapter is based on the paper titled "Probabilistically Safe Control Using Learning-Based High-Order Control Barrier Functions," IEEE Transactions on Automatic Control, Under Review.

To handle RQ4 and achieve RO4, this chapter proposes an enhanced GP-based barrier (EGPBarrier) method that integrates GP-based probabilistic modelling into the HOCBF framework to formulate a probabilistic HOCBF approach. To address model uncertainty affecting the safety constraint, we introduce a novel compound kernel for uncertainty-aware constraint learning. We establish three theoretical conditions to guarantee the feasibility of the proposed method. Finally, we evaluate this method on two numerical examples, comparing its performance with existing approaches.

The content of this chapter is organized as follows. Section 6.1 surveys related studies associated with this work. Section 6.2 provides the necessary preliminaries. The core contributions are discussed in Sections 6.3, 6.4, and 6.5. Section 6.6 presents numerical

examples that demonstrate the effectiveness of the two proposed approaches. A summary of the chapter is given in Section 6.7. In addition, an overview of the proposed methods is illustrated in Figure 6.

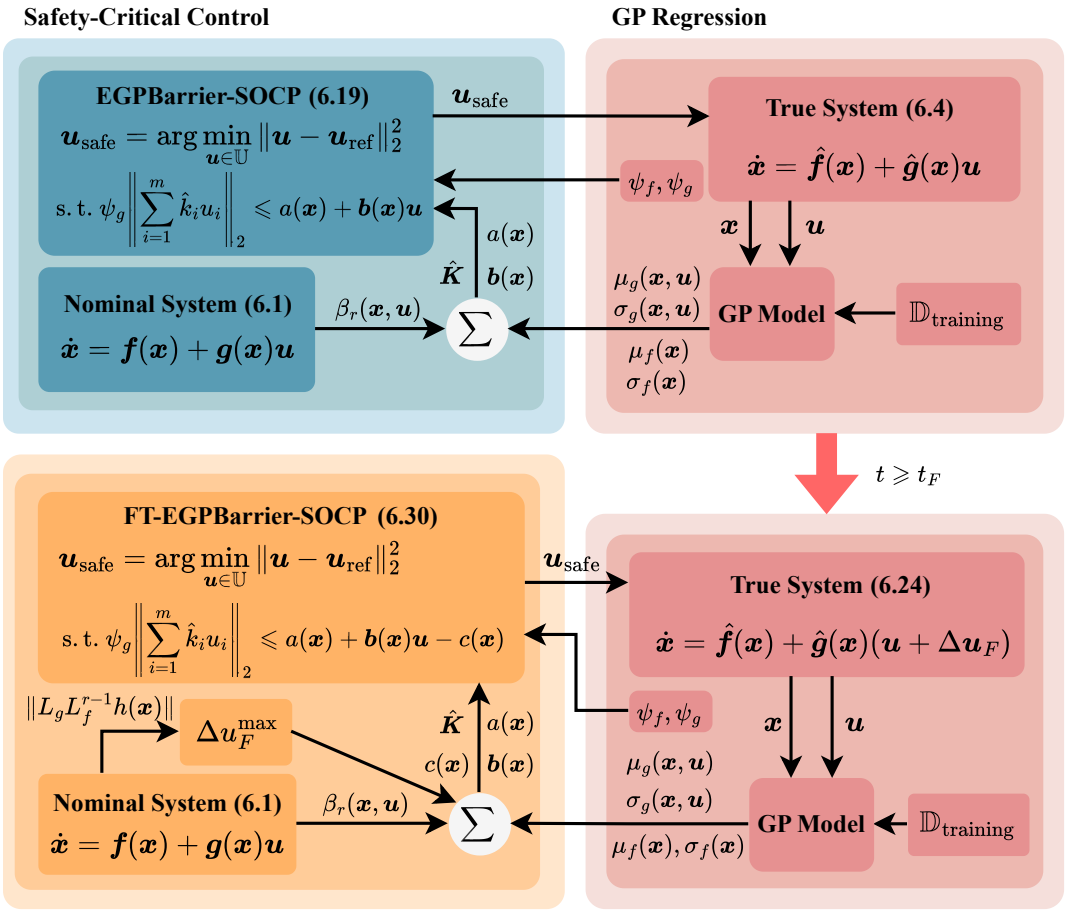

Figure 6.1: An overview of EGPBarrier and FT-EGPBarrier methods, where the uncertain terms in the HOCBF constraint are modelled using GP regression. If the actuator faults occurrence, the EGPBarrier method is switched as the FT-EGPBarrier method.

6.1 Introduction

Safety is a fundamental requirement in autonomous systems during real-time operation. To ensure safe behavior, researchers have developed safety-critical control methods, including CBFs [18], HJ reachability analysis [19], and safe RL [20]. Unlike HJ

reachability and safe RL, CBFs offer rigorous safety guarantees for control systems by enforcing system state forward invariance of safe sets. They have been widely applied in robotic systems, such as legged robot systems [21]. However, CBFs highly rely on accurate system models, and their effectiveness may be affected by model uncertainty. Given this, researchers have explored the GPs method, which provides a probabilistic modeling framework and offers greater robustness to measurement noise [11]. To ensure the safety of uncertain systems using CBFs, some studies use GP regression to model unknown system dynamics [24, 111, 136], while others apply it to fit uncertainties in the safety constraint [89, 92, 93, 137]. As stated in [111], Dhiman et al. presented a matrix variate GP regression method to learning unknown system dynamics and designed a probabilistic CBF method. Wang et al. [93] established a GP-based CBF method and used Bayesian optimization to optimize the safe control performance. However, matrix-variate GP regression, as used in [24, 111, 136] to model unknown system dynamics, is computationally expensive and structurally complex. The studies in [89, 92, 93, 137] assume that only drift dynamics contains model uncertainty. To overcome these issues, few researchers presented an affine dot product kernel method [34] and a compound kernel method [39] to handle both uncertain drift and gain dynamics in control systems. Nevertheless, the proposed method in [34] lacks flexibility and is sensitive to parameter tuning. Although the method in [39] avoids the additional feasibility analysis required by the SOCP formulation in [34], it is limited to systems with a scalar control input due to its underlying model assumptions.

Considering that CBFs are limited to systems with relative degree one, HOCBFs have been proposed as an extension to handle systems with high relative degrees [94]. In contrast to CBFs, model uncertainty impose additional challenges on the design of an HOCBF approach. According to the definition of the HOCBF, unknown drift dynamics can directly influence the constraint expression involving the control input. To tackle

this, some studies, such as [23, 114], provide an assumption of the model uncertainty to avoid the above issue, while others design GP-based HOCBF methods using the affine dot product kernel method to model uncertain terms [25, 38]. As stated in [114], the authors designed a data-driven adaptive control framework that combines high-order robust adaptive CBF and adaptive CLF methods using the concurrent learning strategy. Aali et al. [38] focused on guaranteeing the system safety based on designed the GP-based HOCBF. However, the assumptions of model uncertainty in [23, 114] are conservative and hinder the generality of their methods. Additionally, the kernel methods used in [25, 38] suffer from limited flexibility and sensitivity to parameter tuning. To address these issues, this chapter proposes EGPBarrier and fault-tolerant EGPBarrier methods using a novel compound kernel method.

6.2 Preliminaries

This section provides a brief introduction to the definitions of the HOCBF and GP regression. Then, we begin with the definition of extended class $\mathcal{K}$ functions:

Definition 6.2.1 (Extended class $\mathcal{K}$ function [18])**.** *If a continuous function $\alpha : [-b, a) \to [-\infty, \infty)$ is strictly increasing and $\alpha(0) = 0$, then the function α is said to belong to extended class $\mathcal{K}$ for some $a, b > 0$.*

Consider the following control-affine system of the form:

$$\dot{\boldsymbol{x}} = \boldsymbol{f}(\boldsymbol{x}) + \boldsymbol{g}(\boldsymbol{x})\boldsymbol{u}, \tag{6.1}$$

where $\boldsymbol{x} \in \mathbb{R}^n$ presents the system state. The drift dynamic $\boldsymbol{f} : \mathbb{R}^n \to \mathbb{R}^n$ and the gain dynamic $\boldsymbol{g} : \mathbb{R}^n \to \mathbb{R}^{n \times m}$ are known and locally Lipschitz functions. $\boldsymbol{u} \in \mathbb{U} \subseteq \mathbb{R}^m$ is the control input, along with $\mathbb{U}$ denotes a control constraint set.

6.2.1 High-Order CBFs

The CBF method is reformulated as a safety-critical constraint to ensure system safety. However, it encounters greater challenges when applied to systems with high relative

degrees, due to the term $L_g h(\boldsymbol{x}) = 0$. To handle this issue, the HOCBF is proposed. Then, we first assume the function h fulfilling Definition 2.4.2.

Definition 6.2.2 (HOCBF [94])**.** *Define a sequence of functions $\beta_i : \mathbb{R}^n \to \mathbb{R}, i \in \{1, \cdots, r\}$, recursively as $\beta_i(\boldsymbol{x}) = \dot{\beta}_{i-1}(\boldsymbol{x}) + \alpha_i(\beta_{i-1}(\boldsymbol{x}))$ with base function $\beta_0(\boldsymbol{x}) = h(\boldsymbol{x})$, and denote a sequence of sets $\mathbb{A}_i = \{\boldsymbol{x} \in \mathbb{R}^n : \beta_i(\boldsymbol{x}) \geqslant 0\}$. If there exist a sequence of extended class $\mathcal{K}$ functions $\alpha_i(\cdot)$ such that*

$$\sup_{\boldsymbol{u} \in \mathbb{U}} \{\underbrace{L_f \beta_{r-1}(\boldsymbol{x}) + L_g \beta_{r-1}(\boldsymbol{x})\boldsymbol{u} + \alpha_r(\beta_{r-1}(\boldsymbol{x}))}_{\beta_r(\boldsymbol{x},\boldsymbol{u}) = h^r(\boldsymbol{x},\boldsymbol{u})} \geqslant 0\}, \tag{6.2}$$

for all $\boldsymbol{x} \in \mathbb{A}_1 \cap, \cdots, \cap \mathbb{A}_r$, then function $h : \mathbb{R}^n \to \mathbb{R}$ is said to be a candidate HOCBF of the relative degree r for system (6.1)*, where $L_f \beta_{r-1}(\boldsymbol{x}) = L_f^r h(\boldsymbol{x}) + \sum_{i=1}^{r-1} L_f^i(\alpha_{r-i} \circ \beta_{r-i-1})(\boldsymbol{x}) \in \mathbb{R}$ and $L_g \beta_{r-1}(\boldsymbol{x}) = L_g L_f^{r-1} h(\boldsymbol{x}) \in \mathbb{R}^{1 \times m}$.*

Then, the HOCBF constraint is incorporated into a QP to compute a safe control input $\boldsymbol{u}_{\text{safe}} \in \mathbb{R}^m$ for system (6.1)*, resulting in the following formulation:*

$$\boldsymbol{u}_{\text{safe}} = \arg\min_{\boldsymbol{u} \in \mathbb{U}} \|\boldsymbol{u} - \boldsymbol{u}_{\text{ref}}\|_2^2, \tag{6.3a}$$

$$\text{s.t. } L_f \beta_{r-1}(\boldsymbol{x}) + L_g \beta_{r-1}(\boldsymbol{x})\boldsymbol{u} + \alpha_r(\beta_{r-1}(\boldsymbol{x})) \geqslant 0, \tag{6.3b}$$

where $\boldsymbol{u}_{\text{ref}} \in \mathbb{R}^m$ presents a reference control input, which can be obtained by model predictive control or PID control.

6.3 Uncertainty-Aware Safety Constraint Learning

This section aims to propose a novel compound kernel method for learning uncertain terms in safety constraints.

Consider an uncertain control-affine system as follows:

$$\dot{\boldsymbol{x}} = \hat{\boldsymbol{f}}(\boldsymbol{x}) + \hat{\boldsymbol{g}}(\boldsymbol{x})\boldsymbol{u}, \tag{6.4}$$

where the system state $\boldsymbol{x}$ and control input $\boldsymbol{u}$ have same meanings as in system (6.1). The drift dynamic $\hat{\boldsymbol{f}} : \mathbb{R}^n \to \mathbb{R}^n$ and the gain dynamic $\hat{\boldsymbol{g}} : \mathbb{R}^n \to \mathbb{R}^{n \times m}$ are partially known and locally Lipschitz function. Note that systems (6.1) and (6.4) represent the known nominal system and the partially known true system under model uncertainty.

Based on (6.3), a new QP-based controller for system (6.4) can be derived as follows:

$$\boldsymbol{u}_{\text{safe}} = \arg\min_{\boldsymbol{u}\in\mathbb{U}} \|\boldsymbol{u}-\boldsymbol{u}_{\text{ref}}\|_2^2, \tag{6.5a}$$

$$\text{s.t. } \underbrace{L_{\hat{f}}\beta_{r-1}(\boldsymbol{x}) + L_{\hat{g}}\beta_{r-1}(\boldsymbol{x})\boldsymbol{u} + \alpha_r(\beta_{r-1}(\boldsymbol{x}))}_{\hat{\beta}_r(\boldsymbol{x},\boldsymbol{u})=\hat{h}^r(\boldsymbol{x},\boldsymbol{u})} \geqslant 0, \tag{6.5b}$$

where $L_{\hat{f}}\beta_{r-1}(\boldsymbol{x}) = L_{\hat{f}}^r h(\boldsymbol{x}) + \sum_{i=1}^{r-1} L_{\hat{f}}^i(\alpha_{r-i}\circ\beta_{r-i-1})(\boldsymbol{x}) \in \mathbb{R}$ and $L_{\hat{g}}\beta_{r-1}(\boldsymbol{x}) = L_{\hat{g}}L_{\hat{f}}^{r-1}h(\boldsymbol{x}) \in \mathbb{R}^{1\times m}$.

According to (6.3b) and (6.5b), we define the constraint errors between the true system and the nominal system as follows:

$$\Delta\beta_f(\boldsymbol{x}) = L_{\hat{f}}\beta_{r-1}(\boldsymbol{x}) - L_f\beta_{r-1}(\boldsymbol{x}), \tag{6.6}$$

$$\Delta\beta_g(\boldsymbol{x}) = L_{\hat{g}}L_{\hat{f}}^{r-1}h(\boldsymbol{x}) - L_gL_f^{r-1}h(\boldsymbol{x}), \tag{6.7}$$

where $\Delta\beta_f(\boldsymbol{x}) \in \mathbb{R}$ and $\Delta\beta_g(\boldsymbol{x}) \in \mathbb{R}^{1\times m}$ denote the constraint errors arising from model uncertainty.

Remark 6.3.1. *Unlike CBF constraints, it is more challenging to mitigate the effects of model uncertainty in HOCBF constraints. Even if only the drift dynamic $\hat{\boldsymbol{f}}(\boldsymbol{x})$ in system* (6.4) *contains uncertainties, the uncertain term* (6.7) *still appears and needs to be dealt with. To handle this, prior work [114] introduced relatively conservative assumptions to eliminate the uncertain term* (6.7)*, but this hinders the generality and applicability of the HOCBF method. Therefore, this chapter proposes a novel GP-based learning approach to model the uncertain terms in the HOCBF constraint, aiming to reduce the conservatism introduced by prior assumptions [114].*

Then, safe constraint (6.5b) can be rewritten as follows:

$$\hat{\beta}_r(\boldsymbol{x},\boldsymbol{u}) = L_f\beta_{r-1}(\boldsymbol{x}) + L_gL_f^{r-1}h(\boldsymbol{x})\boldsymbol{u} + \Delta\beta_f(\boldsymbol{x}) + \Delta\beta_g(\boldsymbol{x})\boldsymbol{u} + \alpha_r(\beta_{r-1}(\boldsymbol{x})). \tag{6.8}$$

The QP-based controller (6.5) can be rewritten as follows:

$$\boldsymbol{u}_{\text{safe}} = \arg\min_{\boldsymbol{u}\in\mathbb{U}} \|\boldsymbol{u}-\boldsymbol{u}_{\text{ref}}\|_2^2, \tag{6.9a}$$

$$\text{s.t. } \beta_r(\boldsymbol{x},\boldsymbol{u}) + \Delta\beta_f(\boldsymbol{x}) + \Delta\beta_g(\boldsymbol{x})\boldsymbol{u} \geqslant 0. \tag{6.9b}$$

To fit these errors, we define $\Delta\beta_f(\boldsymbol{x}) \sim \mathcal{GP}(0, k_f(\boldsymbol{x},\boldsymbol{x}'))$ and each $\Delta\beta_g^i(\boldsymbol{x}) \sim \mathcal{GP}(0, k_g^i(\boldsymbol{x},\boldsymbol{x}'))$, $i \in \{1,\cdots m\}$ as independent single-output GPs. Consequently, the composite

term $\Delta\beta(\boldsymbol{x},\boldsymbol{u})$ becomes a single-output GP, as shown in [138]:

$$\begin{aligned}\Delta\beta(\boldsymbol{x},\boldsymbol{u}) &\sim \mathcal{GP}\left(0, k_{\text{com}}((\boldsymbol{x},\boldsymbol{u}),(\boldsymbol{x}',\boldsymbol{u}'))\right)\\ k_{\text{com}}((\boldsymbol{x},\boldsymbol{u}),(\boldsymbol{x}',\boldsymbol{u}')) &= k_f(\boldsymbol{x},\boldsymbol{x}') + \sum_{i=1}^{m} k_g^i(\boldsymbol{x},\boldsymbol{x}')u_i u_i',\end{aligned} \tag{6.10}$$

where $\Delta\beta(\boldsymbol{x},\boldsymbol{u}) = \Delta\beta_f(\boldsymbol{x}) + \Delta\beta_g(\boldsymbol{x})\boldsymbol{u}$ and $k_{\text{com}}(\cdot,\cdot)$ is a compound kernel.

Assumption 6.3.1 (Measurable Variables [35])**.** *Suppose that the system state $\boldsymbol{x}$ is fully observable, along with the $\hat{\beta}_{r-1}(\boldsymbol{x})$ and $\beta_r(\boldsymbol{x},\boldsymbol{u})$ can be computed and estimated.*

Under Assumption 6.3.1 and considering the approximation error and observation noise, the observation of $\Delta\beta(\boldsymbol{x},\boldsymbol{u})$ is expressed as follows [25, 38]:

$$y_j = \frac{\hat{\beta}_{r-1}(\boldsymbol{x}(t+\Delta t)) - \hat{\beta}_{r-1}(\boldsymbol{x}(t))}{\Delta t} - \beta_r(\boldsymbol{x}_j,\boldsymbol{u}_j) + d_j, \tag{6.11}$$

where $j = 1,2,\cdots,N$ is the index of collected data. $d_j \sim \mathcal{N}(0,\sigma_n^2)$ represents the approximation errors and observation noise. Δt denotes the sampling interval. Correspondingly, we define a training dataset $\mathbb{D}_{\text{training}} = \{\boldsymbol{x}_j,\boldsymbol{u}_j,y_j\}_{j=1}^N$.

Based on the given the dataset $\mathbb{D}_{\text{training}} = \{\boldsymbol{x}_j,\boldsymbol{u}_j,y_j\}_{j=1}^N$, the compound kernel $k_{\text{com}}(\cdot,\cdot)$ can be formulated as follows:

$$\boldsymbol{K}_{\text{com}} = \boldsymbol{K}_f + \sum_{i=1}^{m} \boldsymbol{U}_i \boldsymbol{K}_g^i \boldsymbol{U}_i + \sigma_n^2 I_N, \tag{6.12}$$

where covariance matrices $\boldsymbol{K}_f \in \mathbb{R}^{N\times N}$ and $\boldsymbol{K}_g \in \mathbb{R}^{N\times N}$ are defined analogously to (2.1) and (6.10) using $k_f(\boldsymbol{X}_p,\boldsymbol{X}_q)$ and $k_g^i(\boldsymbol{X}_p,\boldsymbol{X}_q)$. Matrix $\boldsymbol{U}_i$ =diag$[u_{i,1},\cdots,u_{i,N}] \in \mathbb{R}^{N\times N}$.

Different from GP-based model learning for $\hat{\boldsymbol{f}}(\boldsymbol{x})$ and $\hat{\boldsymbol{g}}(\boldsymbol{x})$, learning for safety constraint terms $\Delta\beta_f(\boldsymbol{x})$ and $\Delta\beta_g(\boldsymbol{x})\boldsymbol{u}$ are scalar-valued, which reduces both the structural complexity and computational time of GP regression.

Then, we can derive the following lemma:

Lemma 6.3.1 (Posterior Mean and Variance)**.** *According to the training data $\mathbb{D}_{\text{training}}$ and compound kernel* (6.12)*, the GP posterior means and variances for safety constraint terms $\Delta\beta_f(\boldsymbol{x}^\star)$ and $\Delta\beta_g(\boldsymbol{x}^\star)\boldsymbol{u}^\star$ are given as follows:*

$$\begin{aligned}\mu_f(\boldsymbol{x}^\star) &= \boldsymbol{k}_f^\top \boldsymbol{K}_{\text{com}}^{-1}\boldsymbol{y},\ \sigma_f^2(\boldsymbol{x}^\star) = k_f^\star - \boldsymbol{k}_f^\top \boldsymbol{K}_{\text{com}}^{-1}\boldsymbol{k}_f,\\ \mu_g(\boldsymbol{x}^\star,\boldsymbol{u}^\star) &= \sum_{i=1}^{m} u_i^\star (\boldsymbol{k}_g^i)^\top \boldsymbol{U}_i \boldsymbol{K}_{\text{com}}^{-1}\boldsymbol{y},\\ \sigma_g^2(\boldsymbol{x}^\star,\boldsymbol{u}^\star) &= \sum_{i=1}^{m} u_i^\star \left[(k_g^i)^\star - (\boldsymbol{k}_g^i)^\top \boldsymbol{U}_i \boldsymbol{K}_{\text{com}}^{-1}\boldsymbol{U}_i \boldsymbol{k}_g^i\right] u_i^\star,\end{aligned} \tag{6.13}$$

where $\boldsymbol{k}_f = [k_f(\boldsymbol{x}_1, \boldsymbol{x}^\star), \cdots, k_f(\boldsymbol{x}_N, \boldsymbol{x}^\star)]^\top \in \mathbb{R}^N$. $\boldsymbol{k}_g^i = [k_g^i(\boldsymbol{x}_1, \boldsymbol{x}^\star), \cdots, k_g^i(\boldsymbol{x}_N, \boldsymbol{x}^\star)]^\top \in \mathbb{R}^N$. $k_f^\star = k_f(\boldsymbol{x}^\star, \boldsymbol{x}^\star)$. $(k_g^i)^\star = k_g^i(\boldsymbol{x}^\star, \boldsymbol{x}^\star)$ *and* $\boldsymbol{y} = [y_1, \cdots, y_N]^\top \in \mathbb{R}^N$.

Proof. From [29], for test inputs $\boldsymbol{x}^\star$ and $\boldsymbol{u}^\star$, as well as compound kernel (6.12), the joint distribution is provided as

$$\begin{bmatrix} f(\boldsymbol{x}^\star) \\ g(\boldsymbol{x}^\star)\boldsymbol{u}^\star \\ \boldsymbol{y} \end{bmatrix} \sim \mathcal{N}\left(0, \begin{bmatrix} k_f^\star & 0 & \boldsymbol{k}_f^\top \\ 0 & \hat{k}_g^\star & \hat{\boldsymbol{k}}_g^\top \\ \boldsymbol{k}_f & \hat{\boldsymbol{k}}_g & \boldsymbol{K}_{\text{com}} \end{bmatrix}\right), \tag{6.14}$$

where $\hat{k}_g^\star = \sum_{i=1}^m u_i^\star (k_g^i)^\star u_i^\star$ and $\hat{\boldsymbol{k}}_g = \sum_{i=1}^m u_i^\star (\boldsymbol{k}_g^i)^\top \boldsymbol{U}_i$.

Therefore, the posterior mean and variance for the safety constraint term $\Delta\beta_f(\boldsymbol{x}^\star)$ are given by

$$\begin{aligned} &f(\boldsymbol{x}^\star)|\mathbb{D}_{\text{training}} \sim \mathcal{N}(\mu_f(\boldsymbol{x}^\star), \sigma_f^2(\boldsymbol{x}^\star)), \\ &\mu_f(\boldsymbol{x}^\star) = \boldsymbol{k}_f^\top \boldsymbol{K}_{\text{com}}^{-1} \boldsymbol{y}, \\ &\sigma_f^2(\boldsymbol{x}^\star) = k_f^\star - \boldsymbol{k}_f^\top \boldsymbol{K}_{\text{com}}^{-1} \boldsymbol{k}_f, \end{aligned} \tag{6.15}$$

and the posterior mean and variance for the safety constraint term $\Delta\beta_g(\boldsymbol{x}^\star)\boldsymbol{u}^\star$ are provided as follows:

$$\begin{aligned} &g(\boldsymbol{x}^\star)\boldsymbol{u}^\star|\mathbb{D}_{\text{training}} \sim \mathcal{N}(\mu_g(\boldsymbol{x}^\star, \boldsymbol{u}^\star), \sigma_g^2(\boldsymbol{x}^\star, \boldsymbol{u}^\star)), \\ &\mu_g(\boldsymbol{x}^\star, \boldsymbol{u}^\star) = \sum_{i=1}^m u_i^\star (\boldsymbol{k}_g^i)^\top \boldsymbol{U}_i \boldsymbol{K}_{\text{com}}^{-1} \boldsymbol{y}, \\ &\sigma_g^2(\boldsymbol{x}^\star, \boldsymbol{u}^\star) = \sum_{i=1}^m u_i^\star \left[(k_g^i)^\star - (\boldsymbol{k}_g^i)^\top \boldsymbol{U}_i \boldsymbol{K}_{\text{com}}^{-1} \boldsymbol{U}_i \boldsymbol{k}_g^i\right] u_i^\star. \end{aligned} \tag{6.16}$$

■

Remark 6.3.2. *Compared to system modeling using GP regression [24, 111, 136], our modeling method reduces structural complexity and computational time. Although researchers have focused on GP-based CBF [34] and HOCBF [25, 38] by utilizing affine dot product compound kernels, these GP prediction methods lack flexibility and require more effective parameter tuning to guarantee the safety of uncertain systems. Further details are provided in the Section Numerical Examples.*

6.4 Probabilistic Safe Control Framework Designing

In this section, we aim at building upon a probabilistic HOCBF constraint and providing theoretical analysis.

Firstly, we provide the following Lemma:

Lemma 6.4.1 (Probabilistic Bound [43])**.** *Suppose that Assumption 2.1.1 holds, then one gets*

$$\begin{aligned} &\Pr\left\{|\mu_f(\boldsymbol{x}^\star)-\Delta\beta_f(\boldsymbol{x}^\star)|\leqslant\psi_f\sigma_f(\boldsymbol{x}^\star)\right\}\geqslant 1-\varrho,\\ &\Pr\left\{|\mu_g(\boldsymbol{x}^\star,\boldsymbol{u}^\star)-\Delta\beta_g(\boldsymbol{x}^\star)\boldsymbol{u}^\star|\leqslant\psi_g\sigma_g(\boldsymbol{x}^\star,\boldsymbol{u}^\star)\right\}\geqslant 1-\varrho \end{aligned} \tag{6.17}$$

for all test data $\boldsymbol{x}^\star\in\mathbb{A}_1\cap,\cdots,\cap\mathbb{A}_r$*, any* $\boldsymbol{u}^\star\in\mathbb{U}$*, and any probability* $\varrho\in(0,1)$*, where parameters* $\|\Delta\beta_f(\boldsymbol{x}^\star)\|_k^2\leqslant\bar{\beta}_f$ *with* $\psi_f=\sqrt{2\bar{\beta}_f+300\gamma\ln^3\left(\frac{N+1}{\varrho}\right)}$ *and* $\|\Delta\beta_g(\boldsymbol{x}^\star)\boldsymbol{u}^\star\|_k^2\leqslant\bar{\beta}_g$ *with* $\psi_g=\sqrt{2\bar{\beta}_g+300\gamma\ln^3\left(\frac{N+1}{\varrho}\right)}$*. The maximum gain* $\gamma=\frac{1}{2}\log\left(\det\left(I+\sigma_n^{-2}\boldsymbol{K}(\boldsymbol{x},\boldsymbol{x}')\right)\right)$ *and input elements* $\boldsymbol{x},\boldsymbol{x}'\in\left\{\boldsymbol{x}^{\{1\}},\boldsymbol{x}^{\{2\}},\cdots,\boldsymbol{x}^{\{N+1\}}\right\}$.

Proof. This is a direct consequence from [43]. ■

Based on Lemma 6.4.1 and condition (6.9b), the following inequality holds with probability at least $1-\varrho$:

$$\hat{\beta}_r(\boldsymbol{x},\boldsymbol{u})\geqslant\beta_r(\boldsymbol{x},\boldsymbol{u})+\mu_f(\boldsymbol{x})-\psi_f\sigma_f(\boldsymbol{x})+\mu_g(\boldsymbol{x},\boldsymbol{u})-\psi_g\sigma_g(\boldsymbol{x},\boldsymbol{u}) \tag{6.18}$$

for all $\boldsymbol{x}\in\mathbb{A}_1\cap,\cdots,\cap\mathbb{A}_r$ and any $\boldsymbol{u}\in\mathbb{U}$.

Combining (6.18) into the optimization problem (6.9a), one derives the following SOCP:

EGPBarrier-SOCP:

$$\boldsymbol{u}_{\text{safe}}=\arg\min_{\boldsymbol{u}\in\mathbb{U}}\|\boldsymbol{u}-\boldsymbol{u}_{\text{ref}}\|_2^2, \tag{6.19a}$$

$$\text{s.t. }\psi_g\left\|\sum_{i=1}^{m}\hat{k}_i u_i\right\|_2\leqslant a(\boldsymbol{x})+\boldsymbol{b}(\boldsymbol{x})\boldsymbol{u}, \tag{6.19b}$$

---

where $a(\boldsymbol{x})=L_f\beta_{r-1}(\boldsymbol{x})+\alpha_r(\beta_{r-1}(\boldsymbol{x}))+\mu_f(\boldsymbol{x})-\psi_f\sigma_f(\boldsymbol{x})\in\mathbb{R}$. $\hat{k}_i=\sqrt{k_g^i-(\boldsymbol{k}_g^i)^\top\boldsymbol{U}_i\boldsymbol{K}_{\text{com}}^{-1}\boldsymbol{U}_i\boldsymbol{k}_g^i}$ $\in\mathbb{R}$. $\boldsymbol{b}(\boldsymbol{x})=L_gL_f^{r-1}h(\boldsymbol{x})+\hat{\boldsymbol{b}}^\top(\boldsymbol{x})\in\mathbb{R}^{1\times m}$. $\hat{\boldsymbol{b}}(\boldsymbol{x})=[\hat{b}_1(\boldsymbol{x}),\cdots,\hat{b}_m(\boldsymbol{x})]^\top\in\mathbb{R}^m$ and $\hat{b}_i(\boldsymbol{x})=(\boldsymbol{k}_g^i)^\top\boldsymbol{U}_i\boldsymbol{K}_{\text{com}}^{-1}\boldsymbol{y}\in\mathbb{R}$.

To ensure the safety of true system (6.4), we provide the necessary feasibility analysis for constraint (6.19b) as follows:

Theorem 6.4.1. *Given a state $\boldsymbol{x} \in \mathbb{A}_i,\ i = \{1, \cdots, r\}$, EGPBarrier-SOCP* (6.19) *is feasible, if there exists a control input $\boldsymbol{u} \in \mathbb{R}^m$ such that*

$$\begin{bmatrix} 1, \boldsymbol{u}^\top \end{bmatrix} \begin{bmatrix} -a^2(\boldsymbol{x}) & -a(\boldsymbol{x})\boldsymbol{b}(\boldsymbol{x}) \\ -\boldsymbol{b}^\top(\boldsymbol{x})a(\boldsymbol{x}) & \psi_g^2\hat{\boldsymbol{K}} - \boldsymbol{b}^\top(\boldsymbol{x})\boldsymbol{b}(\boldsymbol{x}) \end{bmatrix} \begin{bmatrix} 1 \\ \boldsymbol{u} \end{bmatrix} \leqslant 0,$$

$$a(\boldsymbol{x}) + \boldsymbol{b}(\boldsymbol{x})\boldsymbol{u} \geqslant 0, \tag{6.20}$$

where matrix $\hat{\boldsymbol{K}} = \operatorname{diag}\left[\hat{k}_1, \cdots, \hat{k}_m\right] \in \mathbb{R}^{m \times m}$.

Proof. The first inequality is derived by squaring both sides of (6.19b). Additionally, since the left-hand side of (6.19b) is non-negative, the second inequality follows. ■

Then, we provide two lemmas to guarantee Theorem 6.4.1.

Lemma 6.4.2 (Necessary Condition)**.** *Given a state $\boldsymbol{x} \in \mathbb{A}_i,\ i = \{1, \cdots, r\}$, if EGPBarrier-SOCP* (6.19) *is feasible, then the following condition needs to be fulfilled:*

$$1 - \frac{1}{\psi_g^2}\boldsymbol{b}(\boldsymbol{x})\hat{\boldsymbol{K}}^{-1}\boldsymbol{b}^\top(\boldsymbol{x}) \leqslant 0. \tag{6.21}$$

Proof. From the first inequality of (6.20), one derives that if GP-HOCBF-SOCP (6.19) is feasible, block matrix $F(\boldsymbol{x})$ needs to non-positive definite. According to $F(\boldsymbol{x})$, we obtain that the first inequality of (6.20) holds when and only when

$$1 - \frac{1}{\psi_g^2}\boldsymbol{b}(\boldsymbol{x})\hat{\boldsymbol{K}}^{-1}\boldsymbol{b}^\top(\boldsymbol{x}) = \psi_g^2\hat{\boldsymbol{K}} - \boldsymbol{b}^\top(\boldsymbol{x})\boldsymbol{b}(\boldsymbol{x}) \leqslant 0, \tag{6.22}$$

where $F(\boldsymbol{x}) = \begin{bmatrix} -a^2(\boldsymbol{x}) & -\boldsymbol{b}^\top(\boldsymbol{x})a(\boldsymbol{x}) \\ -a(\boldsymbol{x})\boldsymbol{b}(\boldsymbol{x}) & \psi_g^2\hat{\boldsymbol{K}} - \boldsymbol{b}^\top(\boldsymbol{x})\boldsymbol{b}(\boldsymbol{x}) \end{bmatrix}$. ■

Lemma 6.4.3 (Sufficient Condition)**.** *Let ζ be $\lambda_{\min}(\psi_g^2\hat{\boldsymbol{K}} - \boldsymbol{b}^\top(\boldsymbol{x})\boldsymbol{b}(\boldsymbol{x}))$. Given a state $\boldsymbol{x} \in \mathbb{A}_i,\ i = \{1, \cdots, r\}$, if $\zeta \leqslant 0$, then EGPBarrier-SOCP* (6.19) *is feasible at $\boldsymbol{x}$.*

Proof. This is a direct consequence from [34]. ■

This section establishes three theoretical conditions to guarantee the feasibility of the EGPBarrier-SOCP. While a few prior works, such as [34] and [38], have developed feasibility conditions for the constraints of SOCP, our theoretical results are simpler. Additionally, recent work [39] presents a different GP-based CBF method that avoids SOCP construction using a compound kernel; however, the approach in [39] is limited by the dimension of the control input and cannot handle multi-dimensional control inputs, whereas our method addresses not only this limitation but also the high relative degree.

6.5 Learning-Based Fault-Tolerant Safety Controller

This section designs a learning-based fault-tolerant safe control approach to address unknown actuator bias faults.

6.5.1 Modeling of Faults

In this chapter, we study unknown actuator bias faults that are induced by the component torn-and-worn factors [61], which can lead to decreased control performance and pose a threat to system safety, as detailed below:

$$\boldsymbol{u}_F = \boldsymbol{u} + \Delta\boldsymbol{u}_F, \quad \forall t \geqslant t_F, \tag{6.23}$$

where $\Delta\boldsymbol{u}_F \in \mathbb{R}^m$ is an unknown time-varying actuator bias fault. $0 < t_F \in \mathbb{R}$ indicates an unknown time-instant of fault occurrence. The control input $\boldsymbol{u} = \boldsymbol{u}_F$ if $t \geqslant t_F$.

Substituting (6.23) into (6.4), we can derive that

$$\dot{\boldsymbol{x}} = \hat{\boldsymbol{f}}(\boldsymbol{x}) + \hat{\boldsymbol{g}}(\boldsymbol{x})(\boldsymbol{u} + \Delta\boldsymbol{u}_F), \quad \text{if } t \geqslant t_F. \tag{6.24}$$

Assumption 6.5.1 (Fault Bound [118])**.** *Actuator bias fault $\Delta\boldsymbol{u}_F$ is unknown time-varying but bounded function which fufills $\|\Delta\boldsymbol{u}_F\| \leqslant \Delta u_F^{\max} \in \mathbb{R}$ with $0 < \Delta u_F^{\max} < +\infty$. Parameter $\Delta u_F^{\max}$ is a known constant.*

Then, the safe constraint (6.8) can be rewritten as follows:

$$\begin{aligned}
\hat{\beta}_r(\boldsymbol{x},\boldsymbol{u}) =& L_f\beta_{r-1}(\boldsymbol{x}) + L_g L_f^{r-1} h(\boldsymbol{x})(\boldsymbol{u} + \Delta\boldsymbol{u}_F) \\
&+ \Delta\beta_f(\boldsymbol{x}) + \Delta\beta_g(\boldsymbol{x})(\boldsymbol{u} + \Delta\boldsymbol{u}_F) + \alpha_r(\beta_{r-1}(\boldsymbol{x})) \\
=& L_f\beta_{r-1}(\boldsymbol{x}) + L_g L_f^{r-1} h(\boldsymbol{x})\boldsymbol{u} + L_g L_f^{r-1} h(\boldsymbol{x})\Delta\boldsymbol{u}_F \\
&+ \Delta\beta_f(\boldsymbol{x}) + \Delta\beta_g(\boldsymbol{x})\boldsymbol{u} + \Delta\beta_g(\boldsymbol{x})\Delta\boldsymbol{u}_F + \alpha_r(\beta_{r-1}(\boldsymbol{x})).
\end{aligned} \tag{6.25}$$

For $\Delta\beta_g(\boldsymbol{x})$, its posterior mean and variance can be derived from Lemma 6.3.1 that

$$\begin{aligned}
\boldsymbol{\mu}_g(\boldsymbol{x}^\star) &= \left[(\boldsymbol{k}_g^1)^\top \boldsymbol{U}_1 \boldsymbol{K}_{\text{com}}^{-1}\boldsymbol{y}, \cdots, (\boldsymbol{k}_g^m)^\top \boldsymbol{U}_m \boldsymbol{K}_{\text{com}}^{-1}\boldsymbol{y}\right] \in \mathbb{R}^{1\times m}, \\
\boldsymbol{\sigma}_g^2(\boldsymbol{x}^\star) &= \left[(k_g^1)^\star - (\boldsymbol{k}_g^1)^\top \boldsymbol{U}_1 \boldsymbol{K}_{\text{com}}^{-1}\boldsymbol{U}_1\boldsymbol{k}_g^1, \cdots, (k_g^m)^\star - (\boldsymbol{k}_g^m)^\top \boldsymbol{U}_m \boldsymbol{K}_{\text{com}}^{-1}\boldsymbol{U}_m\boldsymbol{k}_g^m\right] \in \mathbb{R}^{1\times m}.
\end{aligned} \tag{6.26}$$

Lemma 6.5.1 (Probabilistic Bound [43])**.** *Suppose that Assumption 2.1.1 holds, then one obtains*

$$\Pr\left\{\left|\mu_g^i(\boldsymbol{x}^\star) - \Delta\beta_g^i(\boldsymbol{x}^\star)\right| \leqslant \hat{\psi}_g^i \sigma_g^i(\boldsymbol{x}^\star)\right\} \geqslant 1 - \varrho \tag{6.27}$$

for each $\Delta\beta_g^i(\boldsymbol{x})$, $i \in \{1,\cdots,m\}$, *all test data* $\boldsymbol{x}^\star \in \mathbb{A}_1 \cap,\cdots,\cap \mathbb{A}_r$, *and any probability* $\varrho \in (0,1)$, *where parameters* $\hat{\psi}_g^i = \sqrt{2\hat{\beta}_g^i + 300\gamma \ln^3\left(\frac{N+1}{\varrho}\right)}$ *with* $\|\Delta\beta_g^i(\boldsymbol{x}^\star)\|_k^2 \leqslant \hat{\beta}_g^i$. *Parameter gain* γ *has the identical meaning in Lemma 6.4.1.*

Proof. This is a direct consequence from [43]. ■

If the vector $\Delta\beta_g(\boldsymbol{x}^\star)$ satisfy the Lemma 6.5.1, the probability is $(1-\varrho)^m$.

6.5.2 Theoretical Analysis and Strategy Design

This subsection establishes a sufficient condition for the fault-tolerant probabilistic HOCBF (FT-EGPBarrier) constraint as follows:

Theorem 6.5.1 (Fault-tolerant EGPBarrier)**.** *Based on controller* (6.19)*, Assumption 6.5.1, and Lemma 6.5.1, the function* h *is said to be FT-EGPBarrier method for system* (6.24) *if there exist a set of extended class* $\mathcal{K}$ *functions* $\alpha_i(\cdot)$ *such that*

$$\begin{aligned}&\sup_{u\in\mathbb{U}}\left\{L_f\beta_{r-1}(\boldsymbol{x}) + L_gL_f^{r-1}h(\boldsymbol{x})\boldsymbol{u} + \mu_f(\boldsymbol{x}) - \psi_f\sigma_f(\boldsymbol{x}) + \hat{\boldsymbol{b}}^\top(\boldsymbol{x})\boldsymbol{u} - \psi_g\sqrt{\boldsymbol{u}^\top\hat{\boldsymbol{K}}\boldsymbol{u}}\right\}\\ &\geqslant -\alpha_r(\beta_{r-1}(\boldsymbol{x})) + \|L_gL_f^{r-1}h(\boldsymbol{x})\|\Delta u_F^{\max} + \left\|\boldsymbol{\mu}_g(\boldsymbol{x}) + \hat{\boldsymbol{\psi}}_g\boldsymbol{\sigma}_g(\boldsymbol{x})\right\|\Delta u_F^{\max}\end{aligned} \tag{6.28}$$

for all $\boldsymbol{x} \in \mathbb{X}$ *with the high probability* $(1-\varrho)^m$, *where* $\hat{\boldsymbol{\psi}}_g = \operatorname{diag}\left[\hat{\boldsymbol{\psi}}_g^1,\cdots,\hat{\boldsymbol{\psi}}_g^m\right] \in \mathbb{R}^{m\times m}$.

Proof. The r-th Lie derivative of $\hat{h}(\boldsymbol{x})$ along the vector field of system (6.24) is

$$\begin{aligned}\hat{\beta}_r(\boldsymbol{x},\boldsymbol{u}) &= L_f\beta_{r-1}(\boldsymbol{x}) + L_gL_f^{r-1}h(\boldsymbol{x})\boldsymbol{u} + L_gL_f^{r-1}h(\boldsymbol{x})\Delta\boldsymbol{u}_F\\ &\quad + \Delta\beta_f(\boldsymbol{x}) + \Delta\beta_g(\boldsymbol{x})\boldsymbol{u} + \Delta\beta_g(\boldsymbol{x})\Delta\boldsymbol{u}_F\\ &\geqslant L_f\beta_{r-1}(\boldsymbol{x}) + L_gL_f^{r-1}h(\boldsymbol{x})\boldsymbol{u} + \mu_f(\boldsymbol{x}) - \psi_f\sigma_f(\boldsymbol{x}) + \hat{\boldsymbol{b}}^\top(\boldsymbol{x})\boldsymbol{u}\\ &\quad - \psi_g\sqrt{\boldsymbol{u}^\top\hat{\boldsymbol{K}}\boldsymbol{u}} - \|L_gL_f^{r-1}h(\boldsymbol{x})\|\Delta u_F^{\max} - \|\Delta\beta_g(\boldsymbol{x})\|\Delta u_F^{\max}\\ &\geqslant L_f\beta_{r-1}(\boldsymbol{x}) + L_gL_f^{r-1}h(\boldsymbol{x})\boldsymbol{u} + \mu_f(\boldsymbol{x}) - \psi_f\sigma_f(\boldsymbol{x}) + \hat{\boldsymbol{b}}^\top(\boldsymbol{x})\boldsymbol{u}\\ &\quad - \psi_g\sqrt{\boldsymbol{u}^\top\hat{\boldsymbol{K}}\boldsymbol{u}} - \|L_gL_f^{r-1}h(\boldsymbol{x})\|\Delta u_F^{\max} - \|\boldsymbol{\mu}_g(\boldsymbol{x}) + \hat{\boldsymbol{\psi}}_g\boldsymbol{\sigma}_g(\boldsymbol{x})\|\Delta u_F^{\max}\\ &\geqslant -\alpha_r(\beta_{r-1}(\boldsymbol{x})) + \|L_gL_f^{r-1}h(\boldsymbol{x})\|\Delta u_F^{\max} + \|\boldsymbol{\mu}_g(\boldsymbol{x}) + \hat{\boldsymbol{\psi}}_g\boldsymbol{\sigma}_g(\boldsymbol{x})\|\Delta u_F^{\max}\end{aligned} \tag{6.29}$$

for all $\boldsymbol{x} \in \mathbb{X}$ with the high probability $(1-\varrho)^m$. ■

Combining the constraint (6.28) into the optimization problem (6.9a), one derives the following SOCP:

FT-EGPBarrier-SOCP:

$$\boldsymbol{u}_{\text{safe}} = \arg\min_{\boldsymbol{u}\in\mathbb{U}} \|\boldsymbol{u}-\boldsymbol{u}_{\text{ref}}\|_2^2, \tag{6.30a}$$

$$\text{s.t. } \psi_g \left\| \sum_{i=1}^{m} \hat{k}_i u_i \right\|_2 \leqslant a(\boldsymbol{x}) + \boldsymbol{b}(\boldsymbol{x})\boldsymbol{u} - c(\boldsymbol{x}), \tag{6.30b}$$

where $c(\boldsymbol{x}) = \left\| L_g L_f^{r-1} h(\boldsymbol{x}) \right\| \Delta u_F^{\max} + \left\| \boldsymbol{\mu}_g(\boldsymbol{x}) + \hat{\boldsymbol{\psi}}_g \boldsymbol{\sigma}_g(\boldsymbol{x}) \right\| \Delta u_F^{\max}$.

To ensure the safety of true system (6.24) under the unknown actuator faults, we provide the necessary feasibility analysis for constraint (6.30b) as follows:

Theorem 6.5.2. *Given a state $\boldsymbol{x} \in \mathbb{A}_i,\ i = \{1,\cdots,r\}$, FT-EGPBarrier-SOCP* (6.30) *is feasible, if there exists a control input $\boldsymbol{u} \in \mathbb{R}^m$ such that*

$$\begin{bmatrix} 1, \boldsymbol{u}^\top \end{bmatrix} \begin{bmatrix} -(a(\boldsymbol{x})-c(\boldsymbol{x}))^2 & -(a(\boldsymbol{x})-c(\boldsymbol{x}))\boldsymbol{b}(\boldsymbol{x}) \\ -\boldsymbol{b}^\top(\boldsymbol{x})(a(\boldsymbol{x})-c(\boldsymbol{x})) & \psi_g^2 \hat{\boldsymbol{K}} - \boldsymbol{b}^\top(\boldsymbol{x})\boldsymbol{b}(\boldsymbol{x}) \end{bmatrix} \begin{bmatrix} 1 \\ \boldsymbol{u} \end{bmatrix} \leqslant 0,$$

$$a(\boldsymbol{x}) + \boldsymbol{b}(\boldsymbol{x})\boldsymbol{u} - c(\boldsymbol{x}) \geqslant 0. \tag{6.31}$$

Proof. The first inequality is derived by squaring both sides of (6.30b). Additionally, since the left-hand side of (6.30b) is non-negative, the second inequality follows. ■

Lemmas 6.4.2 and 6.4.3 can guarantee the feasibility of the Theorem 6.5.2.

Considering the influences of unknown actuator bias faults, we design a hybrid control method to improve the robustness and flexibility of the safe controller (6.30). This results in the following hybrid controller:

$$\boldsymbol{u} = \begin{cases} \boldsymbol{u}_{\text{safe}}, & \text{if } \boldsymbol{x} \notin \mathbb{X}_{\text{desired}}, \\ -K_{\text{gain}}\boldsymbol{x}, & \text{if } \boldsymbol{x} \in \mathbb{X}_{\text{desired}}, \end{cases}$$

where $\mathbb{X}_{\text{desired}}$ denotes the desired region of the state space.

6.6 Numerical Examples

In this section, we evaluate `EGPBarrier` and `FT-EGPBarrier` methods on two examples: 1) an ACC system [94] and 2) a mobile robotic system [114].

6.6.1 Safety Guarantee for an ACC System

6.6.1.1 EGPBarrier Method

In this case, we aim to compare the `EGPBarrier` method against four different HOCBF methods: 1) `Nominal`, an HOCBF method without GP regression [22]; 2) `Robust`, an HOCBF method using upper bounds on model uncertainty [139]; 3) `GP-SK`, a standard GP-HOCBF with a single SE kernel [23]; 4) `GP-ADP(L)` and `GP-ADP(H)`, two compound kernel GP-HOCBF methods using affine dot product kernels with low and high values of ψ_g, respectively [38].

Consider an ACC system with model uncertainty as follows:

$$\underbrace{\begin{bmatrix} \dot{v} \\ \dot{z} \end{bmatrix}}_{\dot{\boldsymbol{x}}} = \underbrace{\begin{bmatrix} -\frac{F_r(v)}{m+\Delta m} \\ v_0 - v \end{bmatrix} + \begin{bmatrix} -\frac{\Delta F_r(v)}{m+\Delta m} \\ 0 \end{bmatrix}}_{\hat{\boldsymbol{f}}(\boldsymbol{x})} + \underbrace{\begin{bmatrix} \frac{1}{m+\Delta m} \\ 0 \end{bmatrix}}_{\hat{\boldsymbol{g}}(\boldsymbol{x})} u, \tag{6.32}$$

where v and z are defined as velocity and distance between ego vehicle and its preceding vehicle. v_0 denotes preceding vehicle's velocity. m and $F_r(v)$ stand for the known mass and the known aerodynamic drag with $F_r(v) = f_0 + f_1 v + f_2 v^2$ of the ego vehicle. Δm and $\Delta F_r(v) = \Delta f_0 + \Delta f_1 v + \Delta f_2 v^2$ refer to model uncertainty. $u \in \mathbb{R}$ and $m + \Delta m$ indicate the control input and the true mass.

We set known mass $m = 1650$kg, true mass $m + \Delta m = 2200$kg, aerodynamic parameters $f_0 = 0.1, f_1 = 5, f_2 = 0.25$, leader's velocity $v_0 = 16$m/s, uncertainties $\Delta f_0 = 0.2, \Delta f_1 = 2.5, \Delta f_2 = 7$, and initial value $\boldsymbol{x}(0) = [20, 100]^\top$. The control input u is restricted within $[u_{\min}, u_{\max}]$ with $u_{\min} = -0.4$mg and $u_{\max} = 0.4$mg; $g = 9.81\text{m/s}^2$. Define CBF $h(\boldsymbol{x}) = z - D$ with $D = 10$m. According to [34], we set the target speed $v_d = 24$m/s as one of control objectives, and we design a GP-CLF method using (6.13).

To fit the uncertain constraint term $\Delta\beta(\boldsymbol{x}, \boldsymbol{u})$ caused by the uncertainties $\Delta F_r(v)$ and Δm, we leverage controller (6.3) with the CLF constraint in [34]. Data is collected until either $\beta_0(\boldsymbol{x}) < 0$ or $\beta_1(\boldsymbol{x}) < 0$, forming the training dataset $\mathbb{D}_{\text{training}}$. We set approximation error and observation noise $d \sim \mathcal{N}(0, 0.25)$, lengthscales $l_f = 1$ and $l_g = 8 \times 10^{-2}$, as well as signal standard deviations $\sigma_f = 1$ and $\sigma_g = 1 \times 10^{-3}$, parameters $\psi_f = 1.5$ and $\psi_g = 0.1$. Furthermore, for `Robust` method, we select upper bounds of $(m + \Delta m)_{\max} = 2250$kg and uncertain terms $\Delta\bar{f}_0 = 2, \Delta\bar{f}_1 = 6, \Delta\bar{f}_2 = 18$. For `GP-SK` method, the kernel hyperparameters are set as $l = 1$ and $\sigma = 1$, and parameter $\psi_{SK} = 1.5$. For `GP-ADP(L)` and `GP-ADP(H)` methods, kernel hyperparameters are set identically with $l = 0.1$ and $\sigma = 1 \times 10^{-3}$, while parameters differ as $\psi_L = 0.1$ and $\psi_H = 0.6$.

Note that the above parameters $\psi_{\#}, \# = \{f, g, SK, L, H\}$ are tuned empirically based on prior studies and practical experience.

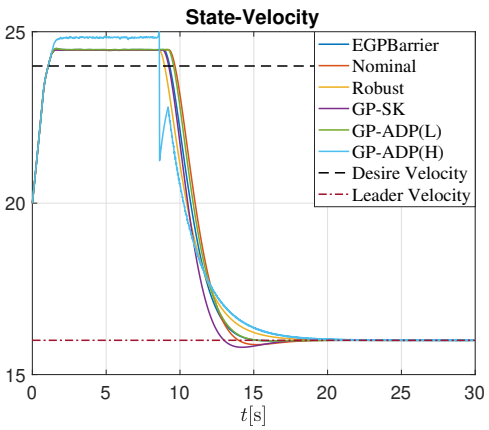

(a) Profiles of the ego vehicle's velocity.

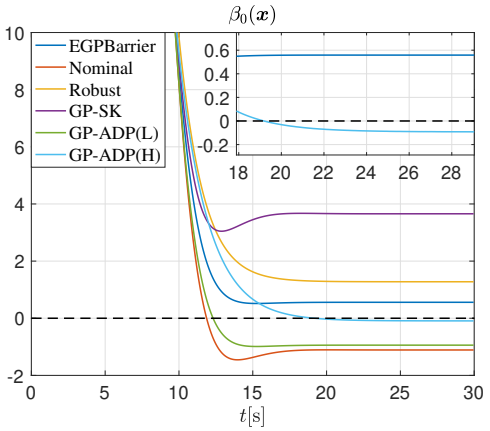

(b) Profiles of CBF $\beta_0(\boldsymbol{x})$.

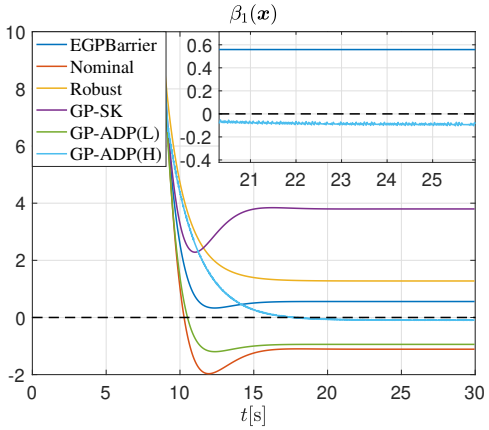

(c) Profiles of CBF $\beta_1(\boldsymbol{x})$.

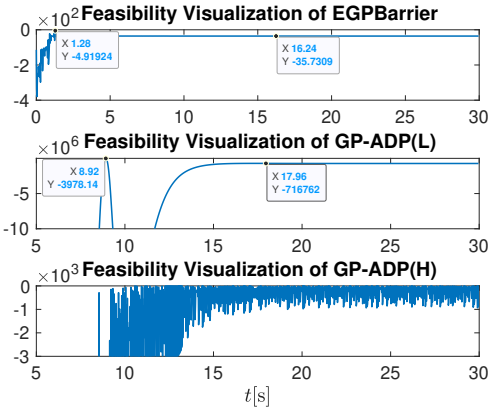

(d) Evolution of feasibility visualization.

Figure 6.2: Comparative results through the uncertain ACC system.

As depicted in Figure 6.2(a), during the interval $t \in [0\text{s}, 10\text{s})$, the velocity curve of `GP-ADP(H)` method exhibits substantial variation, reaching values higher than those of all other methods, followed by a rapid decrease. In the interval $t \in [10\text{s}, 15\text{s})$, the `GP-SK` method yields the lowest velocity values. After 19s, all curves converge to the leader's velocity. In Figures 6.2(b) and 6.2(c), one observes that the values of $\beta_0(\boldsymbol{x})$ and $\beta_1(\boldsymbol{x})$ remain positive under the `EGPBarrier`, `Robust`, and `GP-SK` methods, while they become negative under `Nominal`, `GP-ADP(L)`, and `GP-ADP(H)` methods. Although both `GP-SK` and `Robust` methods are able to maintain safety, they exhibit conservative behavior compared to the `EGPBarrier` method. Figure 6.2(d) illustrates the evolution of feasibility

visualization for `EGPBarrier`, `GP-ADP(L)`, and `GP-ADP(H)` methods, evaluated based on Lemma 6.4.2 and Lemma 2 in [38]. As shown in Figure 6.2(d), all three methods satisfy the feasibility condition, but the curves of the `GP-ADP(H)` method fluctuate rapidly due to the higher parameter value $\psi_H = 0.6$.

These results demonstrate that the `EGPBarrier` method enables the ego vehicle to achieve the control objective while maintaining a safe distance, thereby confirming its effectiveness, competitiveness, and feasibility.

6.6.1.2 FT-EGPBarrier Method

In this case, we aim to compare the `FT-EGPBarrier` method against two different HOCBF methods: 1) `Nominal`, a standard HOCBF method [22]; 2) `FT-Robust`, an HOCBF method using upper bounds on model uncertainty and unknown actuator faults.

According to system (6.32), we construct the following ACC system with unknown actuator faults:

$$\underbrace{\begin{bmatrix} \dot{v} \\ \dot{z} \end{bmatrix}}_{\dot{\boldsymbol{x}}} = \underbrace{\begin{bmatrix} -\frac{F_r(v)}{m+\Delta m} \\ v_0 - v \end{bmatrix} + \begin{bmatrix} -\frac{\Delta F_r(v)}{m+\Delta m} \\ 0 \end{bmatrix}}_{\hat{\boldsymbol{f}}(\boldsymbol{x})} + \underbrace{\begin{bmatrix} \frac{1}{m+\Delta m} \\ 0 \end{bmatrix}}_{\hat{\boldsymbol{g}}(\boldsymbol{x})} (u + \Delta u_F), \quad \text{if } t \geqslant t_F, \tag{6.33}$$

where system parameters v, z, $F_r(v)$, m, Δm, v_0, and u have the same meanings and setting in system (6.32); Δu_F and t_F denote the unknown actuator bias fault and its occurrence time, respectively.

Then, we select the actuator bias fault as $\Delta u_F = 800\cos(t)$ and fault time as $t_F = 5$s. Model uncertainty and GP modeling parameters are chosen from Section 6.6.1.1. Denote CBF $h(\boldsymbol{x}) = z - D$ with $D = 10$m and the target speed $v_d = 24$m/s as one of control objectives. We design a FT-GP-CLF method based on Chapter 4.

As shown in Figure 6.3(a), all methods exhibit small fluctuations caused by unknown actuator bias faults Δu_F after 15s. In Figures 6.3(b) and 6.3(c), the `FT-EGPBarrier` and `Robust` methods ensure the safety of the ACC system under unknown actuator faults. Compared to the `Robust` method, `FT-EGPBarrier` exhibits less conservatism. In contrast, the `Nominal` method fails to guarantee safety. As depicted in Figure 6.3(d), the proposed method remains feasible throughout the entire operation.

These results illustrate that the `FT-EGPBarrier` method enables the ego vehicle under unknown actuator faults to achieve the control objective while maintaining a safe distance, thereby confirming its effectiveness, competitiveness, and feasibility.

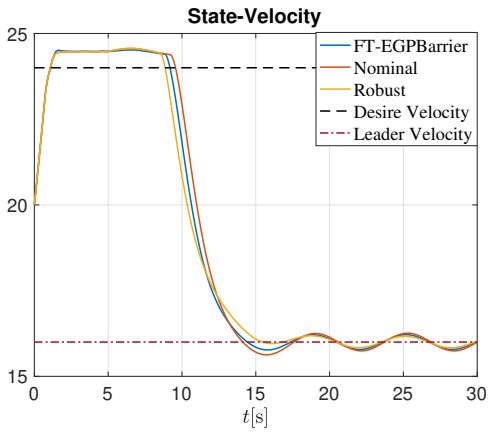

(a) Profiles of the ego vehicle's velocity.

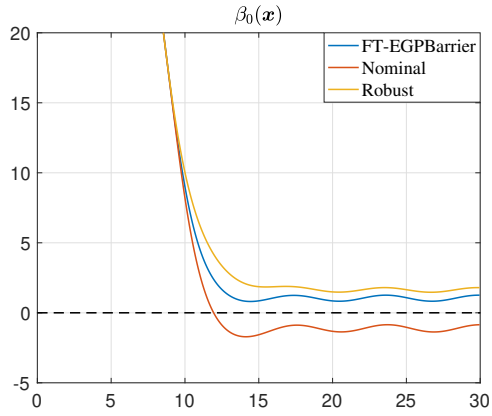

(b) Profiles of CBF $\beta_0(\boldsymbol{x})$.

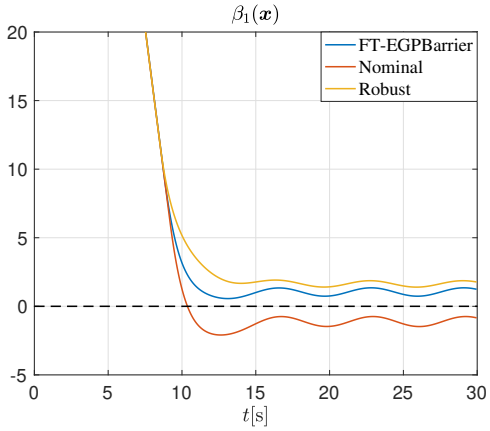

(c) Evolution of CBF $\beta_1(\boldsymbol{x})$.

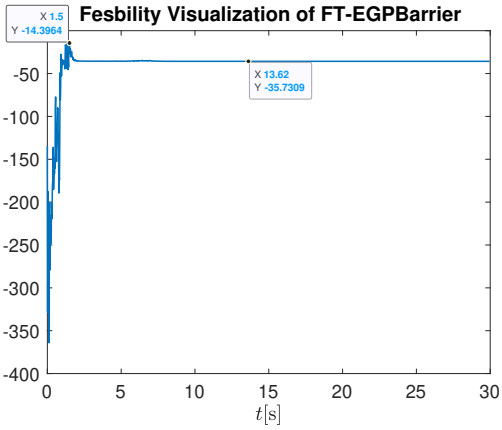

(d) Evolution of feasibility visualization.

Figure 6.3: Comparative results through the uncertain ACC system with faults.

6.6.2 Mobile Robotic System

6.6.2.1 EGPBarrier Method

In this case, we aim to compare the `EGPBarrier` method to existing works, as defined in Section 6.6.1.1, using the following uncertain mobile robotic system:

$$\underbrace{\begin{bmatrix}\dot{x}_1\\ \dot{x}_2\\ \dot{x}_3\\ \dot{x}_4\end{bmatrix}}_{\dot{\boldsymbol{x}}} = \underbrace{\begin{bmatrix}x_3\\ x_4\\ \Delta x_3\\ \Delta x_4\end{bmatrix}}_{\hat{\boldsymbol{f}}(\boldsymbol{x})} + \underbrace{\begin{bmatrix}0 & 0\\ 0 & 0\\ \frac{1}{m}+\Delta m_1 & 0\\ 0 & \frac{1}{m}+\Delta m_2\end{bmatrix}}_{\hat{\boldsymbol{g}}(\boldsymbol{x})} \underbrace{\begin{bmatrix}u_1\\ u_2\end{bmatrix}}_{\boldsymbol{u}}, \tag{6.34}$$

where x_1 and x_2 are the position of the mobile robot. x_3 and x_4 represent the velocity of the mobile robot. m is the known mass of the mobile robot. Δx_3, Δx_4, Δm_1 and Δm_2 stand for uncertainties. u_1 and u_2 refer to control inputs.

We choose known mass $m = 1$kg, uncertain terms $\Delta x_3 = 0.1$, $\Delta x_4 = 0.8$, $\Delta m_1 = 1.5$, and $\Delta m_2 = 1.3$. The initial value is set to $\boldsymbol{x}(0) = [-3.5, 3.5, 0, 0]^\top$. The control input u_1 and u_2 are restricted within $[u_{\min}, u_{\max}]$ with $u_{\min} = -4.5$ and $u_{\max} = 4.5$. Define $h(\boldsymbol{x}) = (x_1+1)^2 - (x_2-1)^2 - 1$. We set the desired control input $\boldsymbol{u}_{\text{ref}} = -K(\boldsymbol{x} - \boldsymbol{x}_{\text{desired}}), K = \begin{bmatrix} 20 & 0 & 20 & 0 \\ 0 & 20 & 0 & 20 \end{bmatrix}^\top$ in controller (6.19) and desired state $\boldsymbol{x}_{\text{desired}} = [0,0,0,0]^\top$.

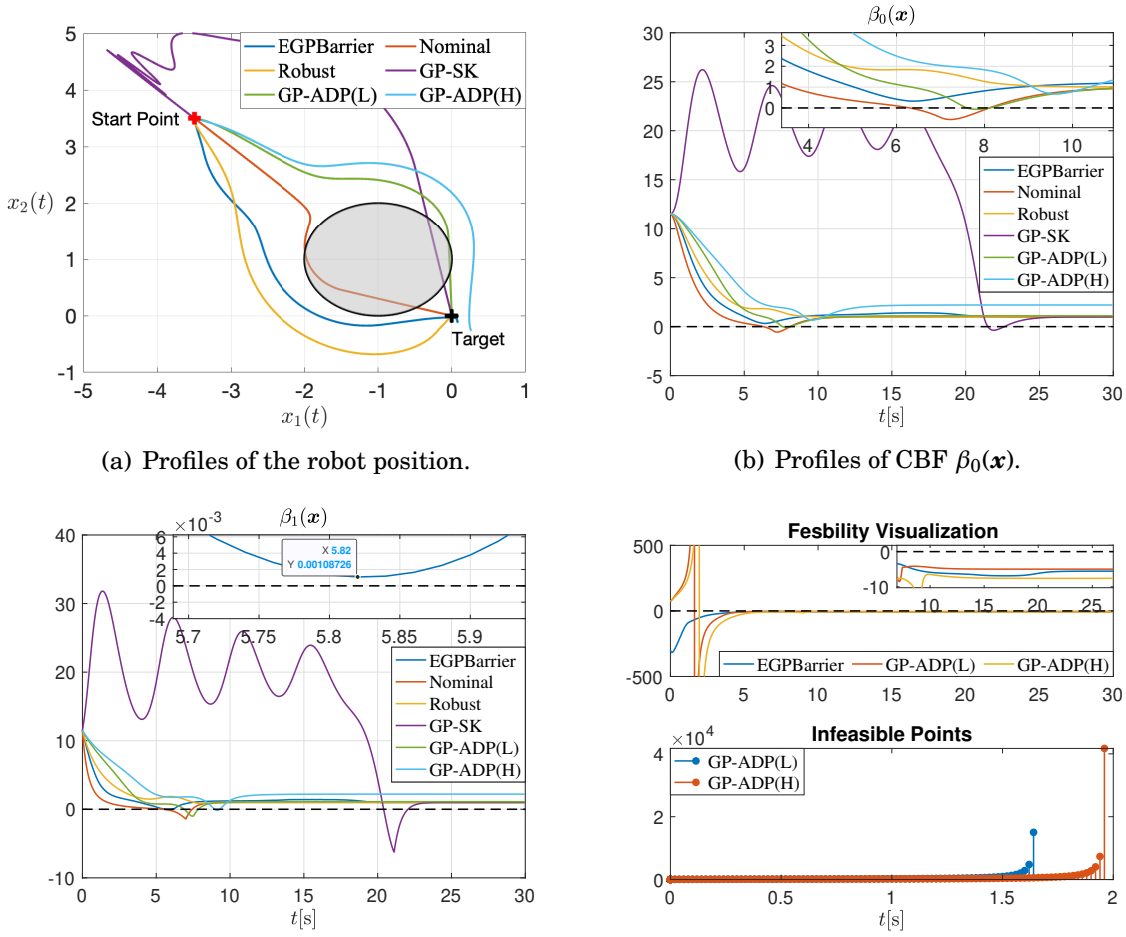

(a) Profiles of the robot position.

(b) Profiles of CBF $\beta_0(\boldsymbol{x})$.

(c) Evolution of CBF $\beta_1(\boldsymbol{x})$.

(d) Evolution of feasibility visualization.

Figure 6.4: Comparative results through the uncertain mobile robotic system.

The data collection and the choice of d are the same as subsection 6.6.1. We select lengthscales $l_f = 1.5$ and $l_g = 0.7$, as well as signal standard deviations $\sigma_f = 0.5$ and

$\sigma_g = 1.3$, parameters $\psi_f = 1.9$ and $\psi_g = 0.85$. Furthermore, for `Robust` method, we set upper bounds of model uncertainty as $\Delta\bar{x}_3 = 1.1$, $\Delta\bar{x}_4 = 18$, $\Delta\bar{m}_1 = 2.5$ and $\Delta\bar{m}_2 = 2.3$. For `GP-SK` method, the kernel hyperparameters are set as $l = 1.5$ and $\sigma = 0.5$, and parameter $\psi_{SK} = 1.9$. For `GP-ADP(L)` and `GP-ADP(H)` methods, the kernel hyperparameters are set identically with $l = 0.7$ and $\sigma = 1.3$, while parameters differ as $\psi_L = 0.85$ and $\psi_H = 1.7$. As illustrated in Figure 6.4(a), one observes that position curves of `Nominal`, `GP-SK`, and `GP-ADP(L)` methods cannot avoid the obstacle. Although the `GP-ADP(H)` method successfully avoids the obstacle, it does not reach the target. In contrast, the `EGPBarrier` method ensures that the position converges to the target with less conservatism than the `Robust` method. In Figures 6.4(b) and 6.4(c), the values of $\beta_0(\boldsymbol{x})$ and $\beta_1(\boldsymbol{x})$ remain positive under both `EGPBarrier` and `Robust` methods. The `GP-ADP(H)` method can guarantee the positivity of $\beta_0(\boldsymbol{x})$, but fails to ensure that of $\beta_1(\boldsymbol{x})$. After 15s, the values of $\beta_0(\boldsymbol{x})$ and $\beta_1(\boldsymbol{x})$ (except those from `GP-SK` method) converge to a fixed value as the mobile robot reaches the target. As shown in Figure 6.4(d), the `EGPBarrier` method satisfies the feasibility condition, while infeasible points arise in the `GP-ADP(L)` and `GP-ADP(H)` methods before 2s. Given this, these results validate the effectiveness, competitiveness, and feasibility of the `EGPBarrier` method.

6.6.2.2 FT-EGPBarrier Method

This case compares the `FT-EGPBarrier` method to existing works, as defined in Section 6.6.1.2, using the following mobile robotic system with unknown actuator faults:

$$\underbrace{\begin{bmatrix}\dot{x}_1\\ \dot{x}_2\\ \dot{x}_3\\ \dot{x}_4\end{bmatrix}}_{\dot{\boldsymbol{x}}} = \underbrace{\begin{bmatrix}x_3\\ x_4\\ \Delta x_3\\ \Delta x_4\end{bmatrix}}_{\hat{\boldsymbol{f}}(\boldsymbol{x})} + \underbrace{\begin{bmatrix}0 & 0\\ 0 & 0\\ \frac{1}{m}+\Delta m_1 & 0\\ 0 & \frac{1}{m}+\Delta m_2\end{bmatrix}}_{\hat{\boldsymbol{g}}(\boldsymbol{x})} \underbrace{\begin{bmatrix}u_1+\Delta u_{F,1}\\ u_2+\Delta u_{F,2}\end{bmatrix}}_{\boldsymbol{u}+\Delta\boldsymbol{u}_F}, \quad \text{if } t \geqslant t_F, \tag{6.35}$$

where system states x_1, x_2, x_3, and x_4, system parameters m, Δm_1, Δm_2, Δx_3, and Δx_4, and control input u_1 and u_2 have the same meanings as those in system (6.32). Variables $\Delta u_{F,1}$, $\Delta u_{F,2}$, and t_F represent the unknown actuator bias faults and their occurrence time, respectively. Then, we choose the actuator bias faults as $\Delta u_{F,1} = 0.2\cos(t)$ and $\Delta u_{F,2} = 0.2\sin(t)$. Fault time is set as $t_F = 1$s. Model uncertainty and GP modeling parameters are selected from Section 6.6.2.1.

As shown in Figure 6.5(a), the `Nominal` method fails to help the mobile robot avoid the obstacle, which eventually results in a collision with the environment. This out-

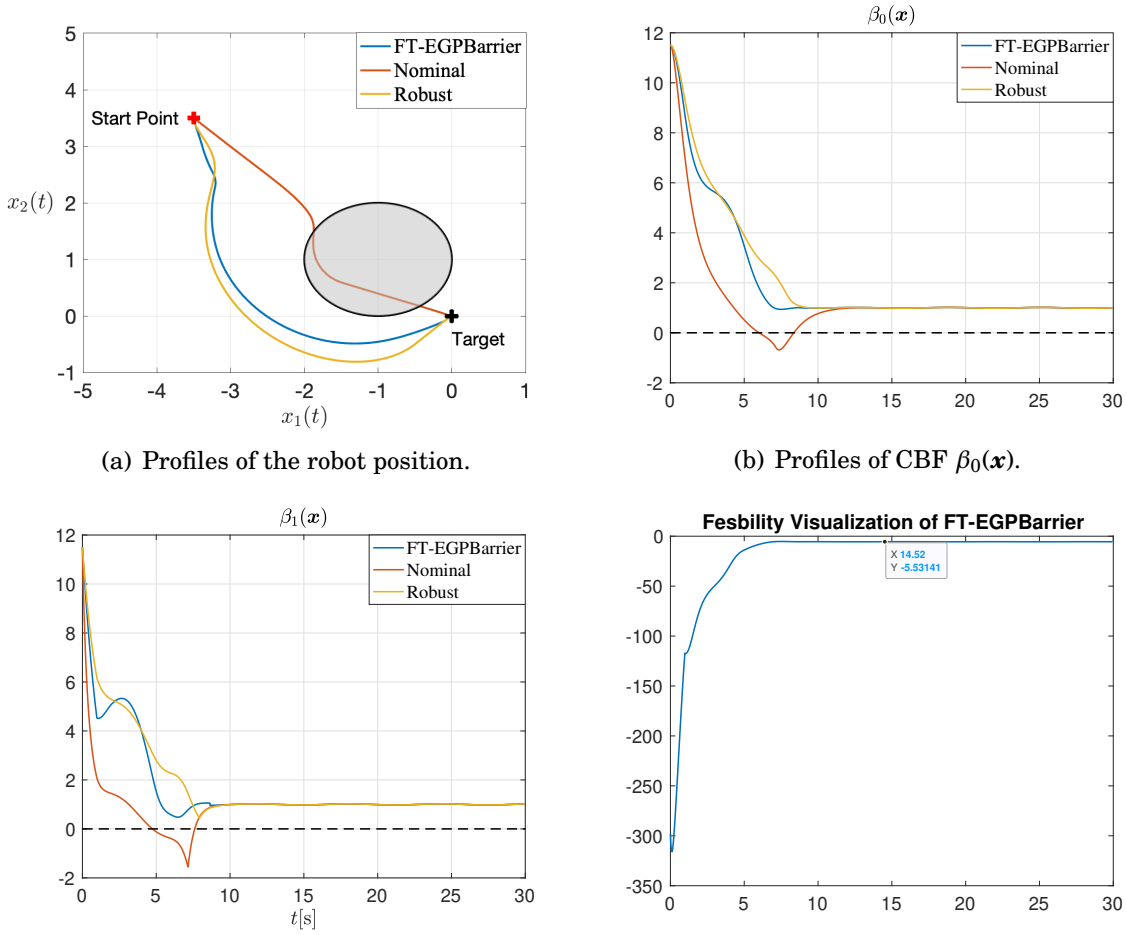

(a) Profiles of the robot position.

(b) Profiles of CBF $\beta_0(\boldsymbol{x})$.

(c) Profiles of CBF $\beta_1(\boldsymbol{x})$.

(d) Evolution of feasibility visualization.

Figure 6.5: Comparative results through the uncertain mobile robotic system with faults.

come reveals that the nominal controller cannot guarantee safety when the system is subject to model uncertainties or unexpected disturbances. In contrast, when using the `FT-EGPBarrier` and `Robust` methods, the mobile robotic system not only successfully avoids the obstacle but also reaches the target position as desired, verifying the effectiveness of incorporating safety mechanisms into the control framework. Compared to the `Robust` method, the `FT-EGPBarrier` method exhibits less conservatism, allowing the system to operate more flexibly while still ensuring constraint satisfaction.

In Figure 6.5(b), one observes that the values of $\beta_0(\boldsymbol{x})$ and $\beta_1(\boldsymbol{x})$ remain strictly positive under both the `FT-EGPBarrier` and `Robust` methods, which indicates that the safety constraints are always satisfied. Moreover, the trajectories of $\beta_0(\boldsymbol{x})$ and $\beta_1(\boldsymbol{x})$

under the `FT-EGPBarrier` method exhibit a faster decay rate, suggesting that the system approaches the constraint boundaries more efficiently without violating them. However, under the `Nominal` method, these values become negative during the time interval $t \in [5\text{s}, 10\text{s})$, implying that the safety conditions are violated and confirming the failure of the nominal controller in maintaining safe operation.

As illustrated in Figure 6.5(c), the proposed method satisfies the feasibility condition throughout the entire operation. This result confirms that the control input remains admissible over time and that the safety guarantees provided by the proposed framework are indeed upheld in practice.

Therefore, these results validate the effectiveness, competitiveness, and practical feasibility of the `FT-EGPBarrier` method.

Remark 6.6.1 (Limitation)**.** *While the EGPBarrier and FT-EGPBarrier methods are flexible and general, demonstrating superior performance compared to existing methods, their computational time is affected by the size of the training dataset. As more training data is collected, the computational time of GP regression will increase due to the use of compound kernels. Therefore, it is essential to explore efficient online data collection strategies, such as event-triggered learning [74], to improve the data efficiency and real-time applicability of the EGPBarrier and FT-EGPBarrier methods.*

6.7 Conclusion

In this chapter, we have proposed the EGPBarrier method, which integrates the HOCBF framework with GP regression via a compound kernel. This method has further been extended to the FT-EGPBarrier method by incorporating fault-tolerant control. We have formulated an SOCP for control synthesis and established several theoretical conditions to guarantee its feasibility. Two numerical examples have been demonstrated that the proposed methods ensure system safety with reduced conservatism, validating their effectiveness and competitiveness compared to existing approaches. Future work will explore online data collection strategies, such as event-triggered learning, to broaden the applicability of the proposed method to a wider range of practical scenarios.

CHAPTER 7

CONCLUSION AND FUTURE RESEARCH

7.1 Conclusion

In this thesis, we have delved into challenges posed by model uncertainty and unknown actuator faults, with the goal of guaranteeing the stability and safety. To address above two issues, reliable and adaptive control methods have been proposed by integrating GP regression and CBFs into FTC frameworks. Considering the computational time of GP regression, we have studied two data collection cases: offline data collection and event-triggered learning methods. In addition, this research has designed GP-based CBFs to address the safe problems for uncertain systems. This approach has also been extended to high relative degrees. To handle unknown actuator bias and gain faults, we have explored robust strategies and online estimation techniques to enhance the performance of GP-based CBF and GP-based HOCBF methods. Furthermore, the influences of drift and gain uncertainties have been investigated, and a compound kernel has been designed to address these modelling challenges.

To answer the RQ1, two types of GP-based adaptive FTC methods have been pro-

posed to ensure the stability of uncertain systems subject to unknown actuator bias faults in Chapter 3. To handle the RQ2, Chapter 4 has developed the GP-based HOCBF method for nonlinear systems with model uncertainty and integrated this approach into FTC frameworks. In Chapter 5, we have designed learning-based adaptive CBFs and HOCBFs to address RQ3 using fault parameter estimation. Chapter 6 has dealt with RQ4 through a compound kernel-based GP regression to model drift and gain uncertain terms, and by establishing a probabilistically fault-tolerant HOCBF framework.

In conclusion, this research has explored learning-based safe FTC methods for uncertain systems in the presence of actuator bias and gain faults. Additionally, compound kernel-based GP regression techniques have been studied to model both drift and gain uncertainties. This work contributes to the advancement of safety-critical control under uncertain and faulty conditions, aiming to develop reliable and safe control frameworks for complex and dynamic environments.

7.2 Future Research

This thesis identifies the following directions as future work:

High dimensional input-based CBFs and HOCBFs

Future research will focus on the development of CBFs and HOCBFs that can effectively handle high-dimensional input data. In autonomous driving scenarios, the environment is typically unknown or only partially observable, and an autonomous car rely on onboard sensors, particularly camera arrays, to perceive obstacles and surroundings. As a result, high-dimensional input data can't be avoided. To address this challenge, we will investigate high-dimensional input-based CBF and HOCBF designs that improve the practical applicability and performance of these methods in real-world environments. Furthermore, advanced image-processing techniques, such as conditional

generative adversarial networks, will be considered for integration into the proposed frameworks to enhance their adaptability to complex and uncertain perception data.

Meta learning-based HOCBFs under dynamic environments

Although our research preliminarily investigates GP-based HOCBFs under drift and gain uncertainties, uncertainty in autonomous systems is dynamic in practical applications. Furthermore, in real-world control tasks, autonomous systems often operate repeatedly in similar environments. Leveraging data from past tasks can facilitate the representation of task similarities as prior knowledge, which can be transferred to new scenarios to improve learning efficiency and safety. In future work, we will explore meta-learning based HOCBFs, aiming to enable fast adaptation to new environments based on prior experiences. Lightweight probabilistic models, such as Bayesian linear regression, will be introduced to represent and generalize task-level knowledge in a computationally efficient manner.

Reinforcement learning-based HOCBFs

RL can be applied not only for system modelling in CBFs and HOCBFs, but also to enhance their control performance. Although RL-based CBFs have been investigated in existing studies, research on RL-based HOCBFs remains at an early stage. In future work, we will develop an RL-based probabilistic HOCBF framework to address model uncertainty in complex systems. Moreover, the penalty terms in HOCBF formulations can be optimized, and the reference input $\boldsymbol{u}_{\text{ref}}$ can be learned through RL policies to further improve control efficiency and adaptability.

References

[1] L. Wang, E. A. Theodorou, and M. Egerstedt, "Safe learning of quadrotor dynamics using barrier certificates," in *2018 IEEE International Conference on Robotics and Automation, ICRA 2018, Brisbane, Australia, May 21-25, 2018*. IEEE, 2018, pp. 2460–2465.

[2] S. Hood, K. Benson, P. Hamod, D. Madison, J. M. O'Kane, and I. Rekleitis, "Bird's eye view: Cooperative exploration by UGV and UAV," in *2017 International Conference on Unmanned Aircraft Systems (ICUAS)*, 2017, pp. 247–255.

[3] W.-C. Chiang, Y. Li, J. Shang, and T. L. Urban, "Impact of drone delivery on sustainability and cost: Realizing the UAV potential through vehicle routing optimization," *Appl. Energ*, vol. 242, pp. 1164–1175, May 2019.

[4] B. Arbanas, A. Ivanovic, M. Car, M. Orsag, T. Petrovic, and S. Bogdan, "Decentralized planning and control for UAVUGV cooperative teams," *Autonomous Robots*, vol. 42, no. 8, pp. 1601–1618, 2018.

[5] W. Zhao, H. Liu, and F. L. Lewis, "Data-driven fault-tolerant control for attitude synchronization of nonlinear quadrotors," *IEEE Trans. Autom. Control.*, vol. 66, no. 11, pp. 5584–5591, 2021.

[6] L. Wang, Y. Bian, D. Cao, H. Qin, and M. Hu, "Hierarchical safe control of heterogeneous connected vehicle systems using adaptive fault-tolerant control," *IEEE Trans. Veh. Technol.*, vol. 73, no. 10, pp. 14 313–14 325, 2024.

[7] W. Cheng, B. Jiang, K. Zhang, and S. X. Ding, "Robust finite-time cooperative formation control of UGV-UAV with model uncertainties and actuator faults," *J. Frankl. Inst.*, vol. 358, no. 17, pp. 8811–8837, 2021.

[8] E. Hüllermeier and W. Waegeman, "Aleatoric and epistemic uncertainty in machine learning: an introduction to concepts and methods," *Mach. Learn.*, vol. 110, no. 3, pp. 457–506, 2021.

[9] I. R. Petersen and R. Tempo, "Robust control of uncertain systems: Classical results and recent developments," *Autom.*, vol. 50, no. 5, pp. 1315–1335, 2014.

[10] E. Lavretsky and K. A. Wise, *Robust and Adaptive Control: With Aerospace Applications*. Springer Cham, 2012.

[11] C. E. Rasmussen and C. K. I. Williams, *Gaussian processes for machine learning*. MIT Press, 2006.

[12] S. X. Ding, *Data-driven design of fault diagnosis and fault-tolerant control systems*. Springer, 2014.

[13] A. A. Amin and K. M. Hasan, "A review of fault tolerant control systems: Advancements and applications," *Measurement*, vol. 143, pp. 58–68, 2019.

[14] Q. Shen, B. Jiang, and S. Peng, *Fault diagnosis and fault-tolerant control based on adaptive control approach*. Springer, 2017.

[15] R. Sheikhbahaei, A. Alasty, and G. Vossoughi, "Robust fault tolerant explicit model predictive control," *Autom.*, vol. 97, pp. 248–253, 2018.

[16] B. Wang, D. Zhu, L. Han, H. Gao, Z. Gao, and Y. Zhang, "Adaptive fault-tolerant control of a hybrid canard rotor/wing UAV under transition flight subject to actuator faults and model uncertainties," *IEEE Trans. Aerosp. Electron. Syst.*, vol. 59, no. 4, pp. 4559–4574, 2023.

[17] X. Yang and J. M. Maciejowski, "Fault tolerant control using gaussian processes and model predictive control," *Int. J. Appl. Math. Comput. Sci.*, vol. 25, no. 1, pp. 133–148, 2015.

[18] A. D. Ames, X. Xu, J. W. Grizzle, and P. Tabuada, "Control barrier function based quadratic programs for safety critical systems," *IEEE Trans. Autom. Control.*, vol. 62, no. 8, pp. 3861–3876, 2017.

[19] S. Bansal, M. Chen, S. L. Herbert, and C. J. Tomlin, "Hamilton-jacobi reachability: A brief overview and recent advances," in *56th IEEE Annual Conference on*

Decision and Control, CDC 2017, Melbourne, Australia, December 12-15, 2017. IEEE, 2017, pp. 2242–2253.

[20] L. Brunke, M. Greeff, A. W. Hall, Z. Yuan, S. Zhou, J. Panerati, and A. P. Schoellig, "Safe learning in robotics: From learning-based control to safe reinforcement learning," *Annu. Rev. Control. Robotics Auton. Syst.*, vol. 5, pp. 411–444, 2022.

[21] A. D. Ames, S. Coogan, M. Egerstedt, G. Notomista, K. Sreenath, and P. Tabuada, "Control barrier functions: Theory and applications," in *17th European Control Conference, ECC 2019, Naples, Italy, June 25-28, 2019*. IEEE, 2019, pp. 3420–3431.

[22] W. Xiao and C. Belta, "High-order control barrier functions," *IEEE Trans. Autom. Control.*, vol. 67, no. 7, pp. 3655–3662, 2022.

[23] L. Zhao, L. Wang, Y. Cao, Y. Yang, and S. Wen, "Learning-based fault-tolerant control with high-order control barrier functions," *IEEE Trans Autom. Sci. Eng.*, vol. 22, pp. 14 689–14 698, 2025.

[24] P. Jagtap, G. J. Pappas, and M. Zamani, "Control barrier functions for unknown nonlinear systems using Gaussian processes," in *59th IEEE Conference on Decision and Control, CDC 2020, Jeju Island, South Korea, December 14-18, 2020*. IEEE, 2020, pp. 3699–3704.

[25] Y. Zhang, L. Wen, X. Yao, Z. Bing, L. Kong, W. He, and A. Knoll, "Real-time adaptive safety-critical control with gaussian processes in high-order uncertain models," in *IEEE International Conference on Robotics and Automation, ICRA 2024, Yokohama, Japan, May 13-17, 2024*. IEEE, 2024, pp. 14 763–14 769.

[26] Q. E. J. van Hilten, "Fault tolerant control barrier functions," Master's thesis, Technical University of Delft, 2024.

[27] Z. Dong, J. Li, and H. Wang, "Fault-tolerant safety-critical control for nonlinear affine system by using high-order control barrier function," *Electronics*, vol. 12, no. 21, p. 4549, 2023.

[28] Z. Wu, R. Yang, L. Zheng, and H. Cheng, "Safe learning-based feedback linearization tracking control for nonlinear system with event-triggered model update," *IEEE Robotics Autom. Lett.*, vol. 7, no. 2, pp. 3286–3293, 2022.

[29] J. Umlauft and S. Hirche, "Feedback linearization based on gaussian processes with event-triggered online learning," *IEEE Trans. Autom. Control.*, vol. 65, no. 10, pp. 4154–4169, 2020.

[30] Y. He and Y. Zhao, "Adaptive robust control of uncertain Euler-lagrange systems using Gaussian processes," *IEEE Trans. Neural Networks Learn. Syst.*, vol. 35, no. 6, pp. 7949–7962, 2024.

[31] E. L. Zhu, F. L. Busch, J. Johnson, and F. Borrelli, "A gaussian process model for opponent prediction in autonomous racing," in *IROS*, 2023, pp. 8186–8191.

[32] W. Zhao, T. He, and C. Liu, "Probabilistic safeguard for reinforcement learning using safety index guided gaussian process models," in *Learning for Dynamics and Control Conference, L4DC 2023, 15-16 June 2023, Philadelphia, PA, USA*, ser. Proceedings of Machine Learning Research, N. Matni, M. Morari, and G. J. Pappas, Eds., vol. 211. PMLR, 2023, pp. 783–796.

[33] R. Yang, L. Zheng, J. Pan, and H. Cheng, "Learning-based predictive path following control for nonlinear systems under uncertain disturbances," *IEEE Robotics Autom. Lett.*, vol. 6, no. 2, pp. 2854–2861, 2021.

[34] F. Castañeda, J. J. Choi, B. Zhang, C. J. Tomlin, and K. Sreenath, "Pointwise feasibility of gaussian process-based safety-critical control under model uncertainty," in *2021 60th IEEE Conference on Decision and Control (CDC), Austin, TX, USA, December 14-17, 2021*. IEEE, 2021, pp. 6762–6769.

[35] S. Wang, K. Li, Y. Yang, Y. Cao, T. Huang, and S. Wen, "Model-assisted probabilistic safe adaptive control with meta-bayesian learning," *CoRR*, vol. abs/2307.00828, 2023.

[36] X. Dai, Z. Yang, M. Xu, S. Zhang, F. Liu, G. Hattab, and S. Hirche, "Decentralized event-triggered online learning for safe consensus control of multi-agent systems with Gaussian process regression," *European Journal of Control*, p. 101058, 2024.

[37] P. Mestres and J. Cortés, "Feasibility and regularity analysis of safe stabilizing controllers under uncertainty," *Autom.*, vol. 167, p. 111800, 2024.

[38] M. Aali and J. Liu, "Learning high-order control barrier functions for safety-critical control with gaussian processes," in *American Control Conference, ACC 2024, Toronto, ON, Canada, July 10-12, 2024*. IEEE, 2024, pp. 1–6.

[39] A. Lederer, A. Begzadic, S. Hirche, J. Cortés, and S. L. Herbert, "Safe barrier-constrained control of uncertain systems via event-triggered learning," *CoRR*, vol. abs/2408.16144, 2024.

[40] N. T. Nguyen, "Model-reference adaptive control," in *Model-Reference Adaptive Control: A Primer*, N. T. Nguyen, Ed. Springer International Publishing, 2018, pp. 83–123.

[41] A. R. Barron, "Approximation and estimation bounds for artificial neural networks," *Mach. Learn.*, vol. 14, no. 1, pp. 115–133, 1994. [Online]. Available: https://doi.org/10.1007/BF00993164

[42] D. Duvenaud, "Automatic model construction with gaussian processes," Ph.D. dissertation, 2014.

[43] N. Srinivas, A. Krause, S. M. Kakade, and M. W. Seeger, "Information-theoretic regret bounds for gaussian process optimization in the bandit setting," *IEEE Trans. Inf. Theory*, vol. 58, no. 5, pp. 3250–3265, 2012.

[44] T. Beckers, D. Kulic, and S. Hirche, "Stable gaussian process based tracking control of euler-lagrange systems," *Autom.*, vol. 103, pp. 390–397, 2019.

[45] A. Lederer, J. Umlauft, and S. Hirche, "Uniform error bounds for gaussian process regression with application to safe control," in *Advances in Neural Information Processing Systems 32: Annual Conference on Neural Information Processing Systems 2019, NeurIPS 2019, December 8-14, 2019, Vancouver, BC, Canada*, H. M. Wallach, H. Larochelle, A. Beygelzimer, F. d'Alché-Buc, E. B. Fox, and R. Garnett, Eds., 2019, pp. 657–667.

[46] J. Umlauft, L. Pöhler, and S. Hirche, "An uncertainty-based control lyapunov approach for control-affine systems modeled by gaussian process," *IEEE Control. Syst. Lett.*, vol. 2, no. 3, pp. 483–488, 2018. [Online]. Available: https://doi.org/10.1109/LCSYS.2018.2841961

[47] J. Umlauft, T. Beckers, and S. Hirche, "Scenario-based optimal control for gaussian process state space models," in *16th European Control Conference,*

ECC 2018, Limassol, Cyprus, June 12-15, 2018. IEEE, 2018, pp. 1386–1392. [Online]. Available: https://doi.org/10.23919/ECC.2018.8550458

[48] F. Castañeda, J. J. Choi, B. Zhang, C. J. Tomlin, and K. Sreenath, "Gaussian process-based min-norm stabilizing controller for control-affine systems with uncertain input effects and dynamics," in *2021 American Control Conference, ACC 2021, New Orleans, LA, USA, May 25-28, 2021*. IEEE, 2021, pp. 3683–3690. [Online]. Available: https://doi.org/10.23919/ACC50511.2021.9483420

[49] R. C. Grande, G. Chowdhary, and J. P. How, "Nonparametric adaptive control using gaussian processes with online hyperparameter estimation," in *Proceedings of the 52nd IEEE Conference on Decision and Control, CDC 2013, Florence, Italy, December 10-13, 2013*. IEEE, 2013, pp. 861–867. [Online]. Available: https://doi.org/10.1109/CDC.2013.6759990

[50] G. Chowdhary, H. A. Kingravi, J. P. How, and P. A. Vela, "Bayesian nonparametric adaptive control using gaussian processes," *IEEE Trans. Neural Networks Learn. Syst.*, vol. 26, no. 3, pp. 537–550, 2015. [Online]. Available: https://doi.org/10.1109/TNNLS.2014.2319052

[51] G. Joshi and G. Chowdhary, "Adaptive control using gaussian-process with model reference generative network," in *57th IEEE Conference on Decision and Control, CDC 2018, Miami, FL, USA, December 17-19, 2018*. IEEE, 2018, pp. 237–243. [Online]. Available: https://doi.org/10.1109/CDC.2018.8619431

[52] L. Hewing, J. Kabzan, and M. N. Zeilinger, "Cautious model predictive control using gaussian process regression," *IEEE Trans. Control. Syst. Technol.*, vol. 28, no. 6, pp. 2736–2743, 2020. [Online]. Available: https://doi.org/10.1109/TCST.2019.2949757

[53] J. Kabzan, L. Hewing, A. Liniger, and M. N. Zeilinger, "Learning-based model predictive control for autonomous racing," *IEEE Robotics Autom. Lett.*, vol. 4, no. 4, pp. 3363–3370, 2019. [Online]. Available: https://doi.org/10.1109/LRA.2019.2926677

[54] G. Cao, E. M. Lai, and F. Alam, "Gaussian process model predictive control of an unmanned quadrotor," *J. Intell. Robotic Syst.*, vol. 88, no. 1, pp. 147–162, 2017. [Online]. Available: https://doi.org/10.1007/s10846-017-0549-y

[55] Y. Xu, J. Sun, Z. Wu, and G. Wang, "Fully distributed adaptive event-triggered control of networked systems with actuator bias faults," *IEEE Trans. Cybern.*, vol. 52, no. 10, pp. 10 773–10 784, 2022.

[56] D. Ye and G. Yang, "Adaptive fault-tolerant tracking control against actuator faults with application to flight control," *IEEE Trans. Control. Syst. Technol.*, vol. 14, no. 6, pp. 1088–1096, 2006.

[57] P. Mellodge, *A practical approach to dynamical systems for engineers*. Woodhead Publishing, 2015.

[58] H. Ouyang and Y. Lin, "Adaptive fault-tolerant control for actuator failures: A switching strategy," *Autom.*, vol. 81, pp. 87–95, 2017.

[59] C. Deng and G. Yang, "Distributed adaptive fault-tolerant control approach to cooperative output regulation for linear multi-agent systems," *Autom.*, vol. 103, pp. 62–68, 2019.

[60] J. Chen and R. J. Patton, *Robust Model-Based Fault Diagnosis for Dynamic Systems*, ser. The International Series on Asian Studies in Computer and Information Science. Kluwer, 1999, vol. 3.

[61] L. Wang, M. Hu, Y. Bian, G. Guo, S. E. Li, B. Chen, and Z. Zhong, "Periodic event-triggered fault detection for safe platooning control of intelligent and connected vehicles," *IEEE Trans. Veh. Technol.*, vol. 73, no. 4, pp. 5064–5077, 2024.

[62] J. Lunze and J. Richter, "Reconfigurable fault-tolerant control: A tutorial introduction," *European Journal of Control*, vol. 14, no. 5, pp. 359–386, 2008.

[63] J. Jiang and X. Yu, "Fault-tolerant control systems: A comparative study between active and passive approaches," *Annu. Rev. Control.*, vol. 36, no. 1, pp. 60–72, 2012.

[64] M. Khalili, X. Zhang, M. M. Polycarpou, T. Parisini, and Y. Cao, "Distributed adaptive fault-tolerant control of uncertain multi-agent systems," *Autom.*, vol. 87, pp. 142–151, 2018.

[65] H. Wang, W. Bai, and P. X. Liu, "Finite-time adaptive fault-tolerant control for nonlinear systems with multiple faults," *IEEE CAA J. Autom. Sinica*, vol. 6, no. 6, pp. 1417–1427, 2019.

[66] T. Yang and J. Dong, "Predefined-time adaptive fault-tolerant control for switched odd-rational-power multi-agent systems," *IEEE Trans Autom. Sci. Eng.*, vol. 20, no. 4, pp. 2423–2434, 2023.

[67] H. Fan, X. Fang, W. Wang, J. Huang, and L. Liu, "Adaptive fault-tolerant control for uncertain nonlinear systems with both parameter estimator and controller triggering," *Autom.*, vol. 151, p. 110954, 2023.

[68] J. Wang, J. Ma, H. Pan, and W. Sun, "Event-triggered adaptive saturated fault-tolerant control for unknown nonlinear systems with full state constraints," *IEEE Trans Autom. Sci. Eng.*, vol. 21, no. 2, pp. 1837–1849, 2024.

[69] Y. Wu, G. Zhang, and L. Wu, "Event-triggered adaptive fault-tolerant control for nonaffine uncertain systems with output tracking errors constraints," *IEEE Trans. Fuzzy Syst.*, vol. 30, no. 6, pp. 1750–1761, 2022.

[70] Z. Zhao, Y. Ren, C. Mu, T. Zou, and K. Hong, "Adaptive neural-network-based fault-tolerant control for a flexible string with composite disturbance observer and input constraints," *IEEE Trans. Cybern.*, vol. 52, no. 12, pp. 12 843–12 853, 2022.

[71] X. Guo, C. Wang, and L. Liu, "Adaptive fault-tolerant control for a class of nonlinear multi-agent systems with multiple unknown time-varying control directions," *Autom.*, vol. 167, p. 111802, 2024.

[72] X. Shao, Q. Hu, Y. Shi, and Y. Zhang, "Fault-tolerant control for full-state error constrained attitude tracking of uncertain spacecraft," *Autom.*, vol. 151, p. 110907, 2023.

[73] C. Deng, X. Jin, W. Che, and H. Wang, "Learning-based distributed resilient fault-tolerant control method for heterogeneous mass under unknown leader dynamic," *IEEE Trans. Neural Networks Learn. Syst.*, vol. 33, no. 10, pp. 5504–5513, 2022.

[74] L. Zhao, G. Wen, Z. Guo, S. Zhu, C. Hu, and S. Wen, "Probabilistic model-based fault-tolerant control for uncertain nonlinear systems," *IEEE Trans. Cybern.*, vol. 55, no. 4, pp. 1838–1847, 2025.

[75] X. Xu, P. Tabuada, J. W. Grizzle, and A. D. Ames, "Robustness of control barrier functions for safety critical control," in *5th IFAC Conference on Analysis*

and Design of Hybrid Systems, ADHS 2015, Atlanta, GA, USA, October 14-16, 2015, ser. IFAC-PapersOnLine, M. Egerstedt and Y. Wardi, Eds., vol. 48, no. 27. Elsevier, 2015, pp. 54–61.

[76] M. Jankovic, "Robust control barrier functions for constrained stabilization of nonlinear systems," *Autom.*, vol. 96, pp. 359–367, 2018.

[77] J. R. Buch, S. Liao, and P. J. Seiler, "Robust control barrier functions with sector-bounded uncertainties," *IEEE Control. Syst. Lett.*, vol. 6, pp. 1994–1999, 2022.

[78] M. H. Cohen, C. Belta, and R. Tron, "Robust control barrier functions for nonlinear control systems with uncertainty: A duality-based approach," in *61st IEEE Conference on Decision and Control, CDC 2022, Cancun, Mexico, December 6-9, 2022*. IEEE, 2022, pp. 174–179.

[79] C. Dawson, Z. Qin, S. Gao, and C. Fan, "Safe nonlinear control using robust neural lyapunov-barrier functions," in *Conference on Robot Learning, 8-11 November 2021, London, UK*, ser. Proceedings of Machine Learning Research, A. Faust, D. Hsu, and G. Neumann, Eds., vol. 164. PMLR, 2021, pp. 1724–1735.

[80] B. T. Lopez, J. E. Slotine, and J. P. How, "Robust adaptive control barrier functions: An adaptive and data-driven approach to safety," *IEEE Control. Syst. Lett.*, vol. 5, no. 3, pp. 1031–1036, 2021.

[81] S. Wang, B. Lyu, S. Wen, K. Shi, S. Zhu, and T. Huang, "Robust adaptive safety-critical control for unknown systems with finite-time elementwise parameter estimation," *IEEE Trans. Syst. Man Cybern. Syst.*, vol. 53, no. 3, pp. 1607–1617, 2023.

[82] Y. Wang and X. Xu, "Adaptive safety-critical control for a class of nonlinear systems with parametric uncertainties: A control barrier function approach," *Syst. Control. Lett.*, vol. 188, p. 105798, 2024.

[83] E. Das and J. W. Burdick, "Robust control barrier functions using uncertainty estimation with application to mobile robots," *CoRR*, vol. abs/2401.01881, 2024.

[84] J. J. Choi, F. Castañeda, C. J. Tomlin, and K. Sreenath, "Reinforcement learning for safety-critical control under model uncertainty, using control lyapunov functions and control barrier functions," in *Robotics: Science and Systems XVI,*

Virtual Event / Corvalis, Oregon, USA, July 12-16, 2020, M. Toussaint, A. Bicchi, and T. Hermans, Eds., 2020.

[85] A. J. Taylor, A. Singletary, Y. Yue, and A. D. Ames, "Learning for safety-critical control with control barrier functions," in *Proceedings of the 2nd Annual Conference on Learning for Dynamics and Control, L4DC 2020, Online Event, Berkeley, CA, USA, 11-12 June 2020*, ser. Proceedings of Machine Learning Research, A. M. Bayen, A. Jadbabaie, G. J. Pappas, P. A. Parrilo, B. Recht, C. J. Tomlin, and M. N. Zeilinger, Eds., vol. 120. PMLR, 2020, pp. 708–717.

[86] L. Lindemann, A. Robey, L. Jiang, S. Tu, and N. Matni, "Learning robust output control barrier functions from safe expert demonstrations," *IEEE Open. J. Control Syst.*, vol. 3, pp. 158–172, 2024.

[87] Y. Emam, P. Glotfelter, S. Wilson, G. Notomista, and M. Egerstedt, "Data-driven robust barrier functions for safe, long-term operation," *IEEE Trans. Robotics*, vol. 38, no. 3, pp. 1671–1685, 2022.

[88] J. Li, Q. Liu, W. Jin, J. Qin, and S. Hirche, "Robust safe learning and control in an unknown environment: An uncertainty-separated control barrier function approach," *IEEE Robotics Autom. Lett.*, vol. 8, no. 10, pp. 6539–6546, 2023.

[89] M. Li and Z. Sun, "Safe stabilization with model uncertainties: A universal formula with gaussian process learning," in *18th IEEE International Conference on Control & Automation, ICCA 2024, Reykjavík, Iceland, June 18-21, 2024*. IEEE, 2024, pp. 180–185.

[90] K. Long, V. Dhiman, M. Leok, J. Cortés, and N. Atanasov, "Safe control synthesis with uncertain dynamics and constraints," *IEEE Robotics Autom. Lett.*, vol. 7, no. 3, pp. 7295–7302, 2022.

[91] M. J. Khojasteh, V. Dhiman, M. Franceschetti, and N. Atanasov, "Probabilistic safety constraints for learned high relative degree system dynamics," in *Proceedings of the 2nd Annual Conference on Learning for Dynamics and Control, L4DC 2020, Online Event, Berkeley, CA, USA, 11-12 June 2020*, ser. Proceedings of Machine Learning Research, A. M. Bayen, A. Jadbabaie, G. J. Pappas, P. A. Parrilo, B. Recht, C. J. Tomlin, and M. N. Zeilinger, Eds., vol. 120. PMLR, 2020, pp. 781–792.

[92] B. Li, Z. Guo, C. Hu, S. Zhu, and S. Wen, "Safe formation control of uncertain multiagent systems from a bayesian perspective," *IEEE Trans. Autom. Control.*, vol. 70, no. 3, pp. 1929–1934, 2025.

[93] S. Wang, K. Li, Z. Yan, Z. Guo, S. Zhu, G. Wen, and S. Wen, "Optimal parameter adaptation for safety-critical control via safe barrier bayesian optimization," *CoRR*, vol. abs/2503.19349, 2025.

[94] W. Xiao and C. Belta, "Control barrier functions for systems with high relative degree," in *58th IEEE Conference on Decision and Control, CDC 2019, Nice, France, December 11-13, 2019*. IEEE, 2019, pp. 474–479.

[95] Q. Nguyen and K. Sreenath, "Exponential control barrier functions for enforcing high relative-degree safety-critical constraints," in *2016 American Control Conference, ACC 2016, Boston, MA, USA, July 6-8, 2016*. IEEE, 2016, pp. 322–328.

[96] H. Khalil, *Nonlinear Systems*. 3rd ed. Englewood Cliffs, NJ, USA: Prentice Hall, 2002.

[97] C. I. G. Chinelato and B. A. Angélico, "Robust exponential control barrier functions for safety-critical control," in *2021 American Control Conference, ACC 2021, New Orleans, LA, USA, May 25-28, 2021*. IEEE, 2021, pp. 2342–2347. [Online]. Available: https://doi.org/10.23919/ACC50511.2021.9482899

[98] P. J. Seiler, M. Jankovic, and E. Hellström, "Control barrier functions with unmodeled input dynamics using integral quadratic constraints," *IEEE Control. Syst. Lett.*, vol. 6, pp. 1664–1669, 2022. [Online]. Available: https://doi.org/10.1109/LCSYS.2021.3130782

[99] V. Azimi and S. Hutchinson, "Exponential control lyapunov-barrier function using a filtering-based concurrent learning adaptive approach," *IEEE Trans. Autom. Control.*, vol. 67, no. 10, pp. 5376–5383, 2022. [Online]. Available: https://doi.org/10.1109/TAC.2021.3120622

[100] C. Wang, Y. Meng, Y. Li, S. L. Smith, and J. Liu, "Learning control barrier functions with high relative degree for safety-critical control," in *2021 European Control Conference, ECC 2021, Virtual Event / Delft, The Netherlands, June 29 - July 2, 2021*. IEEE, 2021, pp. 1459–1464. [Online]. Available: https://doi.org/10.23919/ECC54610.2021.9655206

[101] L. Wang and J. Dong, "Concurrent learning control lyapunov and barrier functions for uncertain nonlinear safety-critical systems with high relative degree constraints," *IEEE Trans Autom. Sci. Eng.*, vol. 21, no. 4, pp. 7170–7179, 2024. [Online]. Available: https://doi.org/10.1109/TASE.2023.3339501

[102] J. Wang, H. Pan, and W. Sun, "Event-triggered adaptive fault-tolerant control for unknown nonlinear systems with applications to linear motor," *IEEE/ASME Trans. Mechatron.*, vol. 27, no. 2, pp. 940–949, 2022.

[103] H. Fan, X. Fang, W. Wang, J. Huang, and L. Liu, "Adaptive fault-tolerant control for uncertain nonlinear systems with both parameter estimator and controller triggering," *Autom.*, vol. 151, p. 110954, 2023.

[104] L. Liu, Y. Liu, and S. Tong, "Neural networks-based adaptive finite- time fault-tolerant control for a class of strict-feedback switched nonlinear systems," *IEEE Trans. Cybern.*, vol. 49, no. 7, pp. 2536–2545, 2019.

[105] S. Roshanravan and S. Shamaghdari, "Adaptive fault-tolerant tracking control for affine nonlinear systems with unknown dynamics via reinforcement learning," *IEEE Trans Autom. Sci. Eng.*, vol. 21, no. 1, pp. 569–580, 2024.

[106] J. Qiu, M. Ma, and T. Wang, "Event-triggered adaptive fuzzy fault-tolerant control for stochastic nonlinear systems via command filtering," *IEEE Trans. Syst. Man Cybern. Syst.*, vol. 52, no. 2, pp. 1145–1155, 2022.

[107] J. Wu, F. He, H. Shen, S. Ding, and Z. Wu, "Adaptive NN fixed-time fault-tolerant control for uncertain stochastic system with deferred output constraint via self-triggered mechanism," *IEEE Trans. Cybern.*, vol. 53, no. 9, pp. 5892–5903, 2023.

[108] J. Kocijan, *Modelling and control of dynamic systems using Gaussian process models*. Springer, 2016.

[109] X. Dai, A. Lederer, Z. Yang, and S. Hirche, "Can learning deteriorate control? analyzing computational delays in gaussian process-based event- triggered online learning," in *Learning for Dynamics and Control Conference, L4DC 2023, 15-16 June 2023, Philadelphia, PA, USA*, N. Matni, M. Morari, and G. J. Pappas, Eds., vol. 211. PMLR, 2023, pp. 445–457.

[110] R. Kamalapurkar, H. T. Dinh, S. Bhasin, and W. E. Dixon, "Approximate optimal trajectory tracking for continuous-time nonlinear systems," *Autom.*, vol. 51, pp. 40–48, 2015.

[111] V. Dhiman, M. J. Khojasteh, M. Franceschetti, and N. Atanasov, "Control barriers in bayesian learning of system dynamics," *IEEE Trans. Autom. Control.*, vol. 68, no. 1, pp. 214–229, 2023.

[112] Y. Li and G. Yang, "Robust adaptive fault-tolerant control for a class of uncertain nonlinear time delay systems," *IEEE Trans. Syst. Man Cybern. Syst.*, vol. 47, no. 7, pp. 1554–1563, 2017.

[113] Y. Su, C. Zheng, and P. Mercorelli, "Nonlinear PD fault-tolerant control for dynamic positioning of ships with actuator constraints," *IEEE/ASME Trans. Mechatron.*, vol. 22, no. 3, pp. 1132–1142, 2017.

[114] M. H. Cohen and C. Belta, "High order robust adaptive control barrier functions and exponentially stabilizing adaptive control Lyapunov functions," in *American Control Conference, ACC 2022, Atlanta, GA, USA, June 8-10, 2022*. IEEE, 2022, pp. 2233–2238.

[115] H. Noura, D. Theilliol, J.-C. Ponsart, and A. Chamseddine, *Fault-tolerant Control Systems: Design and Practical Applications*. Springer London, 2009.

[116] H. Zhang, L. Niu, A. Clark, and R. Poovendran, "Fault tolerant neural control barrier functions for robotic systems under sensor faults and attacks," in *IEEE International Conference on Robotics and Automation, ICRA 2024, Yokohama, Japan, May 13-17, 2024*. IEEE, 2024, pp. 9901–9907.

[117] M. Cohen and C. Belta, *Adaptive and Learning-Based Control of Safety-Critical Systems*. Springer Cham, 2023.

[118] L. Wu and J. H. Park, "Adaptive fault-tolerant control of uncertain switched non-affine nonlinear systems with actuator faults and time delays," *IEEE Trans. Syst. Man Cybern. Syst.*, vol. 50, no. 9, pp. 3470–3480, 2020.

[119] H. Tao, H. Shi, J. Qiu, G. Jin, and V. Stojanovic, "Planetary gearbox fault diagnosis based on FDKNN-DGAT with few labeled data," *Meas. Sci. Technol.*, vol. 35, no. 2, p. 025036, 2023.

[120] L. Chen, C. Edwards, H. Alwi, and M. Sato, "Flight evaluation of a sliding mode online control allocation scheme for fault tolerant control," *Autom.*, vol. 114, p. 108829, 2020.

[121] X. Song, C. Wu, S. Song, V. Stojanovic, and I. Tejado, "Fuzzy wavelet neural adaptive finite-time self-triggered fault-tolerant control for a quadrotor unmanned aerial vehicle with scheduled performance," *Eng. Appl. Artif. Intell.*, vol. 131, p. 107832, 2024.

[122] X. Song, Y. Song, V. Stojanovic, and S. Song, "Improved dynamic event-triggered security control for TS fuzzy LPV-PDE systems via pointwise measurements and point control," *Int. J. Fuzzy Syst.*, vol. 25, no. 8, pp. 3177–3192, 2023.

[123] A. Dosovitskiy, G. Ros, F. Codevilla, A. M. López, and V. Koltun, "CARLA: an open urban driving simulator," in *1st Annual Conference on Robot Learning, CoRL 2017, Mountain View, California, USA, November 13-15, 2017, Proceedings*, ser. Proceedings of Machine Learning Research, vol. 78. PMLR, 2017, pp. 1–16.

[124] F. Pedregosa, G. Varoquaux, A. Gramfort, V. Michel, B. Thirion, O. Grisel, M. Blondel, P. Prettenhofer, R. Weiss, V. Dubourg, J. Vanderplas, A. Passos, D. Cournapeau, M. Brucher, M. Perrot, and E. Duchesnay, "Scikit-learn: Machine learning in Python," *Journal of Machine Learning Research*, vol. 12, pp. 2825–2830, 2011.

[125] S. Diamond and S. P. Boyd, "CVXPY: A python-embedded modeling language for convex optimization," *J. Mach. Learn. Res.*, vol. 17, pp. 83:1–83:5, 2016.

[126] L. Wang, A. D. Ames, and M. Egerstedt, "Safety barrier certificates for collisions-free multirobot systems," *IEEE Trans. Robotics*, vol. 33, no. 3, pp. 661–674, 2017.

[127] H. Ma and L. Xu, "Decentralized adaptive fault-tolerant control for a class of strong interconnected nonlinear systems via graph theory," *IEEE Trans. Autom. Control.*, vol. 66, no. 7, pp. 3227–3234, 2021.

[128] K. P. Wabersich, L. Hewing, A. Carron, and M. N. Zeilinger, "Probabilistic model predictive safety certification for learning-based control," *IEEE Trans. Autom. Control.*, vol. 67, no. 1, pp. 176–188, 2022.

[129] B. Xu, A. Suleman, and Y. Shi, "A multi-rate hierarchical fault-tolerant adaptive model predictive control framework: Theory and design for quadrotors," *Autom.*, vol. 153, p. 111015, 2023.

[130] S. Wang, K. Li, Y. Yang, Y. Cao, T. Huang, and S. Wen, "Model-assisted probabilistic safe adaptive control with meta-bayesian learning," *CoRR*, vol. abs/2307.00828, 2023.

[131] L. Zhao, L. Wang, Y. Cao, Y. Yang, and S. Wen, "Learning-based fault-tolerant control with high-order control barrier functions," *IEEE Trans Autom. Sci. Eng.*, vol. 22, pp. 14 689–14 698, 2025.

[132] H. Noura, D. Theilliol, J.-C. Ponsart, and A. Chamseddine, *Fault-tolerant control systems: Design and practical applications*. Springer Science & Business Media, 2009.

[133] H. Ouyang and Y. Lin, "Adaptive fault-tolerant control and performance recovery against actuator failures with deferred actuator replacement," *IEEE Trans. Autom. Control.*, vol. 66, no. 8, pp. 3810–3817, 2021.

[134] V. Adetola, D. DeHaan, and M. Guay, "Adaptive model predictive control for constrained nonlinear systems," *Syst. Control. Lett.*, vol. 58, no. 5, pp. 320–326, 2009.

[135] A. D. Ames, J. W. Grizzle, and P. Tabuada, "Control barrier function based quadratic programs with application to adaptive cruise control," in *53rd IEEE Conference on Decision and Control, CDC 2014, Los Angeles, CA, USA, December 15-17, 2014*. IEEE, 2014, pp. 6271–6278.

[136] R. Cheng, M. J. Khojasteh, A. D. Ames, and J. W. Burdick, "Safe multi-agent interaction through robust control barrier functions with learned uncertainties," in *59th IEEE Conference on Decision and Control, CDC 2020, Jeju Island, South Korea, December 14-18, 2020*. IEEE, 2020, pp. 777–783.

[137] M. Khan, T. Ibuki, and A. Chatterjee, "Safety uncertainty in control barrier functions using gaussian processes," in *IEEE International Conference on Robotics and Automation, ICRA 2021, Xi'an, China, May 30 - June 5, 2021*. IEEE, 2021, pp. 6003–6009.

[138] A. R. Kumar, S. Liu, J. F. Fisac, R. P. Adams, and P. J. Ramadge, "Probf: Learning probabilistic safety certificates with barrier functions," *CoRR*, vol. abs/2112.12210, 2021.

[139] X. Tan, W. Shaw-Cortez, and D. V. Dimarogonas, "High-order barrier functions: Robustness, safety, and performance-critical control," *IEEE Trans. Autom. Control.*, vol. 67, no. 6, pp. 3021–3028, 2022.